Università degli Studi di
Milano-Bicocca

Scuola di scienze

Dipartimento di Fisica

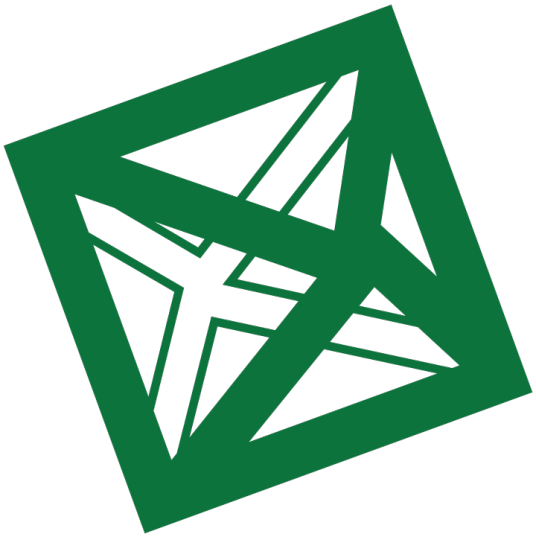

Corso di Laurea Magistrale in Fisica

Control of phase separating systems close to criticality

Relatore interno:
Francesco Montalenti

Relatore esterno:
Olivier Pierre-Louis

Candidato:
Rocco Suanno
Mat: 858885

Seduta del 18-20/09/24

Anno Accademico 2023–2024

Abstract

Domains, characterized by distinct regions of uniform composition or magnetization, frequently emerge as a result of phase transition dynamics. Two-component mixtures, like binary alloys or colloid-polymer mixtures, become unstable when a macroscopic variable, such as temperature or pressure, crosses a critical threshold. This leads to the separation of the homogeneous mixture into domains of two different phases. One notable mechanism for this phase separation is *spinodal decomposition*, characterized by the absence of nucleation barriers and resulting in an interconnected patterned structure of domains. In this work, we questioned how much control can one exert over the size, position, and shape of these domains by *varying in time* some macroscopic parameters, such as temperature. We investigated the problem within the framework of the Time-Dependent Ginzburg-Landau (TDGL) equation (or Allen-Cahn equation). This is a well known model to describe system undergoing spinodal decomposition when temperature is close to the critical value. We found that we cannot control the patterns that emerge in this type of dynamics by varying the temperature in time in two-dimensional systems. However we can control the size of domains in a one-dimensional system and this is consistent with previous machine learning investigations.

Keywords— Time dependent Ginzburg Landau equation, Allen-Cahn equation, Spinodal decomposition, Phase separation, Control theory.

Contents

Introduction

Controlling the morphology of a crystal's surface is a prominent challenge. The surface micro and nano-structure plays a crucial role in determining properties that have applications in various fields, such as regulating the growth of cell populations [1], enhancing the optical absorbance of materials [2], and producing nano-scale emitters with precise frequency outputs, known as *quantum dots*. The last application is relevant also in the semiconductor industry, where quantum dots are involved in the fabrication of nano-scale devices, like the single-electron transistor (Figure 2b).

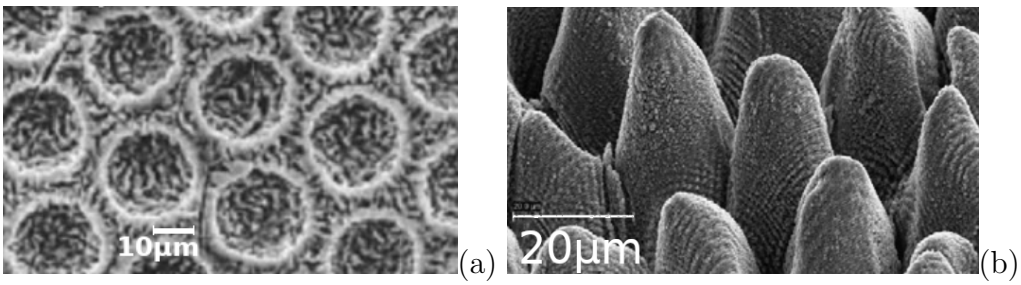

(a) (b)

Figure 1: a) Ti surface with circular cavity of diameter $d = 30\mu m$. Over the cavities, the surface presents an average roughness of $0.7\mu m$. The circular cavities were prepared with photolithography, while the additional roughness was produced by post-treating the surface with an acid [1]. b) Laser treated Ti surface showing the formation of nano-structures after exposing the surface to approximately 450 laser shots with an intensity of 0.9 J/cm2 [2].

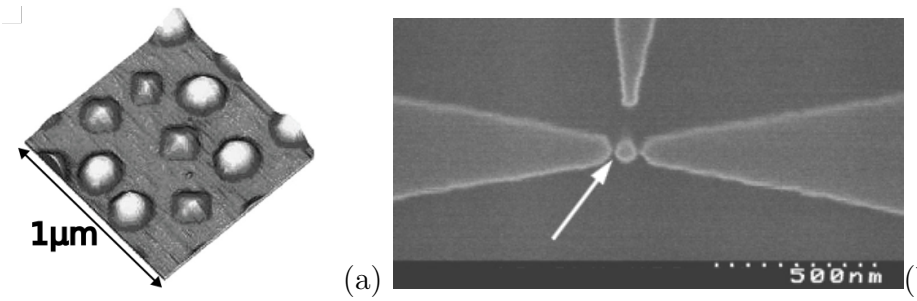

(a) (b)

Figure 2: a) Atomic force microscope image of quantum dots produced by annealing a 50 Å thick $Si_{0.6}Ge_{0.4}$ layer at 550 °C for 18 h [13]. b) Scanning electron microscope image of a single electron transistor. The arrow indicates the quantum dot [14].

Up to now, to carve the surface of crystals, scientists mainly used *lithography* techniques. This involves removing matter from the sample through a chemical compound, which reacts with the surface only where it is illuminated by light or a beam of electrons. But this method presents some limitations: the wavelength of the light limits the accuracy due to diffraction, while electron beam lithography requires expensive instruments. Other methods for shaping surfaces involve driving the system in non-equilibrium conditions. This conditions lead to the spontaneous emergence of micro and nano-structures, such as the ones shown in Figure 1. This class of methods includes adjusting the growth rate during crystal formation or applying an electric current along the surface, that can alter its structure through a process known as electromigration [3]. Other methods involve time depending driving forces

such as applying laser pulses [2]. In this process, matter reorganizes and reaches a new state, revealing the formation of the nano-structures in Figure 1b. However, there is no fundamental theoretical understanding of what can be achieved by time-dependent driving forces.
So in the following work, we are going to investigate how much the morphology of a crystal surface can change by *varying the temperature over time*. We will focus on a simplified scenario involving a very flat substrate that can be covered with atoms only up to a single atomic layer. This is a two-dimensional system, that we call *mono-layer* (Figure 3). We will consider this system exchanging atoms with a gas

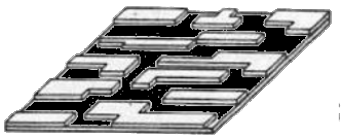

Figure 3: Schematic of a mono-layer. In black is represented a flat substrate and in white the atoms that cover it.

phase. If this is the mechanism driving the dynamics, we will see that the system is equivalent to the 2D Ising model, equipped with the usual Glauber dynamics (so the total magnetization is not conserved in time).
Instead of investigating the dynamics of the individual atoms, we study how the global morphology changes at large scales. We will see that a suitable model to study this system is the **Time Dependent Ginzburg Landau** (TDGL) equation, known also in literature as the Allen-Cahn equation

$$\partial_t m = \Delta m + C(T)m - m^3$$

where $m(x, y)$ is the magnetization field or the density of covered sites of the substrate. While $C(T)$ is a parameter depending on the temperature T.
This equation, along with the Cahn-Hilliard equation (the alternative for conservative dynamics), is the leading model to describe **spinodal decomposition** , a phenomena that takes place in some binary mixtures: binary alloys or colloid-polymer mixtures for instance. Those systems become unstable when a macroscopic variable, such as temperature or pressure, crosses a critical threshold. This leads to the spontaneous separation of the homogeneous mixture into *domains* of two different phases (Figure 4a).
We say that the homogeneous phase is unstable, in the sense that there is no energy barrier preventing the phenomena to happen and this leads to *interconnected* emerging pattern, that are different from the one characteristic of a "nucleation and growth" process (Figure 4).
This model has been extensively studied in the regime where the temperature is kept constant in time[4][6][7]. While neglecting the time dependence of temperature can be a good approximation for studying the dynamics following a rapid quench, future experiments may involve scenarios where the temperature is varied more gradually or in a non-monotonic fashion. However, there has been limited investigation into these systems under time-dependent temperature variations, both experimentally and theoretically. Some experiments have compared scenarios with different quench

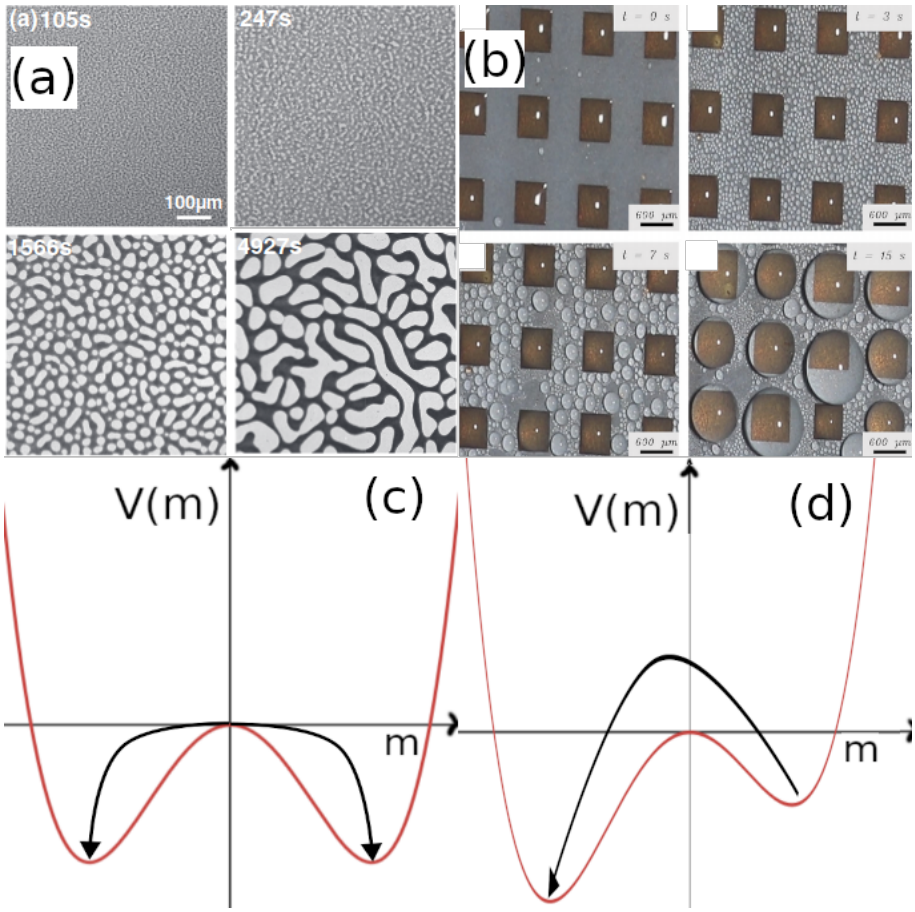

Figure 4: (a) Colloid-polymer mixture resting after being homogenized through steering [11]. The mixture is confined in a μ-channel and this is an image of the central cross section obtained with confocal scanning microscope. (b) Droplets of water condensing on an hydrophobic surface covered with a lattice of square hydrophilic structure of size $600\mu m \times 600\mu m$ and distance of $600\mu m$ [12]. (c), (d) Potentials describing a phase separation phenomena. The maxima is the homogeneous phase, while the minimas are the stable phases: (c) spinodal decomposition, (d) nucleation and growth.

rates [8], while some theorists have studied the Cahn-Hilliard model under conditions where a *quench wave* originates at the center of the system and propagates radially [9].

In this study, we look for a more global understanding of the consequences of time-dependent driving. Our goal is to understand to what extent we can control the pattern emerging from the TDGL equation's dynamics by varying the temperature over time. We will find that in a two-dimensional system, varying the temperature over time does not allow us to control any properties of the emerging pattern. However, in a one-dimensional system, we can control the size of the domains.

Chapter 1

Modelling the dynamics of a mono-layer

In this chapter, we introduce a simple model to describe the dynamics of a *flat crystal surface* in contact with a gas, where atoms from the gas can either bind to the surface or lose this bond and rejoin the gas. This model, known as the **Gas-Lattice model**, represents the surface as a square lattice, where each site can either be occupied by an atom from the gas or remain vacant (Figure 1.1). The energy of the system increases when a site is occupied and decreases when two atoms occupy neighboring sites, which encourages the formation of larger clusters of neighboring atoms, referred to as *domains*. The evolution of the system is simulated using the *Metropolis Monte Carlo* algorithm.
Next, we will demonstrate that this model is equivalent to the *2D Ising model*, meaning the system is characterized by a *critical temperature* T_C. And when the temperature is near this critical value, the system's macroscopic properties can be effectively described by the *Landau-Ginzburg theory*.
Finally, we will explore how the *Time-Dependent Ginzburg-Landau (TDGL)* equation emerges when describing the dynamics of the system as it remains close to the critical condition ($T \simeq T_C$). The dynamics described by this equation will be investigated in the next chapters.

1.1 The Gas-Lattice model

The physical system we are studying consists of a very thin film, just one atom thick (a **mono-layer**), that covers a flat, crystal-like surface (Figure 1.1). While the underlying surface structure remains unchanged over time, the single layer of atoms on top can gain or lose atoms through exchange with a surrounding gas.
The evolution of the system is governed by the internal interactions within the mono-layer, as well as the interactions between the mono-layer, the gas phase, and the crystal surface. This means that specifying the chemical composition of each component is crucial for accurately studying the system's dynamics. However, our goal is to uncover universal principles about the dynamics of this system that are independent of the specific elements involved. Therefore, rather than focusing on a particular real system, we choose to work with a well-known phenomenological

model: the **Gas-Lattice model**. Our aim is not to prove that this model precisely represents real physical systems, but rather we guess that the lack of details in the model will reveal dynamic behaviors common to many real systems.

The model

In this model, atoms can occupy the sites of a square lattice, so the state of the system is described by a sequence of occupation numbers $\{n_{i,j}\}$, where $n_{i,j} = 0$ or 1 indicates whether the site (i, j) of the lattice is unoccupied or occupied by an atom, respectively. It's important to clarify the terminology: in the literature [10], the term "gas" typically refers to the atoms that can occupy the lattice sites, whereas we use "gas" to refer to the reservoir that can exchange atoms with the mono-layer. In this model, only first-neighbor interactions between atoms are considered, and there is an associated energy cost of $+\Delta\mu$ for each atom that condenses from the gas phase onto the mono-layer.

$$U = -J \sum_{<ij>} n_i n_j - \Delta\mu \sum_i n_i \tag{1.1.1}$$

where J is the energy of an horizontal bond between neighbouring adsorbed atoms, while the sum is over all the couples (i,j), each one counted once.

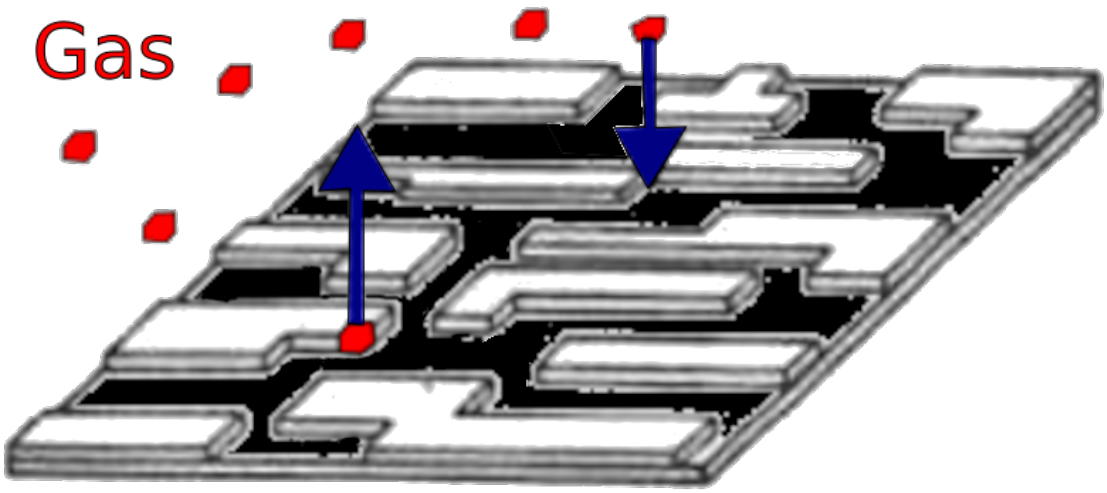

Figure 1.1: Schematic of the attachment/detachment model. The blue arrows indicate the two mechanism that can change the surface's state.

It is possible to show that this model is equivalent to the **2D Ising model**. In fact you can define a new set of state variables $S_i = n_i - \frac{1}{2} \in \{-\frac{1}{2}, +\frac{1}{2}\}$, such that

$$U = -J \sum_{<ij>} S_i S_j - (J\frac{(N-1)}{2}) - \Delta\mu) \sum_i n_i \tag{1.1.2}$$

And this is the energy of the 2D Ising model, in precence of a magnetic field $B = J\frac{(N-1)}{2}) - \Delta\mu$. Now that a link with the 2D Ising model has been established, you should expect to see a second order *phase transition* when the temperature is brought from above to below a critical value T_C and $B = 0$.

1.2 The Landau-Ginzburg theory

In the following section, we will introduce the Landau-Ginzburg theory, which offers a framework for constructing an *effective free energy* functional to describe a phase transition near the critical point ($T = T_C$, $B = 0$), based solely on the symmetries of the system. This functional will be instrumental in the next section for analyzing the system's dynamics when the temperature is maintained near the critical value.
In Ginzburg-Landau theory, the system's free energy $F[m(\mathbf{x}), T, B]$ is assumed to be a functional of a coarse-grained order parameter $m(\mathbf{x})$ and other macroscopic variables that can be controlled experimentally, such as temperature T and magnetic field B. In the Ising model, the order parameter is the magnetization field $m(\mathbf{x})$, which is obtained by averaging the spins S_i at the lattice sites surrounding the position $\mathbf{x}$. The term "coarse-grained" means that this average is taken over a sufficiently large region to avoid atomic-scale fluctuations.
Defining a free energy density $f(m(\mathbf{x}), T, H)$ such that $F = \int f \, d\mathbf{x}$, the fundamental assumption of the theory is that, near the critical temperature, $m(\mathbf{x})$ is small. Consequently, $f(m(\mathbf{x}), T, H)$ can be expanded in powers of $m(\mathbf{x})$ and its derivatives as follows:

$$f(m, T, B) = f_0 + \frac{1}{2}|\nabla m|^2 + hm + am^2 + bm^3 + pm^4 + ... \tag{1.2.1}$$

From the symmetries of the system, we can determine which terms can be eliminated from the expression and how the remaining coefficients $(a, b, p, ...)$ depend on the controllable variables (T, H). This means that systems with the same symmetries share the same effective free energy functional. Consequently, systems that may appear very different can exhibit similar behavior near the critical point. This phenomenon is known as *universality*.
In Appendix A the equivalence between the system and the 2D Ising model is exploited to find that, in the absence of a magnetic field ($B = 0$)

$$f(m, T, 0) = f_0 + \frac{1}{2}|\nabla m|^2 + V(m) \tag{1.2.2}$$

where

$$V(m) = \bar{V}(C - m^2)^2$$

and

$$C(T) = \alpha(T_c - T) \quad \alpha > 0$$

1.3 An equation for the dynamics: the Time Dependent Ginzburg-Landau equation

In this section we will show that by adopting the effective free energy density provided by the Landau-Ginzburg theory (Eq. 1.2.2), it is possible to find an equation to describe the dynamics of the 2D Ising model when the temperature is close to the critical value: the time-dependent Ginzburg-Landau equation.

Usually, the Landau-Ginzburg theory is used to describe the equilibrium states of a system, the states that the system eventually reaches in the absence of external perturbations. These equilibrium states correspond to the configurations that minimize the effective free energy. However, there is a straightforward idea that suggests we can extend the use of the free energy expression derived from this theory to describe the dynamics of the system. Given that the theory is formulated near the critical point, it is expected that this approach remains valid for describing the system's dynamics as long as the temperature is kept close to the critical value.
Before delving into the calculations, it's crucial to understand that the energy expression for the gas lattice system (Eq. 1.1.2) alone is insufficient to fully describe the system's dynamics. To do so, we must establish specific rules for updating the system's state at each discrete time step. The dynamics of the system will vary depending on these rules. Two common updating rules are:

- **Glauber Dynamics**: At each discrete time step, a spin is randomly selected. The spin is then flipped, and the energy change ΔE resulting from this flip is calculated. A random number p is drawn from a uniform distribution in the interval [0,1]. If $e^{-\frac{\Delta E}{k_B T}} > p$, the spin flip is accepted and the new state is retained; otherwise, the system reverts to its original state. This dynamic is simulated by the Metropolis algorithm.

- **Kawasaki Dynamics**: In this rule, instead of flipping a single spin, two spins are selected, and their positions are swapped. Again, the energy change ΔE due to the exchange is calculated, and a random number p is compared with $e^{-\frac{\Delta E}{k_B T}}$. If it is higher than p, the swap is accepted, otherwise is rejected.

The main difference between Glauber dynamics is that Glauber dynamics is a **non-conservative** process, as flipping a spin does not preserve the total magnetization $M = \sum_i S_i$. In contrast, Kawasaki dynamics is **conservative** since swapping the positions of two spins leaves the total magnetization M unchanged. For the purposes of this discussion, we will focus on studying non-conservative dynamics. However, a similar approach can be applied to conservative dynamics, and we will briefly address this at the end of the section.
Since our goal is to derive an equation that captures the system's dynamics, it is reasonable to require that the system tends to minimize its free energy over time. Additionally, as mentioned earlier, we are focusing on non-conservative dynamics. To find an equation that meets both of these criteria, let's consider the prototype equation for a strongly dissipative (over-damped) system. In such systems, the dynamics is non-conservative in the sense that energy is not conserved over time

$$\dot{x} = -\frac{1}{\gamma}\frac{dV}{dx} \tag{1.3.1}$$

where x represent the state variable, such as the position of an oscillator. The prototype equation we consider is essentially Newton's equation of motion, but with the inertial term ($\ddot{x}$) neglected due to the system being over-damped. To model our system, we can naively replace the state variable x with the order parameter $m(\mathbf{x})$ and the potential energy $V(x)$ with the free energy functional $F[m(\mathbf{x})]$.Then, since

we are no longer dealing with a state that is a scalar x, but rather with a function $m(\mathbf{x})$, the ordinary derivative is replaced by a functional derivative with respect to the order parameter $m(\mathbf{x})$.

$$\partial_t m = -\frac{\delta F}{\delta m} \tag{1.3.2}$$

This equation was constructed under the condition that the dynamics is not conservative, but does it satisfy the other condition? Does this equation describe a dynamics in which the free energy F decreases with time?

$$\frac{dF}{dt} = \int \frac{\delta F}{\delta m(\mathbf{x})} \frac{\partial m(\mathbf{x}, t)}{\partial t} d\mathbf{x}$$

Substituting the expression for $\frac{\partial m(\mathbf{x},t)}{\partial t}$ from the dynamics equation 1.3.2

$$\frac{dF}{dt} = -\int (\frac{\delta F}{\delta m(\mathbf{x})})^2 < 0$$

This means that (Eq. 1.3.2) describes a dynamics where the free energy F is monotonically decreasing, as required. Now that we have an equation for the dynamics, it's possible to replace the free energy F with the expression obtained in the previous chapter. The following equation will be the subject of the following chapters: the **Time Dependent Ginzburg Landau Equation (TDGL)**, also known as the Cahn-Allen equation.

$$\partial_t m = \Delta m + C(t)m - m^3 \tag{1.3.3}$$

where $C(t) \propto (T(t) - T_C)$ is a control parameter, because we can change it by changing the temperature T. And if you can vary temperature over time, then the control parameter is time dependent $C = C(t)$.
Before proceeding, it is important to note that a similar equation can be derived by imposing that the dynamics is conservative. By placing a symbol Δ in front of the right-hand side of the Time-Dependent Ginzburg-Landau (TDGL) equation (Eq. 1.3.3), you obtain an equation of the form:

$$\partial_t m = -\Delta J$$

where

$$J = \Delta m + C(t)m - m^3$$

This equation is a continuity equation. It follows directly that $\int m(\mathbf{x})\, d\mathbf{x}$ is a conserved quantity, indicating that the dynamics is conservative. This equation is known in the literature as the *Cahn-Hilliard* equation. However, our focus will remain on the Cahn-Allen equation. In the following section, the state of the art of the TDGL equation is presented. This equation has been intensively studied in the regime where the control parameter has no time dependence. However, there is not much information in the literature about how this dynamics is affected by a time-dependent $C(t)$. And this will be the topic of the next chapters.

Chapter 2

The Time Dependent Ginzburg-Landau equation (TDGL)

In this chapter, we will focus on the dynamics described by the TDGL equation

$$\partial_t m = \Delta m + Cm - m^3$$

in the well-studied regime where the control parameter C is **positive** and **fixed in time**. This condition corresponds to keeping the system's temperature constant and below the critical value.
If the initial state is a small perturbation of zero, as in Figure 2.1, the initial dynamics will be essentially different than the asymptotic (in time) dynamics. At the beginning, only the linear part of the TDGL equation is significant, leading to a straightforward evolution: Fourier modes with large wavelengths grow exponentially fast, while those with short wavelengths decay. This phenomenon is referred to as *linear instability* and we will refer to the initial dynamics as **linear dynamics**. As the perturbation grows and is no longer small, the non-linear terms in the equation become important, and the dynamics become more complex and no longer trivial. While the (*initial*) linear dynamics is essentially the same in any dimension, the (*asymptotic*) **non-linear dynamics**, differs significantly between 1D and 2D ($\mathbf{x} \in \mathcal{R}$ and $\mathbf{x} \in \mathcal{R}^2$).
We will start by discussing the dynamics in 1D. After the initial linear instability, the real axis becomes divided into intervals where the order parameter $m(\mathbf{x})$ is nearly constant (Figure 2.3). If $m(\mathbf{x}) = +\sqrt{C}$ in one interval, it will be $m(\mathbf{x}) = -\sqrt{C}$ in the neighbouring intervals, with smooth variations between $-\sqrt{C}$ and $+\sqrt{C}$ occurring at the extremes of each interval. We will refer to these intervals as *domains* and the regions between neighboring domains as *kinks*. We will calculate the shape of an isolated kink (Eq. 2.2.9) and we'll see that neighboring kinks (Figure 2.5) attract each other, until they meet and disappear together (*annihilation*). This reduces the number of domains, leading to an asymptotic dynamics where the size of the grows in time, a phenomena known in the literature as *coarsening*. In 1D, the size of the domains increases very slowly, specifically as the logarithm of time. So we can consider the size of the domains effectively frozen.

In 2D instead, the interfaces between two domains are curves in the plane, so there is the concept of *curvature*, absent in a 1D system. As a consequence, during the asymptotic dynamics there is a different leading mechanism for the growth of domain sizes: *motion by curvature*. In this mechanism, each point on the interface between two domains moves with a velocity that is normal to the interface and proportional to the local curvature of the interface $\kappa = \frac{1}{R}$, where R is the radius of the circle tangent to the interface at that point. As a result of this mechanism, the size of the domains increases much more rapidly in 2D compared to 1D, as a power law of time $t^{\frac{1}{2}}$.
This chapter is intended to present the state of the art about the study of the TDGL equation. More detailed information can be found in the books [4] and [5].

2.1 Linear instability

Let's consider the TDGL equation (Eq. 1.3.3) with a parameter C that is constant over time and positive. We start with an initial state consisting of a small perturbation from zero, as illustrated in Figure 2.1a. The initial condition is given by:

$$m(x, t = 0) = \delta m(x) \quad \text{where} \quad \delta m(x) \ll 1 \quad \forall x$$

Since this perturbation is small and will remain small at least during the initial

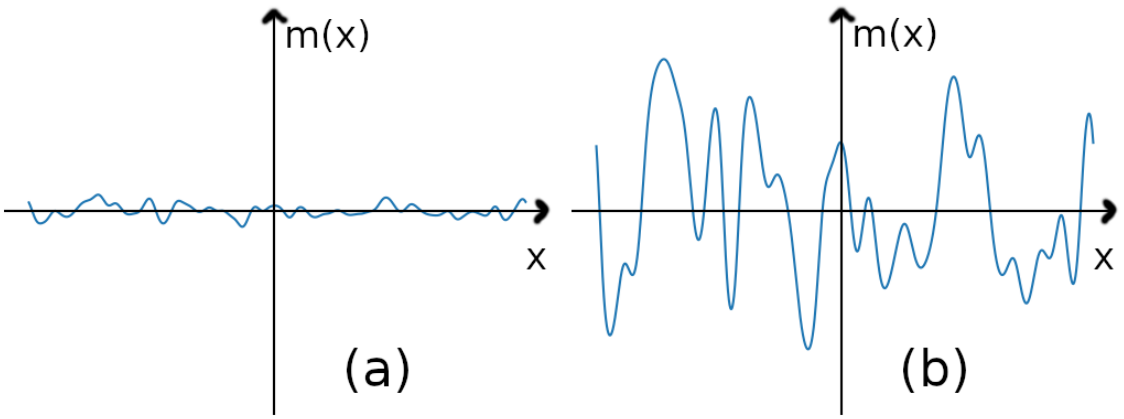

Figure 2.1: (a) The initial state $\delta m(x)$: a small perturbation of zero. (b) The state $m(x)$ after some time is passed. The perturbation is grown due to the growth of the large-wavelength modes.

stages of the dynamics, the non-linear term m^3 can be neglected compared to the linear term Cm. Therefore, the TDGL equation can be approximated with a linear differential equation

$$\partial_t m = \Delta m + Cm = (\Delta + C)m \tag{2.1.1}$$

By performing a Fourier transform in space, it is possible to eliminate the spatial derivative term

$$\partial_t M = (-q^2 + C)M \tag{2.1.2}$$

where q is the conjugate variable of the position x and $M(q)$ is the Fourier transform of $m(x)$ or the amplitude of the Fourier mode with momentum q, as

$$m(x) = \frac{1}{\sqrt{2\pi}} \int M(q) e^{iqx}$$

The Eq. 2.1.2 is solved by

$$M(q,t) = M(q,0) e^{(C-q^2)t} \tag{2.1.3}$$

and in Figure 2.2 is represented the growth rate of the exponent $C - q^2$ as a function of q. When the function $C - q^2$ is positive, the amplitude of the Fourier mode with

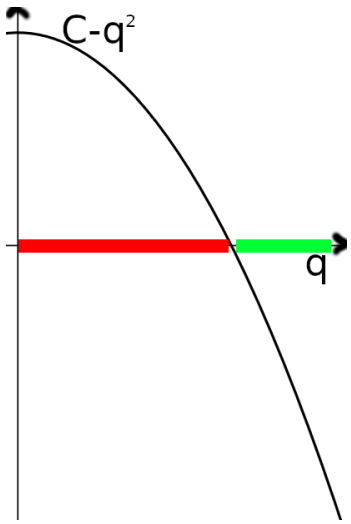

Figure 2.2: The function $C - q^2$ is the growth rate of the Fourier mode with momentum q. The red line represents the unstable modes, that are the ones whose amplitude grows exponentially fast in time. While the green line represents the stable ones, that are the ones which decay to zero. The wavelenght of a mode with momentum q is $\lambda_q = \frac{2\pi}{q}$.

momentum q grows exponentially in time. Conversely, when the function is negative, the amplitude of the corresponding Fourier mode decays to zero. As shown in Figure 2.2, it is evident that the growing Fourier modes are those with small momentum q, which correspond to large wavelengths $\lambda = \frac{2\pi}{q}$. In contrast, the short-wavelength modes with higher q values will decay.
As the large-wavelength modes grow, the amplitude of the perturbation $\delta m(x)$ increases, as shown in Figure 2.1. This phenomenon is referred to as **linear instability** because it is governed by the linear part of the equation, which causes an initially small perturbation to amplify over time. However, once the amplitude of the perturbation becomes significant, the non-linear part of the TDGL equation can no longer be ignored. At this point, the non-linear effects start to play a crucial role, making the system's behavior more complex.
In the following section, we will explore the dynamics that occur after the initial instability. However, it is worth noting that we have not specified the dimensionality of the problem up to this point. This was intentional, because the linear dynamics are consistent across all dimensions, whether the spatial coordinate x parameterizes a line (1D) or a plane (2D).

2.2 Non-linear dynamics

Once the amplitude of the long-wavelenght modes grows enough, the non linear part of the TDGL equation becomes relevant for the dynamics. To study the non-linear dynamics, let's start considering the TDGL equation without the Δm term

$$\partial_t m = Cm - m^3 \tag{2.2.1}$$

this equation does not contain space derivatives. This means that the value of $m(x)$ at a future time depends only on its actual value and not on the values of $m(x')$ with $x' \neq x$.
The Eq. 2.2.1 states that, at each point x of the space, coexist two competitive effects. The linear term $+Cm$ pushes $m \to \pm\infty$, depending on the sign of m, as $C > 0$. While the cubic term $-m^3$ pushes $m \to 0$ due to the minus sign. This competition reaches an equilibrium value that is determined by requiring their strength is the same

$$Cm_{eq} = m_{eq}^3 \implies m_{eq} = \pm\sqrt{C}$$

The consequence is that a state like the one in Figure 2.3a is eventually reached. Regions of the space where $m = \sqrt{C}$ and $m = -\sqrt{C}$ alternate and we call them *domains*.

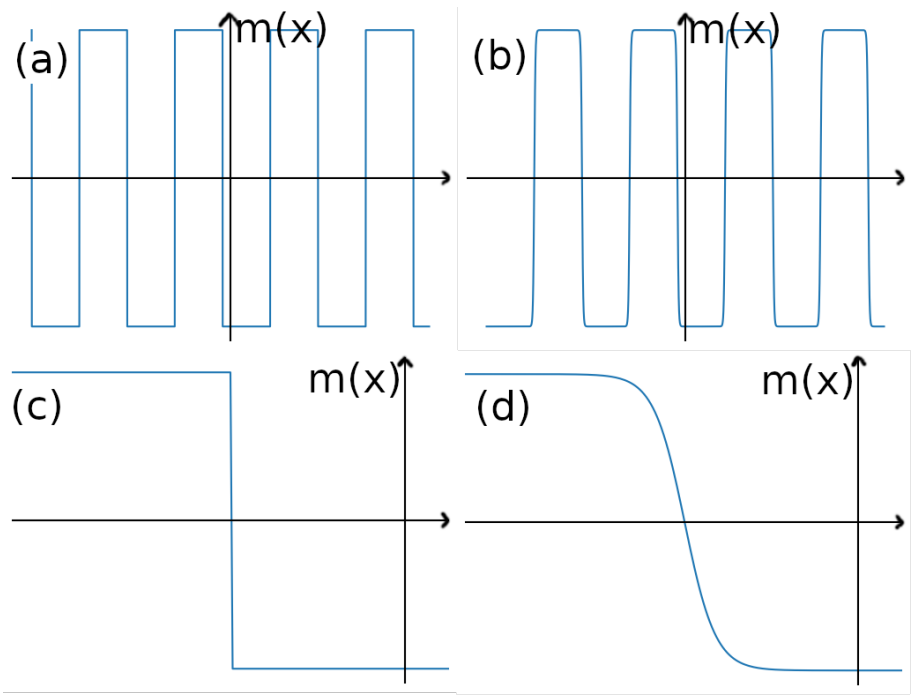

Figure 2.3: (a) Simulation of the 1D TDGL equation without space derivatives (Eq. 2.2.1), for a time sufficiently large to see the kinks. The initial state is a small perturbation of zero $\delta m(x) = \epsilon \sin\left(2\pi \frac{x}{\lambda}\right)$ where $\epsilon = 0.1$, $\lambda \simeq 4$ and $C = 1$. (b) Here the term Δm (Eq. 2.2.2) is included in the equation and the initial condition is the same of (a). (c) and (d) show a magnified view respectively of the kinks in the figures (a) and (b).

At this point we put back in the equation the term with the space derivatives (Δm). As we will see that the non-linear dynamics is essentially different in 1D and 2D, we will threat separately the two cases.
We start by studying the **1D** case, where $\Delta m = \partial_{xx} m$.

$$\partial_t m = \partial_{xx} m + Cm - m^3 \tag{2.2.2}$$

By including this term, the sharp interfaces between two neighbouring domains get smothered, as shown in Figure 2.3b. We call these interfaces between domains *kinks* if $m(x)$ increases or *anti-kink* if it decreases. But what is the shape of a kink?

2.2.1 Stationary states

To study the shape of the kinks, we look for the stationary states of Eq. 2.2.2. So we require that $\partial_t m = 0 \quad \forall x$, that means

$$\partial_{xx} m = -Cm + m^3 \tag{2.2.3}$$

The last equation can be written in the fashion of the Newton equation for a dot particle. In fact, if m is intended as the position of the particle and x as the time coordinate, Eq. 2.2.3 becomes

$$\partial_{xx} m = -\frac{dV}{dm} \tag{2.2.4}$$

where

$$V(m) = \frac{1}{2} C m^2 - \frac{1}{4} m^4$$

is the potential where the dot particle is moving, without experiencing any friction.

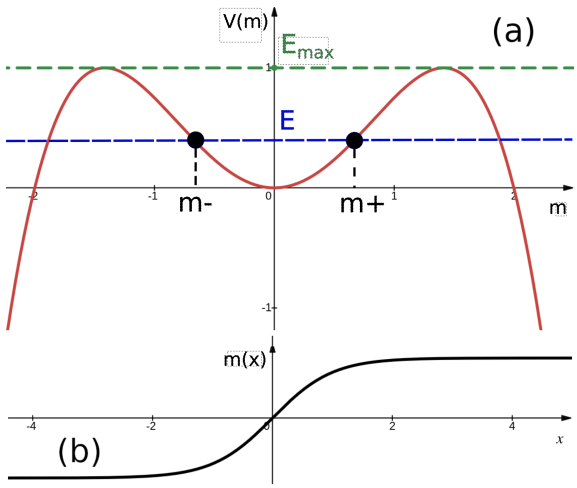

Figure 2.4: (a) Potential in which the particle is moving, with C=1. $E_{\max}$ is maximum value of the Energy for a bounded trajectory. (b) Trajectory with energy $E_{\max}$ (x is the time variable).

Thanks to this *analogy*, we can find the stationary states of Eq. 2.2.3 by looking for the possible trajectories $m(x)$ of the dot particle. We're interested only in the

bounded trajectories, as the stationary states of Eq. 2.2.3 are limited in the interval $m \in [-\sqrt{C}, +\sqrt{C}]$ due to the competition cited before. The bounded trajectories have energy $E \in [0, E_{\max}]$ where $E_{\max} = V(\pm\sqrt{C})$ (Figure 2.4a). And we can find the shape of those trajectories exploiting the fact that the energy of the dot particle is

$$E = \frac{1}{2}(\frac{dm}{dx})^2 + V(m) \tag{2.2.5}$$

and so

$$\frac{dm}{dx} = \sqrt{2(E - V(m))} \implies dx = \frac{dm}{\sqrt{2(E - V(m))}} \tag{2.2.6}$$

Integrating Eq. 2.2.6 it is possible to obtain the trajectory $m(x)$ with energy E, by inverting the equation

$$x = \int_{m(0)}^{m(x)} \frac{dm'}{\sqrt{2(E - V(m'))}} \tag{2.2.7}$$

From the shape of $V(m)$, we can state that those trajectories are periodic ($m(x + T) = m(x)$) with period

$$T(E) = 2\int_{m_-}^{m_+} \frac{1}{\sqrt{2(E - V(m'))}} dm' \quad m_\pm = \pm V^{-1}(E)$$

that increases and approaches infinite if $E \to E_{\max}$ (Figure 2.4b). In general, special functions are needed to express the integral of Eq. 2.2.7. However, for the trajectory with Energy $E = E_{\max}$ it is possible to solve the integral as

$$(E_{\max} - V(m') = V(\pm\sqrt{C}) - V(m') = \frac{1}{4}C^2 - \frac{1}{2}Cm'^2 + \frac{1}{4}m'^4 = \frac{1}{4}(m'^2 - C)^2$$

This means that

$$x = \int_{m(0)}^{m(x)} \frac{dm'}{\sqrt{2}\frac{1}{2}(C - m'^2)} \tag{2.2.8}$$

where $(C - m'^2) > 0 \quad \forall m'$ as $m' \in [-\sqrt{C}, +\sqrt{C}]$. By making a substitution $\tilde{m} = \frac{m'}{\sqrt{C}}$ and recognizing that $\frac{d}{dy}\text{arctanh}(x) = \frac{1}{1-y^2}$ it follows that

$$x = \sqrt{\frac{2}{C}}[\text{arctanh}(\frac{m(x)}{\sqrt{C}}) - \text{arctanh}(\frac{m(0)}{\sqrt{C}})]$$

and by defininining the time $x = 0$ as the one when $m(0) = 0$ we can conclude that the trajectory with energy $E = E_{\max}$ is the one shown in Figure 2.4b

$$m(x) = \sqrt{C}\tanh\left(\sqrt{\frac{C}{2}}x\right) \tag{2.2.9}$$

This stationary state contains only one kink. However, if you consider a state like the one in Figure 2.3b, it is reasonable to expect that if the kinks a more far apart than their spatial extension (so if they do not overlap) then their shape is well approximated by Eq. 2.2.8.

2.2.2 Coarsening

We determined the shape of a kink in Eq. 2.2.9. Now we will see that there is a weak *attractive interaction* between a kink and the neighbouring anti-kink. This attraction reduces the distance between the two, until they meet and *annihilate*. Due to this interaction, every stationary state, except the one with $E = E_{\max}$, is unstable. In addition, this attraction determines the (slow) growth in time of the domains size, where the typical size of a domain increases as $L \sim \log t$.
In order to see the cited behaviours, let's consider an initial state where a kink and an anti-kink are located at positions $\pm R$, as represented in Figure (2.5). Then we assume that the evolution of the state due to the TDGL equation doesn't change the shape of the state, but just affects the kink's positions so $R = R(t)$.

$$m(x,t) = \sqrt{C}\tanh\left((x - R(t))\sqrt{\frac{C}{2}}\right) - \sqrt{C}\tanh\left((x + R(t))\sqrt{\frac{C}{2}}\right) + \sqrt{C} \quad (2.2.10)$$

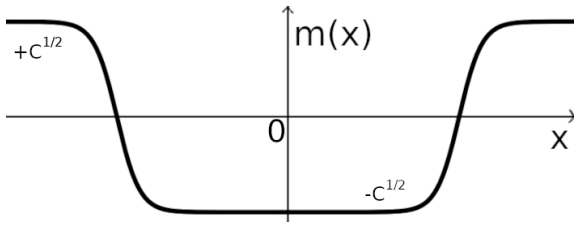

Figure 2.5: State with a neighbouring couple of kink and anti-kink, located respectively at $x = +R$ and $x = -R$.

Immediately, it's possible to notice that

$$\partial_t m = \sqrt{C}\tanh'((x - R(t))\sqrt{\frac{C}{2}})(-\dot{R}) - \sqrt{C}\tanh'((x + R(t))\sqrt{\frac{C}{2}})(+\dot{R})$$

and recognizing that $\tanh'((x \pm R)\sqrt{\frac{C}{2}}) = \partial_x[\tanh\Big((x \pm R(t))\sqrt{\frac{C}{2}}\Big)]$

$$\partial_t m = -\dot{R}\partial_x m \quad (2.2.11)$$

Using this property in the TDGL equation, it follows that

$$-\dot{R(t)}\partial_x m = \partial_{xx} m - V'(m) \qquad V(m) = -\frac{1}{2}Cm^2 + \frac{1}{4}m^4 \quad (2.2.12)$$

By integrating the last equation, as shown in details in Appendix B, it's found that at leading order in $R >> C^{-\frac{1}{2}}$ (that means the kink and the anti-kink are far from each other)

$$\dot{R}(t) = -\alpha e^{-\beta R(t)} \quad (2.2.13)$$

where $\alpha, \beta > 0$ and they both do not depend on time. The last equation can be solved by separating the variables R and t at each member

$$e^{\beta R} dR = -\alpha dt$$

and integrating both sides leads to

$$e^{\beta R(t)} - e^{\beta R(0)} = -\alpha t \tag{2.2.14}$$

Once $R(t) \to 0$, then the size of the central domain $2R \to 0$ and it means that the kink and the anti-kink disappear simultaneously: this is known in physics as **annihilation**. So the time it takes for the couple to annihilate, can be calculated requiring that $R(t) = 0$

$$\tau_{annhilation} = \frac{1}{\alpha}(e^{\beta R(0)} - 1) \sim e^{\beta R(0)} \tag{2.2.15}$$

The time needed for a couple of neighbouring kink and anti-kink to annhilate grows exponentially with their distance. Due to this mechanism, some domains disappear and so the others grow as an effect of the fixed size of the system. The increase of the typical size of domains as time passes is known as **coarsening** in the literature. Even if the state is less-trivial than Eq. 2.2.10, so if there are many domains, their typical size ℓ grows very slowly in time as a consequence of the long annhilation times

$$\ell(t) \sim \log t \tag{2.2.16}$$

Unfortunately, it is difficult to check numerically that the domain size grows respecting this law. The reason is that a logarithmic growth is very slow and so a very long computational time is needed to verify this law.

2.3 The 2D dynamics

In the previous section, we examined the dynamics governed by the 1D Time-Dependent Ginzburg-Landau (TDGL) equation, focusing on solutions along a single spatial dimension $x \in \mathcal{R}$. Now, we turn our attention to the **2D** TDGL equation, where the spatial coordinate $\mathbf{x}$ describes a point in a plane $(x, y) \in \mathcal{R}^2$. The TDGL equation for this two-dimensional case is:

$$\partial_t m = \Delta m + Cm - m^3 \quad \text{where} \quad \Delta = \partial_{xx} + \partial_{yy} \tag{2.3.1}$$

Just as in the 1D case, if the initial state is a small perturbation of zero, there is a linear instability that determines the initial dynamics. This instability leads to the formation of domains, where $m(x, y) = \pm\sqrt{C}$ (Figure 2.6). The interfaces between these domains are now curves in the (x, y) plane, and along a line perpendicular to an interface, the shape resembles that of the 1D kink solutions up to leading order. The key difference in 2D lies in the dynamics of these interfaces, determined by the non-linear part of the equation. Specifically, the interfaces evolve according to a mechanism known as *motion by curvature*. In this context, each point on an interface moves with a velocity perpendicular to the interface and proportional to the local curvature. This mechanism leads to coarsening dynamics, where the characteristic size of domains ℓ grows as a power law of time, $\ell(t) \sim t^{\frac{1}{2}}$, independently on the value of C. This growth is significantly faster than in the 1D case, where the domain sizes could be considered effectively frozen after the linear dynamics.

Figure 2.6: On the left: Simulation of the 2D TDGL equation (Eq. 2.3.1) until a long time after the initial linear instability, such that we can study the asymptotic dynamics, when domains are already formed. White regions represent domains where $m(x, y) = -\sqrt{C}$, while in the blue regions $m(x, y) = +\sqrt{C}$. On the right: Zoom of a region of the interface between two neighbouring domains.

As an example, we will show simulations of the 2D TDGL equation with an initial state comprising an *isolated circular domain*. We will see that the domain shrinks in time with the speed predicted by motion by curvature. We will also make use of simulations to compare the speed of coarsening dynamics between the 1D and 2D cases, highlighting the essential differences in domain growth rates.

2.3.1 The new leading mechanism for the dynamics: motion by curvature

In the following section, we will demonstrate that the dynamics of an interface is primarily governed by its curvature. To achieve this, we will first introduce a new coordinate system $(x, y) \to (\xi, s)$ that is more naturally suited for describing the dynamics of the interface.
After establishing the new coordinate system, we will make some empirical observations about the asymptotic dynamics of the system. These observations will be used as assumptions, forming the basis for our proof that the interface motion is driven by curvature.

A new coordinate system

We can formally define an **interface** as a curve in the plane where the order parameter $m(x, y)$ is constant and equal to zero (Figure 2.7a). This curve represents the boundary between two neighbouring domains, where $m(x, y)$ takes on different values: $\pm\sqrt{C}$. To describe the dynamics of the interface, we'll switch from Cartesian coordinates (x, y) to a more natural coordinate system (ξ, s) relative to the interface. In this new coordinate system:

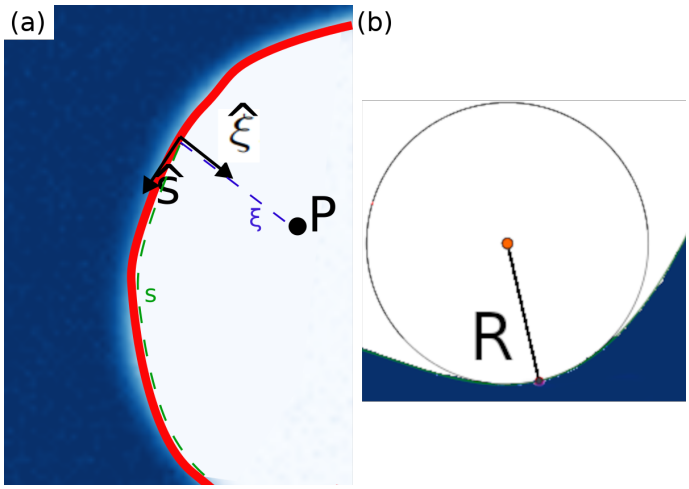

Figure 2.7: (a) Interface between two domains (Figure 2.6). In red is highlighted the interface between two domains, that is the curve where $m(x, y) = 0$. The position of the point P is described by its distance from the interface ξ (in blue) and the position of its projection along the interface s (in green). (b) Circle tangent to the interface at a point P. If R is its radius, then $\kappa = R^{-1}$ is the curvature of the interface at the point P.

- ξ represents the distance of the point P from the interface along the direction normal to the interface.
- s represents the position of the projection of the point P onto the interface. Equivalently, if you take the curve of points with an equal distance $\xi = \bar{\xi}$ from the interface, then s is the coordinate distinguishing the point in this curve.

Since the interface is a curve within the plane, we can define the local **curvature** κ at any given point along the interface. The *modulus* of the curvature κ is mathematically defined as:

$$|\kappa| = \frac{1}{R}$$

Here, R represents the radius of the osculating circle that is tangent to the interface at that specific point, as shown in Figure 2.7b. The modulus $|\kappa|$ quantifies the degree of bending of the interface: a larger curvature indicates a sharper bend (smaller R), while a smaller curvature indicates a more gradual bend or even a flat region (larger R). In 2D, the curvature has a *sign*. Since the unit vector $\hat{\xi}$ must vary smoothly along the interface, it cannot be defined as pointing toward the center of the tangent circle at every point of the interface. Consequently, $\hat{\xi}$ may point either toward the center of the tangent circle or in the opposite direction, resulting in the curvature κ being either negative or positive, as shown in Figure 2.8.

Motion by curvature

During the asymptotic dynamics, simulations show that the curvature of the interfaces is small compared to the *thickness of the interface*, defined as the length of the

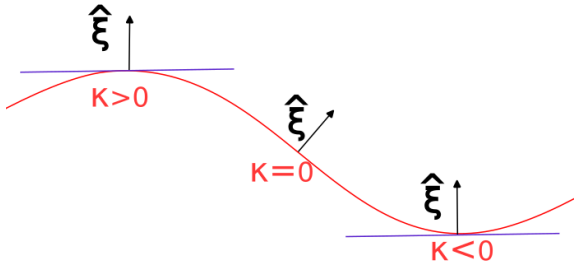

Figure 2.8: The interface (shown in red) is a curve that divides the plane into two regions. At any point along the interface, we can draw a tangent line (shown in blue) and define the "exterior" of the curve as the region where the tangent lies, with the "interior" being the opposite region. Since the unit vector $\hat{\xi}$ can point either toward the interior or exterior, we can introduce the concept of the *sign* of the curvature. We define the curvature as $\kappa > 0$ when $\hat{\xi}$ points toward the exterior of the curve and $\kappa < 0$ when it points toward the interior. At points where the curve is flat (to leading order), this distinction is not possible, consistently with the fact that $|\kappa| = 0$ at such points.

region where $\partial_\xi m$ is significantly different from zero. Additionally, the curvature changes gradually along the interface (as illustrated in Figure 2.6).
The aim of this section is to formalize these empirical observations into assumptions and to prove that the dynamics of the interface is predominantly governed by its curvature, through a mechanism known as **motion by curvature**.
As the existence of the concept of curvature distinguishes the 2D case from the 1D one, we expect that if the curvature is small, the system will exhibit properties similar to those discussed for a 1D system. Specifically, along the direction $\hat{\xi}$, which is orthogonal to the interface, the shape of the interface should resemble that of the 1D kink solutions. This implies that if we consider the curve of points characterized by the same $\xi = \bar{\xi}$ (a curve of points at the same distance from the interface), it will be well approximated by a curve where m is constant. Consequently, m will vary slowly with respect to s. Additionally, since the length of a 1D kink is approximately $\sim C^{-\frac{1}{2}}$, choosing $\mathbf{C} \sim \mathbf{1}$ leads us to conclude that the thickness of the 2D interfaces is also of order ~ 1.
As a consequence of the previous considerations, we can formalize our assumptions as

- κ is small compared with the interface width (~ 1)

$$\kappa = \epsilon_1 K_1 \quad \text{where: } K_1 \sim 1; \quad \epsilon_1 << 1 \tag{2.3.2}$$

- $m(\xi, s)$ depends slowly on s

$$\delta m \sim \epsilon_2 \quad \text{if } \delta_s \sim 1 \quad \text{where: } \epsilon_2 << 1$$

while

$$\delta_m \sim 1 \quad \text{if } \delta\xi \sim 1$$

that can be re-stated as

$$\partial_s m = \epsilon_2 \partial_\xi m \tag{2.3.3}$$

In addition to assumptions 2.3.2 and 2.3.3, we assume that the shape of the interface remains constant during the time it takes for the interface to propagate over a distance of order 1, which is the order of magnitude of the thickness of the interface. Furthermore, we assume the speed v of the interface to be slow, meaning that a considerable amount of time is required for the interface to traverse a length of order 1. Formalizing the last assumptions, we find the properties

$$m(\xi, s, t) = m(\xi - vt, s, 0) \implies \partial_t m = -v\partial_\xi m \tag{2.3.4}$$

$$v = \epsilon_3 V_1 \quad \text{where: } V_1 \sim 1, \epsilon_3 << 1 \tag{2.3.5}$$

Before employing the stated assumptions to demonstrate that curvature drives the dynamics of the interfaces, we notice that we introduced the presence of three *different* small parameters, denoted as ϵ_i. To simplify our analysis, we can invoke an additional assumption known in the literature as the **scaling hypothesis**. This means assuming that all large-scale features of the system are characterized by the same length scale ℓ. This implies that these features are of the same order, leading to the relationship:

$$\epsilon_1 = \epsilon_2 = \epsilon_3 = \epsilon$$

It is important to note that this holds true only for large-scale features, as there is clearly another scale present in the system: the thickness of the interface, which is a short-scale feature.
We're finally able to use the stated assumptions 2.3.2, 2.3.3, 2.3.4 and 2.3.5 in the TDGL equation, along with the expression for Δ in the coordinates (ξ, s), that is calculated in Appendix D

$$\Delta = \frac{\kappa}{1+\xi\kappa}\partial_\xi + \partial_{\xi\xi} + \frac{1}{1+\xi\kappa}\partial_s\left(\frac{1}{1+\xi\kappa}\partial_s\right)$$

By using the assumptions 2.3.2 and 2.3.3, up to leading order in ϵ

$$\Delta = \partial_{\xi\xi} + \epsilon K_1 \partial_\xi + O(\epsilon^2) \tag{2.3.6}$$

Recalling the TDGL equation

$$\partial_t m = \Delta m + Cm - m^3$$

and using 2.3.4, 2.3.5 and 2.3.6, we find at leading order in ϵ

$$-\epsilon V_1 \partial_\xi m = \partial_{\xi\xi} m + \epsilon K_1 \partial_\xi m + Cm - m^3 \tag{2.3.7}$$

Then it is natural to expand also the order parameter in powers of ϵ

$$m = m_0 + \epsilon m_1 + O(\epsilon^2)$$

Equating the terms of order zero (ϵ^0), we find

$$\partial_{\xi\xi} + Cm_0 - m_0^3 = 0 \tag{2.3.8}$$

that is the Eq. 2.2.3 where $x \to \xi$, so we already know the solution

$$m_0(\xi, t) = C(t)^{\frac{1}{2}} \tanh\Big(\xi C(t)^{\frac{1}{2}} 2^{-\frac{1}{2}}\Big)$$

Up to order zero, the shape of the interface along the direction $\hat{\xi}$ is the same of a 1D kink (Eq. 2.2.9). While equating the terms of order ϵ, we find a less trivial result

$$(\partial_{\xi\xi} + C - 3m_0^2)m_1 = -(V_1 + K_1)\partial_\xi m_0 \tag{2.3.9}$$

We could not figure out how to solve this equation for m_1. However it's possible to use a theorem known as the *Fredholm alternative* (and proved in Appendix E) to find a relation between the parameters of the equation (C, V_1, K_1). The theorem states that, given a solution $u(\xi)$ of the in-homogeneous differential equation Eq. 2.3.9 and an homogeneous solution $v(\xi)$

$$\hat{L}u(\xi) = f(\xi)$$
$$\hat{L}v(\xi) = 0$$

where

$$\hat{L} = (\partial_{\xi\xi} + C - 3m_0^2)$$
$$f(\xi) = -(V_1 + K_1)\partial_\xi m_0$$

then

$$\int_{-\infty}^{+\infty} f(\xi)v(\xi)d\xi = [\partial_\xi uv - u\partial_\xi v]_{-\infty}^{+\infty} \tag{2.3.10}$$

We can use this mathematical theorem to retrieve some information from Eq. 2.3.9. The in-homogeneous solution is $u = m_1$ then, deriving Eq. 2.3.8 respect to ξ

$$\partial_{\xi\xi}(\partial_\xi m_0) + C\partial_\xi m_0 - 3m_0^2\partial_\xi m_0 = 0$$

so $v(\xi) = \partial_\xi m_0$ is an homogeneous solution ($\hat{L}u(\xi) = 0$) and we can apply the theorem 2.3.10

$$-(V_1 + K_1)\int_{-\infty}^{+\infty} (\partial_\xi m_0)^2 d\xi = 0$$

where in the last equation we assumed that the right side of Eq. 2.3.10 is zero. As the integral is non-zero, it means that

$$V_1 = -K_1$$

So an interface moves with a velocity orthogonal to itself and it's proportional to the curvature κ. This effect is called **motion by curvature**

$$v = \epsilon V_1 = -\epsilon K_1 = -\kappa \tag{2.3.11}$$

The dynamics of an interface is, up to leading order in ϵ, governed by the curvature κ and the velocity v does not depend on the parameter C.
This result is consistent with the fact that v represents the velocity at which the interface propagates along the direction of $\hat{\xi}$. Indeed, $\hat{\xi}$ can point either inward or outward relative to the interface, but in both cases, the sign of the curvature changes accordingly, ensuring that the velocity always points toward the interior of the curve.

Figure 2.9: Schematic for the dynamics of the interfaces in 2D. The interface moves with a velocity $v = -\kappa$ where κ is the local curvature (Fig. 2.7b).

Example: isolated circular domain

The simplest way for verifying that motion by curvature (Eq. 2.3.11) is the leading mechanism of the dynamics, is studying a simulation of the 2D TDGL equation considering as the initial state an isolated circular domain of radius R_0 (Figure 2.10).
The initial state is set up as follows:

$$m(t=0) = \sqrt{C}\tanh\left(\sqrt{\frac{C}{2}}(r - R_0)\right)$$

where

$$r = \sqrt{x^2 + y^2}.$$

To measure the radius as a function of time $R(t)$, we calculate the average of the radial coordinate r weighted by the squared gradient of the order parameter $|\nabla m|^2$:

$$R^2(t) = \frac{\int r^2 |\nabla m|^2 \, dx\, dy}{\int |\nabla m|^2 \, dx\, dy}.$$

This method is expected to provide a good estimate of the radius of the circular island since $|\nabla m|^2$ is sharply peaked at the interface and nearly zero elsewhere.
In the case of a circular interface, the curvature κ is the same at any point and $\kappa = \frac{1}{R}$, where R is the radius of the circular domain. This means that the velocity of the interface $v = \dot{R}$ satisfies

$$\dot{R} = -R^{-1}$$

and so

$$R^2(t) = R_0^2 - 2t \tag{2.3.12}$$

so the area of the domain ($2\pi R^2$) shrinks linearly in time, until it disappears. In Figure 2.10 this behaviour is verified in a simulation, confirming that motion by curvature is the leading mechanism determining the dynamics in a 2D system.

2.3.2 Coarsening

In 2D, the concept of curvature fundamentally alters the dynamics of the interfaces. However, similar to the 1D case, this curvature-driven dynamics leads to coarsening,

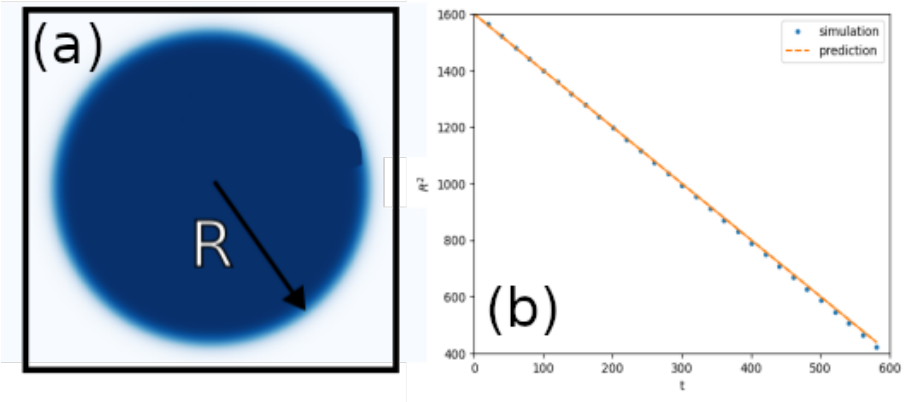

Figure 2.10: (a) Isolated circular domain with radius R. (b) Measure of $R^2(t)$ in a simulation of the 2D TDGL where the initial state is prepared as (a). $C = 0.5, R_0 = 40, L = 128, dt = 0.1$.

the size of the domains increases over time. In two dimensions, the coarsening process is significantly faster: the typical size of the domains scales with time as a power law, specifically $\ell \sim t^{\frac{1}{2}}$. In contrast, in 1D, the scaling is logarithmic, $\ell \sim \log t$, which results in domains that can be considered effectively frozen.
To demonstrate this result, we will employ a dimensional analysis, which is not applicable in the 1D case as it makes use of the motion by curvature $v = -\kappa$ relation. Dimensional $[v] = \frac{[L]}{[t]}$, where v is the interface velocity and $[L], [t]$ represent respectively a length and a time. Then motion by curvature tells that $v = -\kappa$ and $[\kappa] = \frac{1}{[L]}$. Together the relations tell that $1/L \sim L/t$ so

$$\ell(t) \sim t^{\frac{1}{2}} \tag{2.3.13}$$

where $\ell(t)$ is a length-scale describing the size of the domains.
To verify this coarsening law numerically, we need to define a measurable quantity that describes the typical size of the domains. The idea we propose is to consider the function $|\nabla m|^2$ as this function will be significantly different from zero only where there is an interface. In 1D, we can define this length-scale

$$\ell_{DW} = \frac{L}{\int (\partial_x m(x))^2 dx} \int (\partial_x m_0(x))^2 dx \tag{2.3.14}$$

where L is the size of the system (of the simulation box), while m_0 is the stationary state with only one kink, that is defined in Eq. 2.2.9. As the shape of the kinks is the same for each kink and it is defined by Eq. 2.2.9, then the ratio $N = \frac{\int (\partial_x m(x))^2 dx}{\int (\partial_x m_0(x))^2 dx}$ corresponds to the number of kinks. As a consequence, $\ell_{DW} = L/N$ is the average size of a 1D domain.
Then we can extend the definition of ℓ_{DW} to the 2D case

$$\ell_{DW} = \frac{L^2}{\int |\nabla m(x)|^2 dx dy} \int (\partial_x m_0(\xi))^2 d\xi \tag{2.3.15}$$

where we still consider ℓ_{DW} as a measure of the typical size of the domains.

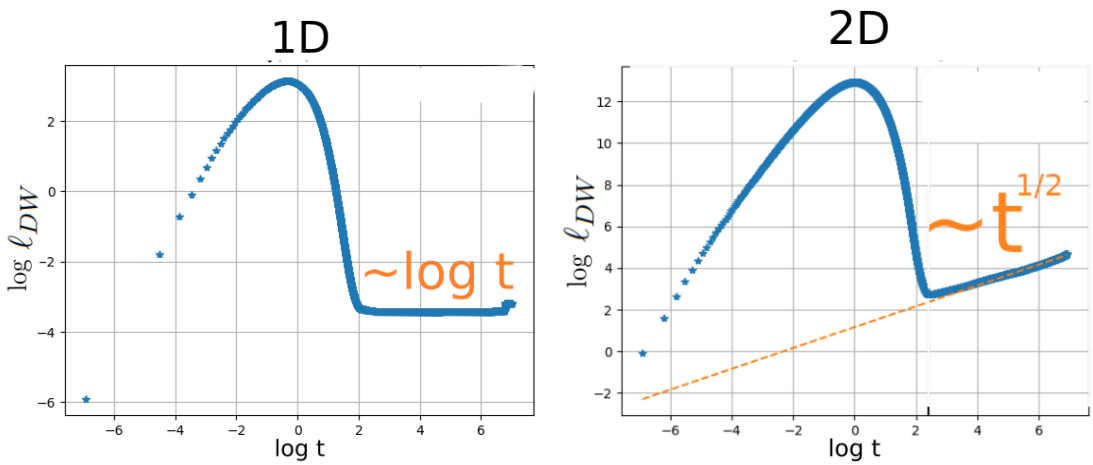

Figure 2.11: Simulations of the 1D and 2D TDGL equations, starting from an initial state that is a small perturbation of zero in both cases. The typical domain size, ℓ_{DW}, is measured as a function of time. The expected coarsening laws, $\ell_{1D} \sim \log t$ for the 1D case and $\ell_{2D} \sim t^{\frac{1}{2}}$ for the 2D case, are verified at long times in the log log scale plots. In the 1D simulation, we would need a much longer duration to observe the expected logarithmic relationship clearly. In shorter simulations, the size of the domains appears frozen. At very early times, domains have not yet formed, meaning that ℓ_{DW} does not accurately represent the size of the domains. During the linear dynamics, we used a time step of $dt = 0.001$ to precisely capture the domain formation process up to time $t = 8$. Following this, we switched to a larger time step of $dt = 0.1$ to simulate the slower coarsening dynamics.

In Figure 2.11 the coarsening laws for the 1D and the 2D cases are verified by simulating the 1D and the 2D TDGL equation for a long time and measuring $\ell_{DW}(t)$ as a function of time. The expected laws are verified only at long times, as at short times domains are not yet formed and so ℓ_{DW} is not a measure of the size of domains. Let's also notice that, as at long times the curvature of any interface is small, the shape of the interface along a perpendicular direction is well approximated by the 1D kink shape $m_0(\xi)$. As a consequence,

$$\int |\nabla m(x)|^2 dxdy \simeq \mathcal{L} \int (\partial_x m_0(\xi))^2 d\xi$$

where $\mathcal{L}$ is the sum of the lengths of all the interfaces. It follows that in 2D

$$\ell_{DW} = \frac{L^2}{\mathcal{L}}$$

meaning that the total length of the interfaces decreases in time, as ℓ_{DW} increases. And this is expected, as the number of domains decreases in time during coarsening dynamics.

Chapter 3

Controlling the linear dynamics

In the previous chapter, we described the dynamics of the Time-Dependent Ginzburg-Landau (TDGL) equation with a fixed, positive control parameter C. In the following chapters, we will explore the possibility of **controlling** the properties of the system's state, such as domain **size** and **position**, by varying the control parameter over time: $= C(t)$. Our analysis will be divided into two separate chapters, each focusing on one of the two distinct regimes of the dynamics. The first chapter will examine how the initial linear dynamics, during which domains are forming, is influenced by variations in $C(t)$. The second chapter will investigate the effects of $C(t)$ on the asymptotic dynamics, when domains coarsen.

In this chapter, we will present that the dynamics of the system is not influenced by the time variations of the control parameter C during the linear dynamics. If $C(t)$ is strictly positive, the dynamic is linear during the initial stages, when domains are forming. However, if $C(t)$ can be negative, the TDGL equation may still be approximated by a linear equation even long after $C(t)$ starts varying. While this chapter places no constraints on $C(t)$, the $C > 0$ case is extensively explored in later chapters, while the other case is under ongoing study (see Appendix H for some numerical results).

Our analysis will show that, during the linear regime, the characteristic length of the system $\ell(t) \sim t^{\frac{1}{2}}$, at any dimension and *independently* on the specific *shape of* $C(t)$. However, the duration of the linear regime can be controlled by the average value $\bar{C}$ around which $C(t)$ oscillates, such that $\tau_{\text{linear}} \sim \bar{C}$. This control over τ_{linear} allows us to influence the value of the characteristic length scale ℓ at the end of the linear regime. In 1D systems, where the subsequent coarsening dynamics is slow, the size of the domains formed during the linear phase can be considered effectively frozen. This enables the control of the 1D domain sizes during their formation. Conversely, in two-dimensional (2D) systems, domains growth cannot be neglected in the asymptotic regime, not giving the possibility of controlling domain sizes through the same mechanism.

3.1 Effects of a time dependent C on the formation of domains

Let's consider an initial condition that is a small and **random** perturbation of zero, this means that the amplitude of each Fourier component $M(\mathbf{q})$ is small and equal to each other

$$M(\mathbf{q},0)=\delta \quad \forall \mathbf{q} \qquad \text{where: } \delta << 1$$

In this case, the initial dynamics will be the ruled by the linear part of the TDGL and will lead to the formation of domains. In this section, we will show that the rules describing the dynamics in this regime are not affected by how $C(t)$ varies in time.
To do so, we define a characteristic length of the system ℓ that represents the typical size of the features appearing in the state of the system $m(\mathbf{x})$. To define ℓ, we follow the idea that the wave-length associated to each Fourier mode is $\lambda_{\mathbf{q}}=\frac{2\pi}{\sqrt{q^2}}$, where $\mathbf{q}$ is the momentum of the mode. Then we can define a typical wave-length of the system, by calculating the average

$$< q^2 >= \frac{\int q^2 |M(\mathbf{q})|^2 d\mathbf{q}}{D\int |M(\mathbf{q})|^2 d\mathbf{q}} \tag{3.1.1}$$

where $M(\mathbf{q})$ is the Fourier transform of the state $m(\mathbf{x})$, or equivalently the amplitude of the Fourier mode with momentum $\mathbf{q}$. While D is the dimension of the system. Then a typical wave-length of the system will be

$$\ell = \frac{2\pi}{\sqrt{< q^2 >}} \tag{3.1.2}$$

We say that ℓ is the typical size of the features of the state, as the presence of a feature of order λ is described by the amplitude of the Fourier mode with wave-length λ.
In the linear regime, the length ℓ increases in time as $\ell \sim t^{\frac{1}{2}}$, independently on the choice of the function $C(t)$. We can see this, noticing that in the linear regime

$$\partial_t M \simeq [-q^2 + C(t)]M$$

so it follows that

$$M(\mathbf{q},t) = M(\mathbf{q},0)e^{-q^2 t + \int_0^t C(t')dt'} \tag{3.1.3}$$

Using this property in the integral

$$< q^2 >= \frac{\int q^2 M(\mathbf{q},0)^2 e^{-2q^2 t} d\mathbf{q} * e^{2\int_0^t C(t')dt'}}{D\int M(\mathbf{q},0)^2 e^{-2q^2 t} d\mathbf{q} * e^{2\int_0^t C(t')dt'}} = \frac{\int q^2 M(\mathbf{q},0)^2 e^{-2q^2 t} d\mathbf{q}}{D\int M(\mathbf{q},0)^2 e^{-2q^2 t} d\mathbf{q}}$$

As the terms containing $C(t)$ got cancelled, it means that $< q^2 >$, and so ℓ, does not depend on the shape of $C(t)$. It is also possible to calculate explicitly the ratio between the integrals, exploiting that the initial state is a random perturbation of zero, so $M(\mathbf{q},0)=\delta \quad \forall \mathbf{q}$ and we can cancel the terms $M(\mathbf{q},0)$ out of the integral.

Then, we notice that if the system has a finite size L^D, Fourier modes that are larger than the system size are not available. So the integration must be restricted to the intervals

$$q_i \in [-q_{min}, +q_{min}]$$

where $q_{min} = \frac{2\pi}{L}$, so

$$< q^2 >= \frac{\int_{-q_{min}}^{+q_{min}} q^2 e^{-2q^2 t} d\mathbf{q}}{D \int_{-q_{min}}^{+q_{min}} e^{-2q^2 t} d\mathbf{q}} \tag{3.1.4}$$

In Appendix C an approximation of the integral is calculated, that is valid in the limit where $t >> \frac{1}{2} q_{min}^{-2}$, but not so large such that the dynamics is still governed by the linear part of the TDGL equation. So, during the initial dynamics, at **any dimension**, the characteristic lenght $\ell(t)$ evolves *independently on the shape of* $C(t)$ and according to the law

$$< q^2 > \simeq \frac{t^{-1}}{4} \implies \ell(t) = 4\pi t^{\frac{1}{2}} \tag{3.1.5}$$

However, even if the linear dynamics does not depend on the control parameter $C(t)$, the time it takes for the non-linear effects to become relevant (the duration of the linear regime) τ_{linear} depends on it. To estimate this characteristic time, we consider the fastest growing mode. As the *growth rate* of each Fourier mode is $-q^2 + \frac{1}{t}\int_0^t C(t')dt'$ (see Eq. 3.1.3), then the one with momentum $\mathbf{q} = \mathbf{0}$ is the one we consider

$$M(0,t) = M(0,0) e^{+\int_0^t C(t')dt'}$$

If we require $C(t)$ to be a *periodic oscillation* with period T and around the average value $\bar{C} = \frac{1}{T}\int_0^T C(t')dt'$, it follows that, if $t >> T$

$$M(0,t) \simeq M(0,0) e^{\bar{C}t}$$

and so the characteristic time for the growth of $M(0,t)$ is

$$\tau_{\text{linear}} \sim \bar{C}^{-1}$$

Inserting this result in Eq. (3.1.5) the typical size of the features of the system, at the end of the linear regime, is

$$\ell(\tau_{\text{linear}}) \sim 4\pi \bar{C}^{-\frac{1}{2}}$$

In a 1D system, it is possible to take advantage of this result, to control the typical size of the domains. In fact, during the asymptotic dynamics, the size of the domains is effectively frozen in a 1D, so the sizes they have at the end of the linear regime, do not change anymore, as shown in Figure 3.1.
In the same figure, one can see that a different choice of C (that is equal to $\bar{C}$ as $C(t)$ is kept constant in time) determines a different position for the peak of ℓ_{DW}. This behaviour is expected, as the position of the peak describes the duration of the linear regime $\tau_{\text{linear}} \sim C^{-1}$.

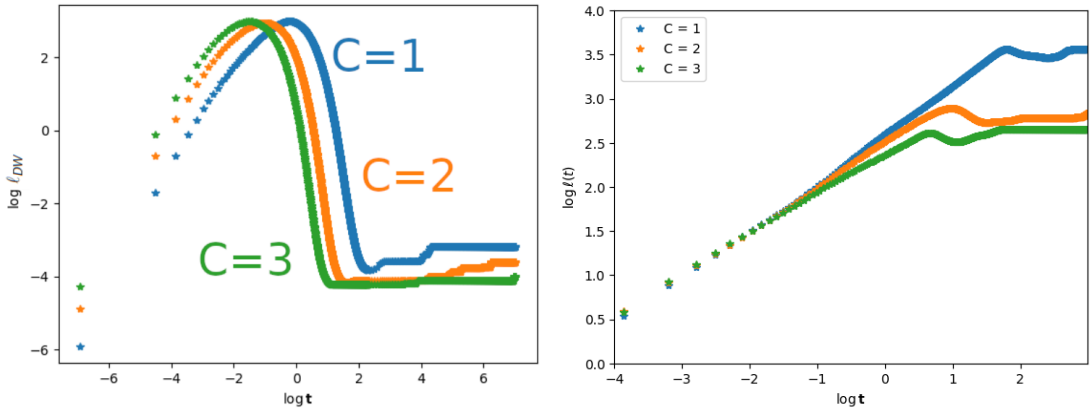

Figure 3.1: Evolution of the characteristic lenghts ℓ_{DW}(average domain size) and ℓ in a simulation of the 1D TDGL equation with different values of C (constant). The initial state is the same and it is a random perturbation of zero. In the asymptotic regime, λ_{DW} is about constant in time (precisely $\lambda_{DW} \sim \log t$, but a longer simulation is needed to see this time dependence) and takes different "final" values depending on the choice of C.

However, it is important to note that the characteristic length ℓ is not specifically defined to measure the average size of the domains. While $C(t)$ influences the typical size of the domains, this size will not necessarily correspond to $\ell(\tau_{\text{linear}})$.
In a 2D system, the characteristic size ℓ, along with the size of the domains (denoted as ℓ_{DW}), continues to increase even after the initial dynamics (as shown in Figure 3.2). This makes not possible to control the size of the domains.
It is worth to notice that, during the asymptotic dynamic, the quantities ℓ and ℓ_{DW} are not independent. In fact in Appendix G it is proved an equation linking the two.

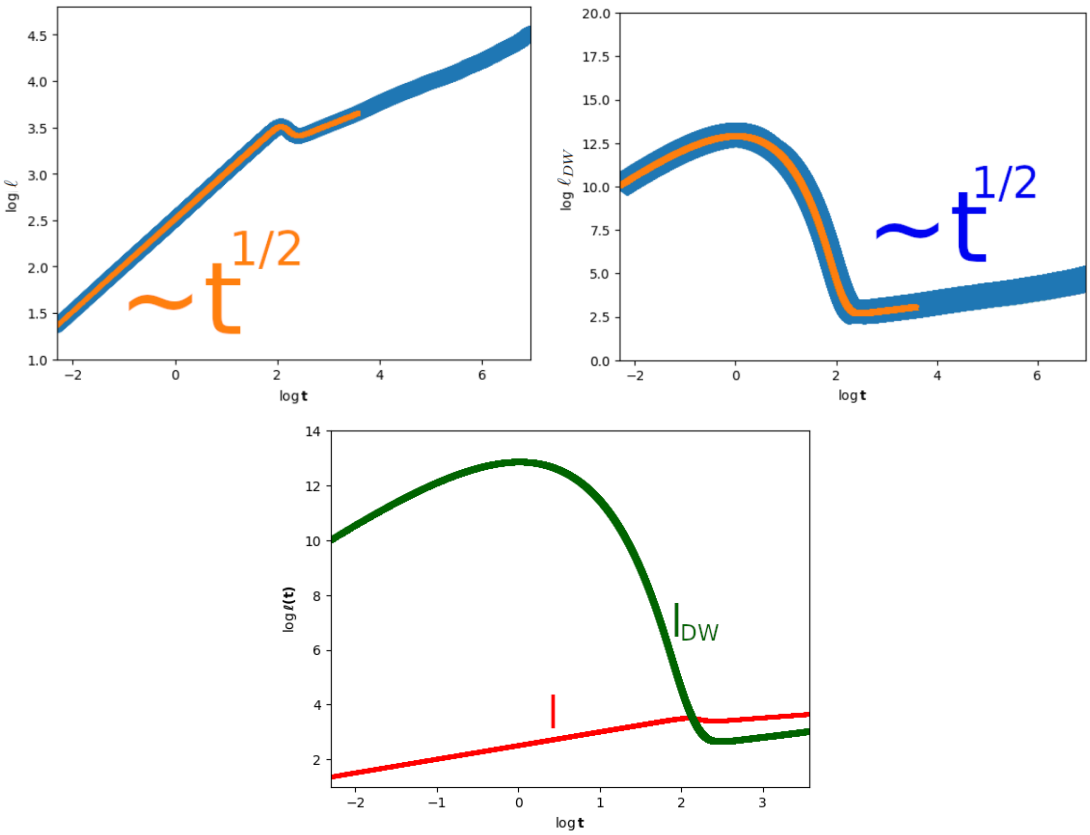

Figure 3.2: Evolution of the characteristic lengths of the system $\ell(t)$ (left) and ℓ_{DW} (right) measured during a simulation of the 2D TDGL equation with $C = 1$ (blue curve) and $C = 1 + \frac{1}{4}\sin\left(2\pi\frac{t}{T}\right); T = 0.025$ (orange curve). After the linear regime, $\ell(t)$ still grows in time as $\ell \sim t^{\frac{1}{4}}$. In the last plot both $\ell(t)$ (red) and $\ell_{DW}(t)$ (dark green) are represented on the same canvas. Notice the two function overlap at the end of the linear regime, suggesting the possibility of estimating the initial domain size as $l(t)$ evaluated at the end of the linear regime.

Chapter 4

Controlling the non-linear dynamics

In the previous chapter, we studied how the dynamics of the system is affected by varying the control parameter $C(t)$ during the (initial) linear dynamics, while domains are forming. In this chapter, we will explore whether it is possible to control the position or size of the domains by varying $C(t)$ during the asymptotic non-linear dynamics, once the domains have already formed.

Our study will examine systems of increasing dimensionality, starting with a 0D system where the order parameter is independent of spatial coordinates. In this case, we will solve the time-dependent Ginzburg-Landau (TDGL) equation exactly, through a closed-form expression. When $C(t)$ oscillates around an average value $\bar{C} \neq 0$, the order parameter converges to zero if $\bar{C} < 0$ or to $\pm\sqrt{\bar{C}}$ if $\bar{C} > 0$, both occurring exponentially fast. Conversely, if $\bar{C} = 0$, the order parameter converges to zero as a power law of time.

Next, we will consider both the 1D and 2D cases. Rather than solving the dynamics exactly, we will focus on the limiting cases where $C(t)$ oscillates either slowly or rapidly relative to the other time scales of the system. In these limiting cases, we will analyze the dynamics performing *multiple-scale expansions*. For the slow-varying scenario, to expand the state in powers of a small parameter, it is necessary to assume that $C(t)$ oscillates in such a way that it remains *strictly positive*. This ensures the system always admits a kink-like stationary solution (Eq. 2.2.9). In contrast, when analyzing the fast-varying limit, it will be sufficient to assume that the average value of $C(t)$ is positive.

We will find that, to leading order, the dynamics of the kinks in 1D and the interfaces in 2D are not affected by the oscillations of $C(t)$. Although these oscillations cause a deviation in the kink shape from the usual form (Eq. 2.2.9), so we will calculate the leading-order correction to the kink shape in the limit where the oscillations of $C(t)$ are slow.

Since the dynamics of the interfaces is not affected by the oscillations of $C(t)$, the coarsening laws (Eq. 2.2.16 and Eq. 2.3.13) remain unchanged as well. Thus, we **cannot control** the position and size of the domains by introducing *strictly positive* oscillations of $C(t)$ during the asymptotic dynamics.

4.1 The 0D case

For zero-dimensional system, we mean a system where the order parameter $m(\mathbf{x}, \mathbf{t})$ depends only on time t, while it is uniform in space. This means that the space derivative of the order parameter is zero and so the **0D TDGL** equation is reduced to

$$\partial_t m = C(t)m - m^3 \tag{4.1.1}$$

We can find an analytical solution to the equation, recognizing that dividing both sides by m^3

$$\frac{\partial_t m}{m^3} = \frac{C}{m^2} - 1$$

then, as $\frac{\partial_t m}{m^3} = -\frac{1}{2}\partial_t(\frac{1}{m^2})$, we can rewrite Eq. 4.1.1 as a simpler differential equation for the function $[\frac{1}{m^2}]$

$$\partial_t[\frac{1}{m^2}] = -2(C[\frac{1}{m^2}] - 1)$$

The corresponding homogeneous equation has the usual exponential solution. The the general in-homogeneous equation can be easily verified

$$\frac{1}{m^2(t)} = e^{-2\int_0^t C(t')dt'}\{\frac{1}{m_0^2} + 2\int_0^t e^{2\int_0^{t'} C(t'')dt''}dt'\} \tag{4.1.2}$$

This expression describes the *exact* dynamics of the system, when $C(t)$ is an arbitrary function.
From now on, we will make our analysis less general, requiring $C(t)$ to be an *oscillation* around an average value $\bar{C}$

$$C(t) = \bar{C} + b(t)$$

where $b(t+T) = b(t)$ is a periodic function, so also $B(t) = \int_0^t b(t)dt'$ is a function of period T. We will see that asymptotically (in time) the dynamics is governed by the value of the average $\bar{C}$ and the oscillation $b(t)$ is negligible: $m(t)$ will converge exponentially fast whether to zero or $\pm\sqrt{\bar{C}}$. Instead, the $\bar{C} = 0$ case is singular, as here the convergence to zero is much slower ($m(t) \sim t^{-\frac{1}{2}}$) and will present oscillations decreasing in amplitude and with the period of $C(t)$.

$$\frac{1}{m^2(t)} = e^{-2[\bar{C}t+B(t)]}\{\frac{1}{m_0^2} + 2\int_0^t e^{2[\bar{C}t'+B(t')]}dt'\}$$

If $\bar{C} \neq 0$, asymptotically ($t >> T$) we can approximate $[\bar{C}t + B(t)] \simeq \bar{C}$ both in the pre-factor and in the integral

$$\frac{1}{m^2(t)} \simeq e^{-2\bar{C}t}\{\frac{1}{m_0^2} + 2\int_0^t e^{2\bar{C}t'}dt'\} = \frac{1}{m_0^2}e^{-2\bar{C}t} + \frac{1}{\bar{C}}(1 - e^{-2\bar{C}t})$$

If $\bar{C} > 0$, asymptotically $(1 - e^{-2\bar{C}t}) \simeq 1$, so

$$(\frac{1}{m^2(t)} - \frac{1}{C}) \sim e^{-2\bar{C}t}$$

While if $\bar{C} < 0$, asymptotically $(1 - e^{-2\bar{C}t}) \simeq -e^{-2\bar{C}t}$, so

$$\frac{1}{m^2(t)} \sim e^{-2\bar{C}t}$$

In both cases, $m(t)$ converges to $\pm\sqrt{\bar{C}}$ or zero exponentially fast. While the $\bar{C} = 0$ case is singular, as in this case the oscillation $B(t)$ cannot be neglected and

$$\frac{1}{m^2(t)} = e^{-2B(t)}\{\frac{1}{m_0^2} + 2\int_0^t e^{2B(t')}dt'\}$$

As the function under the integral symbol is periodic with period T, asymptotically (when $t = nT + \delta t$ with $\delta t << nT$)

$$\frac{1}{m^2(t)} \simeq e^{-2B(t)}\{\frac{1}{m_0^2} + 2n\int_0^T e^{2B(t')}dt'\} \simeq 2ne^{-2B(t)}\int_0^T e^{2B(t')}dt'$$

By writing $n = \frac{t}{T}$, we conclude that $m(t)$ decays to zero as a power law of time

$$m(t) \sim t^{-\frac{1}{2}} \quad \text{if } \bar{C} = 0$$

up to an oscillation of period T, whose amplitude decays exponentially fast and that is present even when $\bar{C} \neq 0$, as shown in Figure 4.1

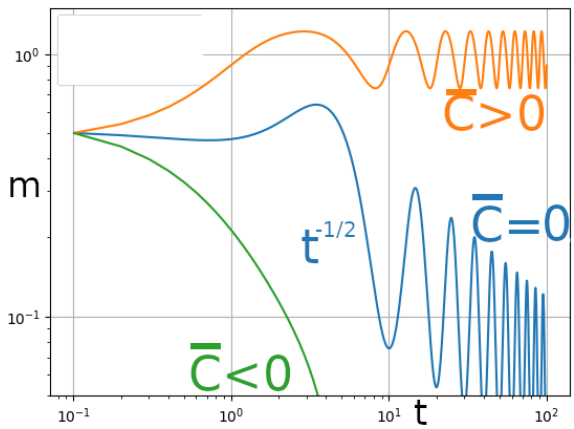

Figure 4.1: Simulation of the TDGL equation with uniform initial condition $m(\mathbf{x}, 0) = \frac{1}{2} \quad \forall t$, such that $\Delta m = 0$ and the TDGL equation is reduced to Eq. 4.1.1. Here $C(t) = \bar{C} + \sin\left(\frac{2\pi t}{T}\right)$ with $T = 10$ and $\bar{C} = -1$ (green), $\bar{C} = 0$ (blue), $\bar{C} = -1$ (orange).

4.2 The 1D case

The analysis of the zero-dimensional case can be applied to study the evolution of the order parameter's value inside a domain, where it's almost uniform. However, to understand if we can control position and size of the domains, we should question

how the interfaces between domains in a 2D system (or the kinks in a 1D system) are affected by a time dependent $C(t)$.
In this section we will study study a one-dimensional system. The analysis of a two-dimensional system will be a generalization of the present one, as in the limit where the curvature of an interface $\kappa \to 0$ the interface is flat, so the system is reduced to a one-dimensional system. However, for didactic reason we think it's worth to present the 1D analysis before the 2D one and not only the second one.
In the following analysis, we will assume $C(t)$ to be a periodic oscillation around an average value $\bar{C}$

$$C(t) = \bar{C} + b(t) > 0 \quad \forall t$$

where $b(t+T) = b(t)$. Then we will study the dynamics in the limits when $C(t)$'s oscillations are **fast** or **slow** respect to the other timescales of the system, using a mathematical tool known as multiple-scale expansion.
The **multiple-scale expansion** consists in a perturbative approach to study the dynamics. The core idea is that the dynamics of the system is the sum of many process that in principle may me characterized by different time scales τ_i (some processes can be faster than others). So you can introduce some *new time variables* t_i, such that

$$\delta t_i \sim 1 \iff \delta t \sim \tau_i$$

hoping to capture the description of each process occurring with a timescale τ_i, inside the dependence of the state $m(\mathbf{x}, t_1, t_2, ...)$ on t_i. The new variables $\{t_i\}$ will be treated as independent variables and we'll define them as

$$t_0 = t, t_1 = \epsilon t, t_2 = \epsilon^2 t, ...$$

this means that

$$\partial_t = \partial_{t_0} + \epsilon \partial_{t_1} + ... \tag{4.2.1}$$

where $\epsilon << 1$ is a small parameter that represent the ratio between two time scales of the system. By using Eq. 4.2.1 inside the TDGL equation, and expanding the order parameter

$$m(x,t) = m_0(x,t) + \epsilon m_1(x,t) + ...$$

will lead to a set of differential equations, one for each power of ϵ.

4.2.1 Slow varying temperature

We say that the temperature is slowly varying, if the time scale τ_C associated with the time variation of $C(t)$ (that, as $C(t)$ is periodic, can be identified as its period T) is large compared to the other scales of the system. In a 1D system, there is only another one time scale, that is the one associated with the growth of the Fourier modes during the initial dynamics. In Sec 3.1 we noticed that this time scale is $\tau_{\text{linear}} \sim \bar{C}^{-1}$. Therefore requiring that the temperature is slow varying in time, corresponds to requiring that

$$\frac{\tau_{\text{linear}}}{\tau_C} = \epsilon \quad ; \quad \epsilon << 1$$

Notice that, if we assume that $\bar{C} \sim 1$, then $\tau_{\text{linear}} \sim 1$.
The limit $\tau_C \to 0$, means that $C(t)$ is constant, so the dynamics is trivial. If, instead, τ_C is finite but still $\tau_C >> \tau_{\text{linear}}$, we *intuitively* expect that the state $m(x,t)$ will *follow* the stationary solution of the TDGL equation associated with $C = C(t)$

$$m(x,t) \simeq \sqrt{C(t)} \tanh\left(x\sqrt{\frac{C(t)}{2}}\right) \tag{4.2.2}$$

Notice that, this is a stable stationary solution of the system only if $C(t) > 0$, otherwise the only stationary solution admitted by the system would be $m = 0$. Thus, in the present analysis of the slow oscillations limit, we are assuming that $C(t)$ never reaches zero, but instead remains a strictly positive, oscillatory function. Now we will study quantitatively this dynamics, calculating, up to leading order in ϵ, how $m(x,t)$ deviates from Eq. 4.2.2. As there are only two time scales in this system, we introduce the time variables

$$t_0 = t, \tau = \epsilon t$$

to describe respectively the processes occurring at a timescale $\tau_{\text{linear}} \sim 1$ and τ_C. This means that $C(t)$ depends only on τ and not on t_0

$$C(t) = \tilde{C}(\tau) \implies \partial_{t_0}\tilde{C}(\tau) = 0$$

and the time derivative can be rewritten as

$$\partial_t = \partial_{t_0} + \epsilon\partial_\tau \tag{4.2.3}$$

If we expand the state $m(x,t)$ in powers of ϵ

$$m(x,t) = m_0(x,t) + \epsilon m_1(x,t) + O(\epsilon^2) \tag{4.2.4}$$

we can use Eq. 4.2.3 togheter with Eq. 4.2.4 inside the 1D TDGL equation

$$\partial_t m = \partial_{xx} m + \tilde{C}(\tau)m - m^3$$

so we find

$$\partial_{t_0} + \epsilon\partial_\tau = \partial_{xx}m_0 + C(t)m_0 - m_0^3 + \epsilon[\partial_{xx}m_1 + \tilde{C}(\tau)m_1 - 3m_0^2 m_1] + O(\epsilon^2)$$

By requiring the term on the left side of order ϵ^n to be equal to the term on the right side of the same order, we find one differential equation for every order n. The equation corresponding to the order zero (ϵ^0) is

$$\partial_{t_0} m_0 = \partial_{xx} m_0 + \tilde{C}(\tau)m_0 - m_0^3$$

and, as t_0 and τ are considered as independent variables, this is the 1D TDGL equation in the case when $C = \tilde{C}(\tau)$ is constant (Eq. 2.2.3). We already know that there is only one stationary solution and that it contains a single kink. So, *asymptotically* (in time)

$$m_0(x,t) = \sqrt{\tilde{C}(\tau)} \tanh\left(x\sqrt{\frac{\tilde{C}(\tau)}{2}}\right)$$

This is what we expected intuitively: in the presence of slow oscillations of $C(t)$, the state $m(x,t)$ deviates from the solution when C is constant by a small correction of order ϵ. From this result, we notice that, up to order zero, $C(t)$ affects only the height and the width of the kink, but not its analytical shape. So we *assume* that this is the case also for the first order correction ϵm_1

$$m_1(x,t) = \beta_1(t) m_{k_1}(\alpha_1(t)x)$$

Above we stated why it is reasonable to make the last assumption. However it's important to say that this assumption, along with the following ones, are designed to be able to find a solution to the TDGL equation to leading order in ϵ. Writing $m_0(x,t)$ in the same fashion $m_0 = \alpha_0 m_{k_0}(\alpha_0 x)$

$$\alpha_0(\tau) = \beta_0(\tau) = \sqrt{\tilde{C}(\tau)}; \quad m_{k_0} = \tanh\Big(\frac{x}{2}\Big)$$

We also assume that

$$\alpha_1(t) = \alpha_0(t) \equiv \alpha(\tau)$$

such that, up to first order in ϵ, the state $m(x,t)$ still presents a kink at any time t. And we assume that $\beta_1(t)$ depends only on the time scale of $C(t)$'s oscillations ($\partial_{t_0}\beta_1 = 0$) as this correction to m_0 is present only if $C(t)$ is time dependent. As α_1 and β_1 are functions of τ, it follows $\partial_{t_0} m_1 = 0$.
We made many assumptions on the solution $m(x,t)$. Now we have to check if, in light of these assumptions, the TDGL equation is solvable up to first order in ϵ. From the assumptions, it follows that

$$\partial_t m = \partial_{t_0} m_0 + \epsilon(\partial_\tau m_0 + \partial_{t_0} m_1) = \epsilon(\beta_0' m_{k_0} + \beta_0 m_{k_0}' \chi \frac{\alpha'}{\alpha})$$

$$\partial_{xx} m = \partial_{xx} m_0 + \epsilon \partial_{xx} m_1 = \beta_0 \alpha^2 u_{k_0}'' + \epsilon \beta_1 \alpha^2 m_{k_1}''$$

$$m^3 = m_0^3 + 3m_0^2 m_1 = \beta_0^3 m_{k_0^3} + 3\epsilon \beta_0^2 m_{k_0}^2 \beta_1 m_{k_1}$$

where, as $m_{k_i} = m_{k_i}(\alpha x)$ (where $i = 0, 1$), we introduced the variable $\chi \equiv \alpha(\tau)x$ and the notation $m_{k_i}' \equiv \partial_\chi$ and $\alpha' = \partial_\tau \alpha$ as $\beta_i' = \partial_\tau \beta_i$. Putting those equations inside the TDGL equation and considering only the terms of order one (ϵ^1)

$$\alpha'(m_{k_0} + m_{k_0}'\chi) = \tilde{C}(\tau)\beta_1(m_{k_1}'' + m_{k_1} - 3m_{k_0}^2 m_{k_1}') \tag{4.2.5}$$

This is a differential equation that contains both derivatives respect to τ and χ. Although it is not a partial differential equation, as we derive respect to τ the function α and respect to χ the function m_{k_1}. In this case we can put a condition to separate the dependence on τ and the one on χ in two separate equations. So we require that all the terms depending on τ, depend on it in the same fashion, so they simplify and disappear from the equation

$$C\beta_1 = \alpha' = \partial_\tau \sqrt{C} = \frac{1}{2} C' C^{-\frac{1}{2}}$$

This assumption determines the shape of $\beta_1(\tau)$

$$\beta_1(\tau) = \frac{1}{2} C'(\tau) C^{-\frac{3}{2}} \tag{4.2.6}$$

Then the τ-dependence disappears from the equation

$$m_{k_0} + m'_{k_0}\chi = m''_{k_1} + m_{k_1} - 3m^2_{k_0} m'_{k_1} \tag{4.2.7}$$

We could not find the analytical solution of Eq. 4.2.7, however we could find a numerical solution $\tilde{m}_{k_1}(\chi)$ (red line in Figure 4.2).
The Eq. 4.2.6 and the numerical solution $\tilde{m}_{k_1}(\chi)$ of Eq. 4.2.7 represent our results. Together, they enable us to calculate the first order correction to the kink's shape m_0 (Eq. 2.2.9) as

$$m(x,t) = m_0(x,t) + \epsilon\beta_1(t)\tilde{m}_{k_1}(x,t) + O(\epsilon^2) \tag{4.2.8}$$

Notice that, up to leading order, the symmetry $\chi \to -\chi$ is still present, as Eq. 4.2.7 is invariant under that transformation. It means that, up to leading order, the position of the kink is not affected by the time dependent $C(t)$. Notice also that we expect those results to be valid *asymptotically*, once, up to order zero, the state is well approximated by the usual kink's shape m_0.

Numerical evidence

We checked numerically the validity of Eq. 4.2.8, when

$$C(t) = \bar{C} + A\sin\left(\frac{2\pi t}{T}\right); \quad \bar{C} = 1, A = 0.2$$

The small parameter ϵ represents the ratio between the two timescales of the system $\epsilon = \frac{\tau_{\text{linear}}}{\tau_C}$. And with this choice of $C(t)$

$$\tau_{\text{linear}} = \frac{1}{\bar{C}} = 1; \quad \tau_C = T \implies \epsilon = T^{-1}$$

Writing $C(t)$ as a function of $\tau = \epsilon t = \frac{t}{T}$

$$C(t) = \bar{C} + A\sin\big(2\pi\bar{C}\tau\big) \tag{4.2.9}$$

From which it's possible to calculate

$$\beta_1(t) = \pi\bar{C}\frac{A\cos\big(\frac{2\pi t}{T}\big)}{[\bar{C} + A\sin\big(\frac{2\pi t}{T}\big)]^{\frac{3}{2}}}$$

To verify Eq. 4.2.8 simulated the 1D TDGL equation and we calculated $m_{k_1}(\chi)$ by inverting Eq. 4.2.8

$$m^{(EXP)}_{k_1} \equiv \frac{m^{(EXP)} - m_0}{\epsilon\beta_1(t)} \tag{4.2.10}$$

where the apex "EXP" indicates that the value is the one observed in the simulation. While the others are the predicted ones. In Figure 4.2 we present the results of two simulations, together with the numerical solution $\tilde{m_{k_1}}$ of Eq. 4.2.7. The two simulations differ from the choice of the period T, such that in the former $T = 100$ and $\epsilon = 0.01$, while in the second $T = 10$, so $\epsilon = 0.1$. It is clear that the mismatch decreases as ϵ decreases. This suggests that the mismatch is due to higher order correction, while our predictions are correct up to leading order.

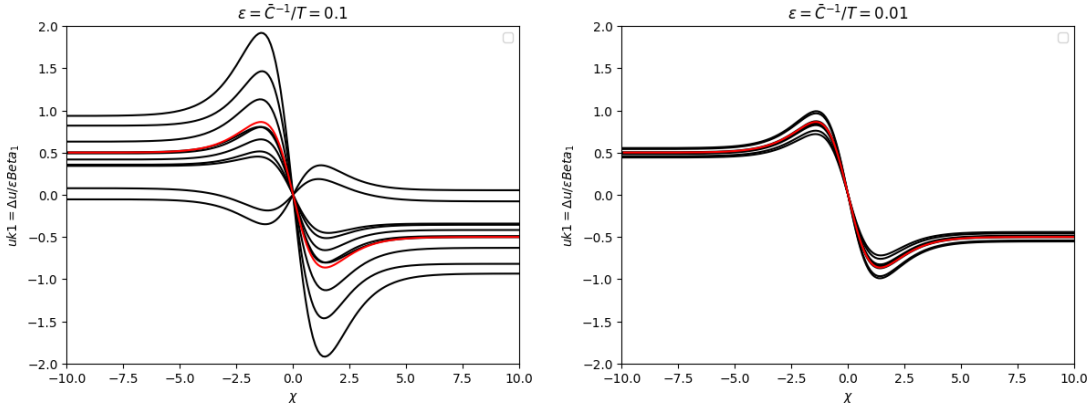

Figure 4.2: Simulations of the 1D TDGL equation compared with the numerical solution $\tilde{m_{k_1}}$ of Eq. 4.2.7. Within the simulations, $C(t)$ has the shape described in Eq. 4.2.9 where $T = 10$ in the left one and $T = 100$ in the right one. During the simulations, the state $m(x,t)$ was measured, to estimate the plotted function $m_{k_1}(\chi)$ calculated as in Eq. 4.2.10. In each figure, the black lines lines correspond to the same simulation, but the measure of the state m is performed at different times. Ten measures are done starting from 3 periods after $t = 0$ and separated by $\Delta t = T/10$, such that a whole period is sampled, and a possible transient behaviour is excluded from the measures. The Eq. 4.2.7 was solved using the function *NDSolve* of *Mathematica*. The adopted initial conditions are $m_{k_1}(0) = 0$, while $m'_{k_1}(0) = -1.12491$ was determined with many trials and choosing a value for which the numerical solution $\tilde{m}_{k_1}(\chi)$ diverges slowly when $\chi \to \pm\infty$.

4.2.2 Fast varying temperature

This is the opposite limit, when $\frac{\tau_{\text{linear}}}{\tau_C} >> 1$, so we can define a small parameter ϵ as

$$\frac{\tau_C}{\tau_{\text{linear}}} = \epsilon \quad ; \quad \epsilon << 1$$

Following the same reasoning presented while analyzing the opposite limit, we introduce new time variables to capture, separately, the processes characterized by different timescales. In this case we introduce the following variables

$$t_{-1} = \epsilon^{-1} t; \quad t_0 = t$$

Following the idea of the multiple scale expansion, we can, in principle, introduce as many variables as we want. However, introducing many variables makes the calculations more messy and so we introduce only a few ones, that we *guess* to be relevant. This time, the variable t_{-1} is the one that describes the processes occurring with the time scale of $C(t)$'s oscillations, as

$$\delta t_{-1} \sim 1 \implies \delta t \sim \epsilon$$

and $\epsilon \sim \tau_C$ if we assume that $\bar{C} \sim 1$ (so $\tau_{\text{linear}\sim 1}$). It means that

$$C(t) = C_0 + D_0(t_{-1})$$

where C_0 is the average value of $C(t)$, while $D_0(t_{-1})$ is an oscillation with period T, around zero

$$\int_{t_{-1}}^{(t_{-1}+T)} D_0(t'_{-1})dt'_{-1} = 0 \quad \forall t_{-1}$$

Within the present analysis, of the limit where $\tau_C << \tau_{\text{linear}}$, it is not necessary to assume that $C(t)$ is a strictly positive function. However we need at least $C_0 > 0$, such that the stationary state associated with $C = C_0$ is kink-shaped.
As $\partial_{t_0} D_0(t_{-1}) = 0$, it follows that $\partial_{t_0} C = 0$, while the time derivative can be written as

$$\partial_t = \epsilon^{-1}\partial_{t_{-1}} + \partial_{t_0}$$

Expanding the state in powers of ϵ

$$m(x,t) = m_0(x,t) + \epsilon m_1(x,t) + \epsilon^2 m_2(x,t) + O(\epsilon^3)$$

and using this expansion inside the 1D TDGL equation

$$\partial_t m = \partial_{xx} m + C(t)m - m^3$$

leads to

$$\epsilon^{-1}\partial_{t_{-1}} m_0 + \partial_{t_0} m_0 + \partial_{t_{-1}} m_1 + \epsilon(\partial_{t_0} m_1 + \partial_{t_{-1}} m_2) =$$

$$= (C_0 + D_0(t_{-1})m_0 - m_0^3 + \partial_{xx} m_0 + \epsilon[(C_0 + D_0(t_{-1})m_1 - 3m_0^2 m_1 + \partial_{xx} m_1] + O(\epsilon^2)$$

Up to order ϵ^{-1}, we find

$$\partial_{t_{-1}} m_0 = 0$$

While, up to order ϵ^0

$$\partial_{t_{-1}} m_1 + \partial_{t_0} m_0 = (C_0 + D_0(t_{-1}))m_0 - m_0^3 + \partial_{xx} m_0$$

This time, these equations are not sufficient to determine m_0. However, it is reasonable to consider that if the oscillations of $C(t)$ are too rapid, the system doesn't have "enough time" to respond to the variations in $C(t)$. Therefore, we assume that, to leading order, the *asymptotic* dynamics is the same as if C were constant and equal to its average value C_0.

$$m_0 = \sqrt{C_0}\tanh\left(x\sqrt{\frac{C_0}{2}}\right) \tag{4.2.11}$$

Notice that, in order for this state to be a stationary state of the system with $C = C_0$ constant, we need that $C_0 > 0$. Otherwise the only stationary state admitted by the system will be $m = 0$.
Assuming that m_0 is a stationary solution of the 1D TDGL equation with $C = C_0$ constant, means that

$$\partial_{xx} m_0 + C m_0 - m_0^3 = 0; \quad \partial_t m_0 = 0$$

So the equation for the order ϵ^0 simplifies to

$$\partial_{t_{-1}} m_1 = D_0(t_{-1})m_0 \tag{4.2.12}$$

That can be integrated, so

$$m_1(t_{-1}, t_0, x) = m_0(x) \int_0^{t_{-1}} D_0(t'_{-1}) dt'_{-1} + f(0, t_0, x) \tag{4.2.13}$$

In this context, we chose not to label the integration constant as $u_1(t_{-1} = 0)$ because the assumption we made about m_0 holds asymptotically, rather than from $t = 0$. There might be a transient regime influenced by the initial condition $m(x, t = 0)$, which we are not interested in analyzing here. Consequently, we can express

$$m_1(t_{-1}, t_0, x) = m_0(x) \int_{\tau_{-1}(t_0,x)}^{t_{-1}} D_0(t'_{-1})\, dt'_{-1}$$

This equation provides a formula to find the first-order correction m_1. However, since we do not have additional equations to determine the function $\tau_{-1}(t_0, x)$, we are unable to calculate the first-order correction to the kink's shape m_1 in this limit of rapidly-oscillating $C(t)$.
The position of the kink is not affected by $C(t)$. We decided to not prove this statement here, but in the next section, while studying the fast oscillations limit in a 2D system. Then a 1D system can be recovered from a 2D one by taking the limit where the curvature of any interface $\kappa \to 0$.

4.3 The 2D case

In the previous chapter, we showed that it is not possible to control the position of a kink in a 1D system using a time-dependent control parameter $C(t)$. Precisely, this conclusion was reached by examining two limiting cases: first, when the oscillations of $C(t)$ are slow relative to the system's intrinsic timescale τ_{linear} and $C(t)$ remains strictly positive, and second, when the oscillations are fast compared to τ_{linear}, requiring just the average value of $C(t)$ being positive.
In this chapter, we will demonstrate that a similar result holds for 2D systems: the *motion by curvature*, which governs the dynamics of interfaces, remains unaffected by the modulation of $C(t)$ in these limiting cases, at least to leading order.
The key difference between the 1D and 2D analysis of dynamics is the introduction of curvature in 2D. This introduces a new timescale, linked to the time required for an interface to move over a distance comparable to its thickness. We will examine the scenario where $C(t)$ varies slowly over time, such that the timescale of $C(t)$'s variation aligns with the new timescale introduced by curvature. This curvature timescale is shorter than the system's intrinsic timescale, $\tau_{\text{linear}} \sim \frac{1}{C}$. We will also examine the case where $C(t)$ varies rapidly compared to the intrinsic timescale τ_{linear}. In both scenarios, we will find that, to leading order, the motion by curvature is not influenced by the time-dependent $C(t)$.

4.3.1 Slow varying temperature

In Sec. 2.3, we noted that during the asymptotic dynamics, the curvature κ at any point on the interface is small, and the interface propagates slowly without

changing its shape to leading order. By combining these observations with the scaling hypothesis, we derived the following equations:

$$\kappa = \epsilon K_1; \quad K_1 \sim 1, \tag{4.3.1}$$

$$\Delta = \partial_{\xi\xi} + \epsilon K_1 \partial_\xi + O(\epsilon^2); \quad \epsilon \ll 1, \tag{4.3.2}$$

$$\partial_t m = -\epsilon V_1 \partial_\xi m; \quad V_1 \sim 1. \tag{4.3.3}$$

In Sec. 2.3, the control parameter C was held constant. However, in the present analysis, we consider a time-dependent $C(t)$, given by:

$$C(t) = \bar{C} + D_0(t),$$

where $D_0(t)$ is a periodic oscillation with $D_0(t+T) = D_0(t)$, and $\bar{C}$ is the average value around which $C(t)$ oscillates.
We define $C(t)$ as slowly varying if its variation occurs at a timescale that is slow compared to the intrinsic timescale of the dynamics, $\tau_{\text{linear}} \sim \frac{1}{\bar{C}} \sim 1$ (assuming $\bar{C} \sim 1$). Specifically, $C(t)$ is considered slowly varying if its timescale is comparable to the timescale of the interface propagation, a phenomena described by Eq. 4.3.3. Introducing the new time variables:

$$t_0 = t; \quad \tau = \epsilon t,$$

the slow varying limit, similar to the 1D analysis, corresponds to:

$$C(t) = \tilde{C}(\tau) \implies \partial_t C = \epsilon \partial_\tau C,$$

where the small parameter ϵ appearing in the last equation is the same as that in Eq. 4.3.3. In general, the introduction of t_0 and τ leads to the relation:

$$\partial_t = \partial_{t_0} + \epsilon \partial_\tau.$$

However, to incorporate in the last expression the phenomena of interface propagation described in Eq. 4.3.3, we state:

$$\partial_t = \partial_{t_0} + \epsilon \partial_\tau - \epsilon V_1 \partial_\xi. \tag{4.3.4}$$

And using the properties 4.3.1, 4.3.2 and 4.3.4 in the TDGL equation

$$\partial_t m = \Delta m + C(t) m - m^3$$

we find, up to leading order in ϵ

$$\partial_{t_0} m + \epsilon \partial_\tau m = \partial_{\xi\xi} m + \epsilon (K_1 + V_1) \partial_\xi m + \tilde{C}(\tau) m - m^3 \tag{4.3.5}$$

As we did during the 1D analysis, we expand the order parameter in powers of ϵ

$$m = m_0 + \epsilon m_1 + O(\epsilon^2)$$

and by putting this expansion in the TDGL equation (Eq. 4.3.5) and equating the terms of order zero (ϵ^0), we find

$$\partial_{t_0} m_0 = \partial_{\xi\xi} m_0 + \tilde{C}(\tau) m_0 - m_0^3 \tag{4.3.6}$$

To order zero, we find the same equation we found in the 1D analysis, where $x \to \xi$. In that previous analysis, we found

$$m_0(\xi, t) = \sqrt{C(\tau)} \tanh\left(\xi \sqrt{\frac{\tilde{C}(\tau)}{2}}\right)$$

Before equating the terms of order ϵ^1 in Eq. 4.3.5, we apply the same assumptions as in the 1D analysis:

$$m_i(\xi, t) = \beta_i(t) m_{k_i}(\alpha_i(t)\xi),$$
$$\alpha_1 = \alpha_0 \equiv \alpha,$$
$$\partial_{t_0}\alpha = \partial_{t_0}\beta_1 = 0.$$

Under these assumptions, equating the terms of order ϵ^1 in the TDGL equation yields:

$$\alpha^2\beta_1\left(m''_{k_1} + m_{k_1} - 3m_{k_0}^2 m_{k_1}\right) = \alpha'\left(m_{k_0} + u'_{k_0}\chi\right) - (K_1 + V_1)\alpha^2 m'_{k_0}. \tag{4.3.7}$$

Here, $\chi \equiv \alpha\xi$, $\alpha' \equiv \partial_\tau \alpha$, and $m'_{k_i} \equiv \partial_\chi m_{k_i}$.
Note that this is the same equation found in the 1D analysis (Eq. 4.2.5), but with an additional term $(K_1)\alpha^2 m'_{k_0}$. The term containing V_1 was also absent in the 1D analysis, though not for any physical reason. Rather, we decided to take into account the influence of $C(t)$ on the kink's position directly in the current analysis of a 2D system, whereas this was not accounted for in the previous 1D study.
The presence of additional terms in the equation neglects the possibility of retrieving an equation with only spatial derivatives, as was done in the 1D analysis. That's because, if we follow the same approach and require:

$$\alpha^2\beta_1 = \alpha' = \alpha^2,$$

considering that $\alpha = \sqrt{\tilde{C}(\tau)}$, we obtain a constraint on $\tilde{C}(\tau)$ that does not align with the requirement for $C(t)$ to be a periodic function.
However, we can still extract useful information from Eq. 4.3.7 by applying the Fredholm alternative, a theorem discussed in Sec. 2.3. As we're dealing with a differential equation of this kind

$$\hat{L}u(\chi) = f(\chi),$$

where

$$\hat{L} = \partial_{\chi\chi} + (1 - 3u_{k_0}^2)$$

It follows that, if $v(\chi)$ is an homogeneous solution ($\hat{L}v = 0$), then

$$\int_{-\infty}^{+\infty} f(\chi)v(\chi)\,d\chi = [\partial_\chi uv - u\partial_\chi v]_{-\infty}^{+\infty}. \tag{4.3.8}$$

In our case, a solution of the homogeneous equation is gived by $u_{k_1} = \partial_\chi u_{k_0}$, as this follows from differentiating Eq. 4.3.6. While

$$f(\chi) = \alpha'(u_{k_0} + \partial_\chi u_{k_0}\chi) - \alpha^2(K_1 + V_1)\partial_\chi u_{k_0}.$$

Assuming the boundary terms are zero, we apply the Fredholm alternative:

$$\int f(\chi)\partial_\chi u_{k_0}(\chi)\,d\chi = 0.$$

$$\int \alpha'(u_{k_0}\partial_\chi u_{k_0} + (\partial_\chi u_{k_0})^2\chi)d\chi - \int \alpha^2(K_1 + V_1)(\partial_\chi u_{k_0})^2 d\chi = 0$$

And recognizing the properties:

- u_{k_0} is odd, so $\partial_\chi u_{k_0}$ is even;
- $(\partial_\chi u_{k_0})^2$ is always positive (or its integral is strictly positive);
- The integration domain is symmetric.

We conclude that:

$$V_1 = -K_1.$$

This implies that, up to leading order, the motion by curvature is unaffected by a time-dependent control parameter $C(t)$. Notably, by utilizing the identity $V_1 = -K_1$ in Eq. 4.3.7, we recover the corresponding equation found in the 1D analysis (Eq. 4.2.5). Thus, we can conclude, without requiring further calculations, that up to leading order, the shape of an interface along a direction perpendicular to it is the same as that of a 1D kink.

Numerical evidence

We numerically verified the motion by curvature equation $v = -\kappa$ by examining an isolated circular domain, whose radius $R(t)$ decreases over time. This example is detailed in Sec. 2.3, where the preparation of the initial state and the method for measuring the radius $R(t)$ over time are explained.
In Sec. 2.3, the control parameter C was constant over time, whereas in this section, $C(t)$ is time-dependent. Specifically, we used the form:

$$C(t) = \bar{C} + A\sin\left(2\pi\frac{t}{T}\right),$$

with the requirement that $C(t)$ be slowly varying over time, which translates to $T \sim \epsilon^{-1}$. This small parameter ϵ also describes the smallness of the curvature $\kappa \sim \epsilon$, given that $\kappa = \frac{1}{R}$ for a circular domain. Consequently, we prepared the initial state by selecting

$$T = R_0,$$

where R_0 is the initial radius of the isolated circular domain.

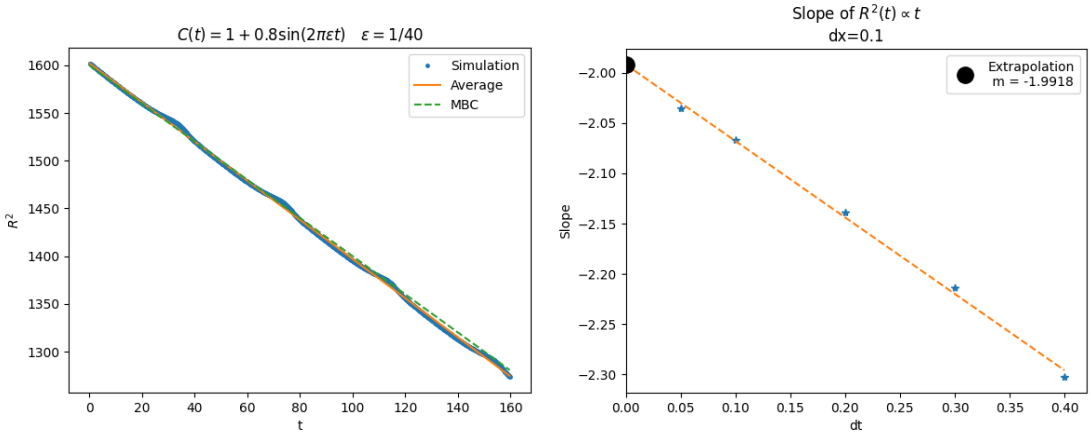

Figure 4.3: On the **left**: Square of the radius of an isolated circular domain $R(t)^2$ as a function of time, where $C(t) = 1 + 0.8\sin(2\pi\epsilon t)$ and $\epsilon = R(0)^{-1} = 1/40$. The blue curve correspond to the measured value of $R(t)^2$. The orange line is a time average, computed making a linear fit of the blue curve. While the green line corresponds to the expected relation if motion by curvature ($v = -\kappa$) holds: $R(t)^2 = R_0^2 - 2t$. The simulation parameters are $dt = 0.1$, $dx = 0.1$, $L = 128$, $R(0) = 40$. On the **right**: The simulation on the left was carried for multiple values of dt. Each time the slope of the experimental curve (the blue one) was estimated with a linear fit. Here the estimated slope is represented as a function of dt. A linear regression to extrapolate the slope value at $dt \to 0$ returns the value -1.992 ± 0.006, that is compatible with the expected value (-2) within two standard deviations.

In Figure 4.3 (left), the measured value of $R^2(t)$ during the simulation is plotted as a function of time. If motion by curvature is valid, we expect $R^2(t)$ to decay linearly, as demonstrated in Sec. 2.3:

$$R^2(t) = R_0^2 - 2t.$$

This linear decay is observed, particularly when the measures of $R^2(t)$ (shown by the blue curve) are averaged over time (orange line). However, the decay appears to be slightly faster than expected (green line).
This discrepancy can be attributed to the discreteness of time steps used in the simulations. To address this, Figure 4.3 (right) illustrates the estimation of the slope of the orange curve by running simulations with various time step values dt. An extrapolation to $dt \to 0$ confirms the expected value of the slope, thereby validating the motion by curvature behavior in the simulations.

4.3.2 Fast varying temperature

This scenario represents the opposite limit, where the time scale associated with the variations of $C(t)$ is one order of magnitude larger than the intrinsic time scale

τ_{linear}. To analyze this, we introduce the time variables:

$$t_{-1} = \epsilon^{-1}t; \quad t_0 = t; \quad t_1 = \epsilon t.$$

In this limit, we define $C(t)$ as follows:

$$C(t) = C_0 + D_0(t_{-1}),$$

where C_0 is the average value of $C(t)$ and $D_0(t_{-1})$ represents an oscillation around zero with period T:

$$\int_{t_{-1}}^{(t_{-1}+T)} D_0(t'_{-1})dt'_{-1} = 0 \quad \forall t_{-1}.$$

Consequently, we have

$$\partial_{t_0} C = \partial_{t_1} C = 0,$$

while in general, the time derivative can be expressed as:

$$\partial_t = \epsilon^{-1}\partial_{t_{-1}} + \partial_{t_0} + \epsilon\partial_{t_1}.$$

It is important to note that this small parameter ϵ is the same one that appears in the equations 4.3.1, 4.3.2, and 4.3.3; it characterizes the smallness of the curvature of an interface.
Following the same approach used in the analysis of the slow-varying $C(t)$ limit, we incorporate the interface propagation phenomena into the time derivative as follows:

$$\partial_t = \epsilon^{-1}\partial_{t_{-1}} + \partial_{t_0} + \epsilon\partial_{t_1} - \epsilon V_1\partial_\xi. \tag{4.3.9}$$

Next, we expand the state in powers of ϵ:

$$m(x,t) = m_0(x,t) + \epsilon m_1(x,t) + \epsilon^2 m_2(x,t) + O(\epsilon^3).$$

By substituting this expansion, along with Equations 4.3.1, 4.3.2, and 4.3.9, into the two-dimensional TDGL equation

$$\partial_t m = \Delta m + C(t)m - m^3,$$

we obtain

$$\epsilon^{-1}\partial_{t_{-1}}m_0 + \partial_{t_0}m_0 + \partial_{t_{-1}}m_1 + \epsilon(\partial_{t_0}m_1 + \partial_{t_{-1}}m_2 + \partial_{t_1}m_0 - V_1\partial_\xi m_0) =$$
$$= \partial_{\xi\xi}m_0 + (C_0 + D_0(t_{-1})m_0 - m_0^3 + \epsilon[\partial_{\xi\xi}m_1 + K_1\partial_\xi m_0 + (C_0 + D_0(t_{-1})m_1 - 3m_0^2 m_1] + O(\epsilon^2)$$

Equating the terms of order ϵ^{-1} we find

$$\partial_{t_{-1}}m_0 = 0$$

while for the order ϵ^0 we find

$$\partial_{t_{-1}}m_1 + \partial_{t_0}m_0 = (C_0 + D_0(t_{-1}))m_0 - m_0^3 + \partial_{\xi\xi}m_0$$

The last two equations, are the same ones we found in the 1D analysis of the fast varying $C(t)$ limit, where $x \to \xi$. In that analysis, these equations led to Eq. 4.2.11 and Eq. 4.2.13, that we recall

$$m_0 = \sqrt{C_0}\tanh\left(\xi\sqrt{\frac{C_0}{2}}\right)$$

$$m_1 = m_0(\xi)\int_{\tau_{-1}(t_0,t_1,\xi)}^{t_{-1}} D_0(t'_{-1})dt'_{-1} \tag{4.3.10}$$

where during the 1D analysis we couldn't determine $\tau_{-1}(t_0, t_1, \xi)$ due to lack of additional equations. As we're interested in the motion of the interfaces, that is a first order (ϵ^1) phenomena, this time we consider also the equation associated with order ϵ^1

$$\partial_{t_{-1}}m_2 + \partial_{t_0}m_1 + \partial_{t_1}m_0 - V_1\partial_\xi m_0 = (C_0 + D(t_{-1}))m_1 - 3m_0^2m_1 + \partial_{\xi\xi}m_1 + K_1\partial_\xi m_0$$

We know that $m_0 = m_0(\xi)$, so $\partial_{t_1}m_0 = 0$. We then make the following assumption to solve the equation. Although we were unable to fully interpret its physical significance, it simplifies the equation, enabling us to find a solution, even if it is not the most general one.

$$\partial_{t_0}\tau_{-1} = \partial_\xi\tau_{-1} = 0$$

Which implies, using Eq. 4.3.10

$$\partial_{t_0}m_1 = 0$$

$$\partial_{\xi\xi}m_1 = \partial_{\xi\xi}m_0\int_{\tau_{-1}}^{t_{-1}} D_0(t'_{-1})dt'_{-1}$$

As a consequence, the equation associated with order ϵ^1 becomes

$$\partial_{t_{-1}}m_2 - V_1\partial_\xi m_0 = (C_0 + D(t_{-1}))m_1 - 3m_0^2m_1 + \partial_{\xi\xi}m_0\int_{\tau_{-1}}^{t_{-1}} D_0(t'_{-1})dt'_{-1} + K_1\partial_\xi m_0$$

$$\partial_{t_{-1}}m_2 = [(C_0m_0 + D_0(t_{-1})m_0 - 3m_0^2 + \partial_{\xi\xi}m_0]\int_{\tau_{-1}}^{t_{-1}} D_0(t'_{-1})dt'_{-1} + (V_1 + K_1)\partial_\xi m_0$$

Remembering that $m_0(\xi)$ is a stationary solution of the 1D TDGL equation with $C = C_0$ constant, it holds

$$C_0m_0 - m_0^3 + \partial_{\xi\xi}m_0 = 0$$

And using this statement in the previous equation

$$\partial_{t_{-1}}m_2 = [D_0(t_{-1})m_0 - 2m_0^3]\int_{\tau_{-1}}^{t_{-1}} D_0(t'_{-1})dt'_{-1} + (V_1 + K_1)\partial_\xi m_0 \tag{4.3.11}$$

To derive a formula for the interface velocity V_1, we must introduce an additional assumption. We anticipate that the order parameter u remains bounded at all times.

Since m_0 does not depend on time and m_1 is periodic—due to the periodic nature of $D_0(t_{-1})$. We also assume that m_2 is periodic with the same period as $D_0(t_{-1})$:

$$m_2(t_{-1} + T) = m_2(t_{-1}).$$

This periodicity leads to the condition:

$$\Delta m_2 \equiv \int_{\tau_{-1}}^{\tau_{-1}+T} \partial_{t'_{-1}} m_2(t'_{-1})\, dt'_{-1} = 0.$$

We can use this last statement if we integrate $\int_{\tau_{-1}}^{\tau_{-1}+T} dt_{-1}$ the Eq. 4.3.11

$$\mathbf{0} = m_0 \int_{\tau_{-1}}^{\tau_{-1}+T} D_0(t_{-1})dt_{-1} \int_{\tau_{-1}}^{t_{-1}} D_0(t'_{-1})dt'_{-1} + \tag{4.3.12}$$

$$-2m_0^2 \int_{\tau_{-1}}^{\tau_{-1}+T} dt_{-1} \int_{\tau_{-1}}^{t_{-1}} D_0(t'_{-1})dt'_{-1} + (V_1 + K_1)\partial_\xi m_0 T$$

Next, we observe that we have a sum of three terms that depend on ξ in different ways: specifically, as m_0, m_0^2, and $\partial_\xi m_0$. Since the equation must hold for all ξ, each of these three terms must individually be zero for their sum to equal zero.
It follows that

$$(V_1 + K_1)\partial_\xi m_0 T = 0 \quad \forall \xi \tag{4.3.13}$$

so we find the usual equation for motion by curvature

$$V_1 = -K_1$$

. We couldn't prove rigorously this statement, however we can at least prove (in Appendix F) that is exists a value for τ_{-1} such that Eq. 4.3.12 reduces to Eq. 4.3.13. This result tells that, up to leading order, motion by curvature is not affected by a time dependent $C(t)$.

Numerical evidence

Similar to our analysis in the opposite limit, we verified the motion by curvature relation $v = -\kappa$ by simulating the dynamics of an isolated circular domain. For the time dependence of $C(t)$, we used the expression

$$C(t) = \bar{C} + A \sin\left(2\pi \frac{t}{T}\right).$$

In the previous case, we established that $T \sim \epsilon^{-1}$ since $C(t)$ was slowly varying over time. In this instance, however, the time scale describing the variation must be small, so we set $T \sim \epsilon$. Consequently, we make the following choice for the initial radius:

$$T = R_0^{-1}.$$

A simulation of this type is presented in Figure 4.4. The results validate the analytical analysis, confirming that motion by curvature serves as the driving mechanism of the dynamics when $C(t)$ varies rapidly over time.

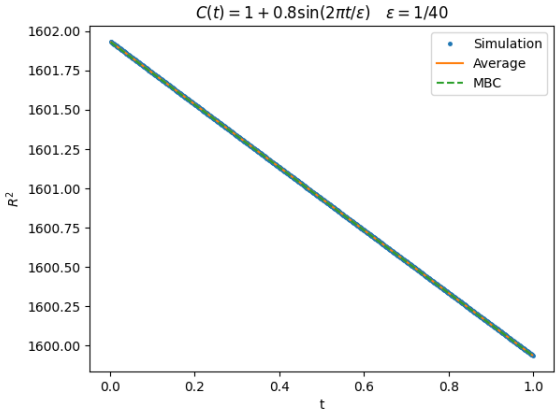

Figure 4.4: Square of the radius of an isolated circular domain $R(t)^2$ as a function of time, where $C(t) = 1 + 0.8\sin(2\pi t/\epsilon)$ and $\epsilon = R(0)^{-1} = 1/40$. The blue curve corresponds to the measured value of $R(t)^2$. The orange line is a time average, computed making a linear fit of the blue curve. While the green line corresponds to the expected relation if motion by curvature ($v = -\kappa$) holds: $R(t)^2 = R_0^2 - 2t$. The simulation parameters are $dt = 0.1$, $dx = 0.1$, $L = 128$, $R(0) = 1/40$.

4.3.3 Controlling the coarsening dynamics

In the previous sections, we numerically verified the motion by curvature relation $v = -\kappa$ by examining the dynamics of a specific system initially prepared with a single isolated circular domain. However, as discussed in Sec. 2.3.2, starting from random initial conditions, the number of domains decreases asymptotically while their average size increases as a power law of time, specifically $\ell \sim t^{\frac{1}{2}}$. We motivated this behavior, known as coarsening dynamics, by applying the motion by curvature relation $v = -\kappa$ within a dimensional analysis framework. This indicates that motion by curvature can be validated by observing that the typical size of the domains grows as a power law over time, particularly with an exponent of $\ell \sim t^{\frac{1}{2}}$.
In this section, we will present simulations of the asymptotic dynamics in the two distinct limits where the time variations of $C(t)$ are either slow or fast relative to the intrinsic timescale of the system. In both scenarios, we will demonstrate that the coarsening dynamics remains unaffected by a time-dependent $C(t)$. Specifically, we'll verify that the characteristic power-law growth of domain size, $\ell \sim t^{\frac{1}{2}}$, persists regardless of whether $C(t)$ changes slowly or rapidly over time.
As in the previous section, we adopted a time-dependent $C(t)$ given by

$$C(t) = \bar{C} + A\sin\left(2\pi\frac{t}{T}\right)$$

In the slow-varying limit, the period T of $C(t)$ is much larger than the intrinsic timescale of the system, $\tau_{\text{linear}} \sim \frac{1}{\bar{C}}$ (which is approximately 1, since $\bar{C} = 1$). Specifically, we chose $T = 25 \gg 1$ to represent this slow-varying case.
Conversely, to study the fast-varying limit of $C(t)$, we set $T = 0.025 \ll 1$, such that the period of $C(t)$ is much smaller than the system's intrinsic timescale.
In Figure 4.5, we present the results of two simulations illustrating how the average

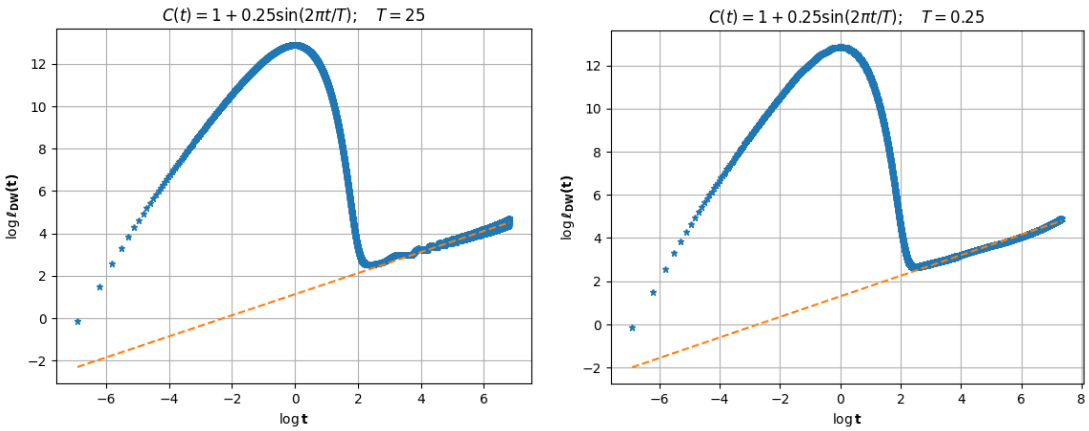

Figure 4.5: We measured the typical domain size ℓ_{DW} (as defined in Eq. 2.3.15) as a function of time in a 2D system where $C(t) = 1 + \frac{1}{4}\sin(2\pi t/T)$ with $T = 25$ (left) and $T = 0.25$ (right). The orange line in the plots shows the result of a linear fit to the experimental curve (the blue one) during the asymptotic dynamics. The fit suggests that the data is well approximated respectively by the laws $\ell_{DW} \simeq 0.98\pi t^{0.5}$ and $\ell_{DW} \simeq 1.18\pi t^{0.48}$. During the linear dynamics, we used a time step of $dt = 0.001$ to accurately capture the process of domain formation. Subsequently, we adopted $dt = 0.1$ to integrate the slower coarsening dynamics.

domain size ℓ_{DW} evolves over time under different time dependencies of $C(t)$. The results indicate that in both scenarios, whether $C(t)$ varies slowly or rapidly, the average domain size ℓ_{DW} grows over time following a power law with an exponent $\ell_{DW} \sim t^{\frac{1}{2}}$. This behavior is highlighted by the orange curve, which represents the time-averaged data of the experimental blue curve. This provides an alternative verification of the motion by curvature mechanism, demonstrating that the coarsening dynamics remain unchanged even when $C(t)$ is time-dependent.
In both simulations, due to the complexity involved in directly calculating the integral of $(\partial_\xi m)^2$ along a line perpendicular to the interface (a term that appears in Eq. 2.3.15 for calculating ℓ_{DW}), we instead computed this integral using the zeroth-order approximation of m. Specifically, we used $m_0 = \sqrt{C(t)}\tanh\left(\sqrt{\frac{C(t)}{2}}\xi\right)$ for the case of slowly varying $C(t)$, and $m_0 = \sqrt{\bar{C}}\tanh\left(\sqrt{\frac{\bar{C}}{2}}\xi\right)$ for the case of rapidly varying $C(t)$.
Indeed, there is an alternative method for numerically verifying the coarsening law $\ell_{DW} \sim t^{\frac{1}{2}}$. In the asymptotic regime, ℓ_{DW} can be expressed in terms of the other length scale ℓ (Appendix G), which we previously defined during the analysis of the linear dynamics. This relationship allows us to verify the coarsening law by verifying that $\ell \sim t^{\frac{1}{4}}$. This result is noteworthy because it allows us to verify the coarsening law by monitoring a quantity, $\ell(t)$, that has physical interpretation (it is the typical size of the features in the system) even during the linear dynamics, when domains are not there and so ℓ_{DW} does not yet reflect the average domain size. However, for the sake of simplicity, we chose to verify the coarsening law by directly calculating ℓ_{DW}.

Chapter 5

Conclusions

In this work, we investigated the dynamics of the time-dependent Ginzburg-Landau equation in a regime that has not been extensively studied in the past: the scenario where the temperature is time-dependent.
We analytically examined two limiting cases: the former where the temperature oscillates much slower than the intrinsic timescale of the system with $T(t) < T_C$, and the other where the temperature oscillates much faster than the intrinsic timescale, requiring only that the average value of $T(t)$ remains below T_C. Using a multiple scale expansion, we could calculate the effects of the time dependence of T on the dynamics, up to the leading order. These analytical predictions were then validated through numerical simulations.
The questions that inspired this research were whether we could control the position or size of domains by varying the temperature over time. Our findings in the two studied cases indicate that, up to leading order, it is not possible to control these domain properties through temperature variation over time. However, we discovered that varying the temperature during the domain formation process (i.e. during the linear regime), it is possible to select their typical size, particularly in one-dimensional systems.
Then, our latest simulations show that in a one-dimensional system with two neighboring kinks, if temperature oscillations occasionally exceed T_C for a sufficiently long period, the kinks start to vanish (their height approaches zero) while their distance decreases. Then, when the temperature drops below T_C again, the kinks regain their original shape and height, and the reduced distance between them is maintained. This intriguing result, presented in Appendix H, points to the possibility of accelerating the slow coarsening process in one-dimensional systems by periodically varying the temperature. However, this phenomenon is still being explored through simulations, and no theoretical explanation is currently available.

Appendix A

Ginzburg-Landau free energy functional for the 2D Ising model

We start from the core assumption of the Landau-Ginzburg theory: close to the critical condition ($T \simeq T_C$)

$$f(m, T, B) = f_0 + \frac{1}{2}|\nabla m|^2 + hm + am^2 + bm^3 + pm^4 + ... \tag{A.0.1}$$

where $m(\mathbf{x})$ is the magnetization field $m(\mathbf{x})$, which is calculated by taking a local average of the spins S_i at the lattice sites around the position $\mathbf{x}$. Then T and B are respectively the temperature and the magnitude of a magnetic field perpendicular to the plane of the system. Those two represent the variable of the system that can be controlled during the experiment.
To understand how the coefficients $(a, b, p, ...)$ depend on the controllable variables T, B, we will use the symmetries of the 2D Ising model. Firstly, we take into account that in the absence of a magnetic field ($B = 0$), there is no preferred direction. Consequently, the function $f(m)$ must be an even function of the order parameter m.

$$f(m, T, 0) = f_0 + \frac{1}{2}|\nabla m|^2 + am^2 + pm^4 \tag{A.0.2}$$

Let's consider now the other coefficients (a, p) and let's look for their temperature dependence. In the 2D Ising model, a second order phase transition occurs when T becomes lower than the critical value T_c. When the temperature is $T < T_C$, the average magnetization has a non-zero value $< m >= \pm m_0(T)$, while if $T > T_c$, $< m >= 0$ up to thermal fluctuations. In order for the theory to describe this phenomena, $f(m, T)$ must predict two degenerate stable states $m = \pm m_0(T)$ when $T < T_c$ and a non-degenerate stable state $m = 0$ when $T > T_c$. Putting this requirement in the formulas

$$f(m, T, 0) = f_0 + \frac{1}{2}|\nabla m|^2 + V(m) \tag{A.0.3}$$

where the potential $V(m)$ has two degenerate minimas $m = \pm m_0$ when $T < T_C$ and a non-degenerate minima $m = 0$ when $T > T_C$. This means

$$V(m) = am^2 + pm^4 \tag{A.0.4}$$

where $a \propto (T - T_C)$, while $p > 0$. And as this effective free energy is supposed to be adopted when $T \simeq T_C$, we can expand $p(T)$ close to the critical point

$$p(T) = p(T = T_c) + p_1(T - T_c) + ...$$

and as $p > 0 \quad \forall T$ (also when $T = T_C$), then $p_0 \neq 0$ and the expansion can be truncated at order zero

$$V(m) = a_0(T - T_C)m^2 + p_0 m^4 \qquad a_0 > 0, p_0 > 0$$

In a different fashion, if we define

$$C(T) = \frac{a_0}{2p_0}(T_c - T) \quad \bar{V} = p_0$$

the potential appears like

$$V(m) = \bar{V}(C - m^2)^2$$

where additive constants to the potential have been neglected.

Appendix B

Interaction between kinks in the 1D TDGL equation

In this section will be presented in details the calculation that shows the existance of an interaction mechanism between a kink and a neighbouring anti-kink (Figure 2.5). The results have been reported in the section 2.2.2 of the text.
We start from Eq. 2.2.12

$$-\dot{R(t)}\partial_x m = \partial_{xx} m - V'(m) \qquad V(m) = -\frac{1}{2}Cm^2 + \frac{1}{4}m^4$$

where $2R(t)$ is the distance between the pair of kink and antikink, while $m(x)$ is defined in Eq. 2.2.10.
For simplicity, in the following calculations we will consider $C = 1$. In this way no generality is lost, as it's possible to *re-scale* x, t, m such that the TDGL equation becomes a parameter-free equation: itself where $C = 1$. In fact, if we define the new set of variables

$$\tilde{t} = Ct \quad \tilde{x} = C^{\frac{1}{2}}x \quad \tilde{m} = C^{-\frac{1}{2}}m$$

it follows that

$$\partial_t = C\partial_{\tilde{t}} \quad \partial_x = C^{\frac{1}{2}}\partial_{\tilde{x}}$$

and so the TDGL equation in the new variables looks like

$$C^{\frac{3}{2}}\partial_{\tilde{t}}\tilde{m} = C^{\frac{3}{2}}\partial_{\tilde{x}\tilde{x}}\tilde{m} + C^{\frac{3}{2}}\tilde{m} - C^{\frac{3}{2}}\tilde{m}^3$$

that simplifying $C^{\frac{3}{2}}$ everywhere is the TDGL equation with $C = 1$. This means that the results of the following calculations will be general, if you rescale in the result any lenght and any time as

$$\ell \to C^{-\frac{1}{2}}\ell \quad \tau \to C^{\frac{1}{2}}\tau \tag{B.0.1}$$

Now let's put the focus back on the first equation. We can multiply both sides by $(\partial_x m)$ and integrate $\int_0^{+\infty} dx$

$$-\dot{R}I = \int_0^\infty (\partial_x m)(\partial_{xx} m) - \int_0^\infty V'(m)(\partial_x m)dx$$

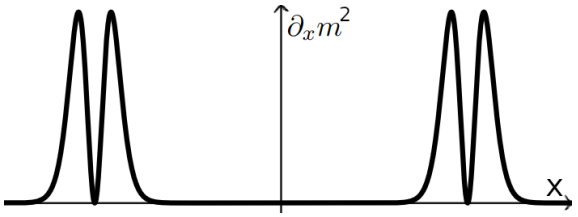

Figure B.1: Plot of $(\partial_x m)^2$, where $m(x)$ is the state with a couple of neighbouring kink and anti-kink defined in Eq. 2.2.10 and represented in Fig 2.5.

where $I = \int_0^\infty (\partial_x m)^2$ is independent on time if the distance $2R$ is big enought. This can be seen from Figure B.1, where the peaks position changes in time as $R = R(t)$, but not their shape.
To solve the other two integrals, we notice that $\frac{1}{2}\partial_x(\partial_x m) = (\partial_x m)(\partial_{xx} m)$, while $V'(m)(\partial_x m)dx = \frac{dV}{dm}\frac{dm}{dx}dx = dV$. It follows that

$$-\dot{R}I = \frac{1}{2}(\partial_x m)|_{x=0}^{x=\infty} - V(m)|_{m(0)}^{m(\infty)}$$

From Figure B.1 it's clear that $(\partial_x m(x))^2 \to 0$ if $x \to \infty$. While $(\partial_x m)(x = 0) = 0$, because $m(x)$ is an even function. For what concerns $V(m)$, we see in Figure 2.5 that $m(\infty) = +\sqrt{C}(= 1)$, while $m(0)$ is not exactly zero. In fact

$$m(0) = \tanh\left(\frac{(-R)}{\sqrt{2}}\right) - \tanh\left(\frac{(+R)}{\sqrt{2}}\right) + 1 = 1 - 2\tanh\left(\frac{(R)}{\sqrt{2}}\right)$$

and if $R >> 1$, it's possible to expand asymptotically the hyperbolic tangent as

$$\tanh\left(\frac{R}{\sqrt{2}}\right) = 1 - 2e^{-2\frac{R}{\sqrt{2}}} + O[e^{-4\frac{R}{\sqrt{2}}}]$$

As a consequence,

$$m(0) \simeq 1 - 2 + 4e^{-\sqrt{2}2R} = 4e^{-\sqrt{2}2R} - 1 = \epsilon - 1 \qquad \epsilon << 1$$

Using this approximation inside $V(m)$, it follows that

$$V(m(0)) \simeq -\frac{1}{2}(\epsilon - 1)^2 + \frac{1}{4}(\epsilon - 1)^4$$

that, at leading order in ϵ, is $V(m(0)) \simeq V(1) + \epsilon^2$, so

$$-\dot{R}I = -[V(m(\infty)) - V(m(0))] = -[V(1) - V(1) - \epsilon^2] = 16e^{-2\sqrt{2}2R}$$

$$\dot{R}(t) = -\alpha e^{-\beta R(t)} \tag{B.0.2}$$

$$\alpha = \frac{16}{I} \quad ; \quad \beta = 2\sqrt{2}$$

From the last equation, in section 2.2.2 we found that the time to wait for the annhilation of the kink and antikink pair is

$$\tau \sim e^{+\beta R(0)}$$

where $2R(0)$ is the initial distance between them. If we remember that space and time where rescaled in order to have a parameter-less TDGL, we can do the inverse operation (Eq. B.0.1). In this way

$$\tau \to C\tau \qquad R(0) \to C^{\frac{1}{2}} R(0)$$

This means that

$$\log(C\tau) \sim \beta C^{\frac{1}{2}} R(0)$$

$$R(0) \sim C^{-\frac{1}{2}} \log \tau$$

Suggesting that the dependance on C of the typical size of the domains ℓ (Eq. 2.2.2) is

$$\ell(t) \sim C^{-\frac{1}{2}} \log t$$

This last result states that it is possible to control the speed of the coarsening (increase of the domains size) by selecting C. However, this process is very slow compared to processes that scale as $\sim t^n$ (that is the case of the 2D TDGL equation, for istance). From this perspective, the size of the domains is frozen in time and so the prefactor of the logarithm is not relevant for the growth speed.

Appendix C

Calculation of $\langle q^2 \rangle$ during linear dynamics

In this appendix, we explicitly calculate the value of $\langle q^2 \rangle$ as defined in Eq. 3.1.1. As demonstrated in Sec. 3.1, the expression for $\langle q^2 \rangle$ is given by:

$$\langle q^2 \rangle = \frac{\int_{-q_{\min}}^{+q_{\min}} q^2 e^{-2q^2 t} d\mathbf{q}}{D \int_{-q_{\min}}^{+q_{\min}} e^{-2q^2 t} d\mathbf{q}}$$

To proceed, we define the integral

$$I(q_{\min}, t) \equiv \int_{-q_{\min}}^{+q_{\min}} e^{-2q^2 t} d\mathbf{q}$$

and notice that

$$\langle q^2 \rangle = -\frac{1}{2D} \frac{\frac{d}{dt} I(q_{\min}, t)}{I(q_{\min}, t)} = -\frac{1}{2D} \frac{d}{dt} \log I(q_{\min}, t)$$

To calculate $I(q_{\min}, t)$ explicitly, we recognize that the integration spans all dimensions $i = 1, 2, \ldots, D$, and the domain of integration is $q_i \in [-q_{\min}, +q_{\min}]$ for all i:

$$I(q_{\min}, t) = \int_{-q_{\min}}^{+q_{\min}} dq_1 \int_{-q_{\min}}^{+q_{\min}} dq_2 \cdots \int_{-q_{\min}}^{+q_{\min}} dq_D \, e^{-2(q_1^2 + q_2^2 + \cdots + q_D^2)t}$$

Making the substitution $x_i = \sqrt{2t} q_i$, the expression simplifies to:

$$I(q_{\min}, t) = \left(\frac{1}{\sqrt{2t}} \right)^D \int_{-x_{\min}}^{+x_{\min}} e^{-x_1^2} dx_1 \cdots \int_{-x_{\min}}^{+x_{\min}} e^{-x_D^2} dx_D = \left(\frac{\tilde{I}(q_{\min}, t)}{\sqrt{2t}} \right)^D$$

where $x_{\min} = \sqrt{2t} q_{\min}$ and $\tilde{I}(q_{\min}, t) = \int_{-x_{\min}}^{+x_{\min}} e^{-x^2} dx$.
The integral of the Gaussian function is known as the error function:

$$\operatorname{erf}(x) \equiv \frac{2}{\sqrt{\pi}} \int_0^x e^{-t^2} dt \tag{C.0.1}$$

Thus,

$$\tilde{I}(q_{\min}, t) = \sqrt{\pi}\,\mathrm{erf}(\sqrt{2t}q_{\min})$$

Subsequently, using the properties of the logarithm, we have:

$$\langle q^2 \rangle = -\frac{1}{2D}\frac{d}{dt}\log I(q_{\min}, t) = -\frac{1}{2}\frac{d}{dt}\log\left(\frac{\mathrm{erf}(\sqrt{2t}q_{\min})}{\sqrt{t}}\right)$$

Or:

$$\langle q^2 \rangle = -\frac{1}{2}\frac{d}{dt}\left[\log\Big(\mathrm{erf}(\sqrt{2t}q_{\min})\Big) + \log t^{-\frac{1}{2}}\right]$$

Calculating the time derivatives:

$$\frac{d}{dt}\log t^{-\frac{1}{2}} = -\frac{1}{2t}$$

$$\frac{d}{dt}\log \mathrm{erf}(\sqrt{2t}q_{\min}) = \frac{\partial_t \mathrm{erf}(\sqrt{2t}q_{\min})}{\mathrm{erf}(\sqrt{2t}q_{\min})}$$

Therefore,

$$\langle q^2 \rangle = \frac{1}{2}\left[\frac{1}{2t} - \frac{\partial_t \mathrm{erf}(\sqrt{2t}q_{\min})}{\mathrm{erf}(\sqrt{2t}q_{\min})}\right]$$

From Eq. C.0.1, we find:

$$\partial_t \mathrm{erf}(\sqrt{2t}q_{\min}) = q_{\min}\left(\frac{2}{\pi t}\right)^{\frac{1}{2}} e^{-2tq_{\min}^2}$$

Thus,

$$\langle q^2 \rangle = \frac{1}{4}t^{-1} - q_{\min}\left(\frac{1}{2\pi}\right)^{\frac{1}{2}} t^{-\frac{1}{2}}\frac{e^{-2tq_{\min}^2}}{\mathrm{erf}(\sqrt{2t}q_{\min})}$$

This is the most explicit expression for $\langle q^2 \rangle$ that we could derive.
Now, we seek an approximate expression valid in the large time limit, defined as $t \gg \frac{1}{2q_{\min}^2}$. However, t should not be so large that nonlinear effects on the dynamics can no longer be neglected.
In this limit:

$$\mathrm{erf}(\sqrt{2t}q_{\min}) \to 1$$

$$t^{-\frac{1}{2}} e^{-2t^2 q_{\min}} \to 0 \quad \text{faster than} \quad t^{-1}$$

As a result:

$$< q^2 > \simeq \frac{1}{4}t^{-1} \qquad \text{if} \quad t >> \frac{1}{2}q_{\min}^{-2}$$

Appendix D

Laplacian operator in the curvilinear coordinate system

In Section 2.3, we introduced a curvilinear coordinate system where the coordinates ξ and s are defined as follows:

- ξ represents the distance of a point from the interface along the direction normal to the interface.
- s describes the position of the point along a line that is equidistant from the interface (a blue line in Figure D.1).

These coordinates are illustrated in Figure D.1. In this section, we will determine

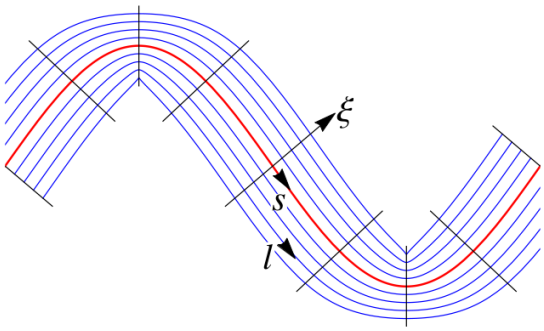

Figure D.1: In the figure, the interface is depicted in red, while each blue lines represent a set of points that are equidistant from the interface (i.e., lines of constant ξ). The coordinate ξ specifies the distance of a point from the interface, while the coordinate s indicates the position of the point along the corresponding blue line to which it belongs.

how to express the Laplacian operator $\Delta = \nabla \cdot \nabla = \partial_{xx} + \partial_{yy}$ in terms of the curvilinear coordinates ξ and s, as well as the corresponding partial derivatives ∂_ξ and ∂_s. Specifically, we will derive an approximation for Δ that is valid in the limit where the curvature is large, which corresponds to the regime studied in the text. In the limit of large curvature, the interface can be locally approximated by an arc of circle (see Figure D.2). The unit vector $\hat{n}$ represents the direction perpendicular

to the interface, which coincides with the radial direction. The unit vector $\hat{\tau}$, on the other hand, is tangent to the circle.
In this context, the radial coordinate r is related to the distance from the interface ξ by the relation

$$r = R + \xi,$$

where R is the radius of the circle that locally approximates the interface. Thus, the local curvature of the interface is $\kappa = 1/R$. Consequently, the derivative along the radial direction is given by $(\hat{n} \cdot \nabla) = \partial_r = \partial_\xi$.

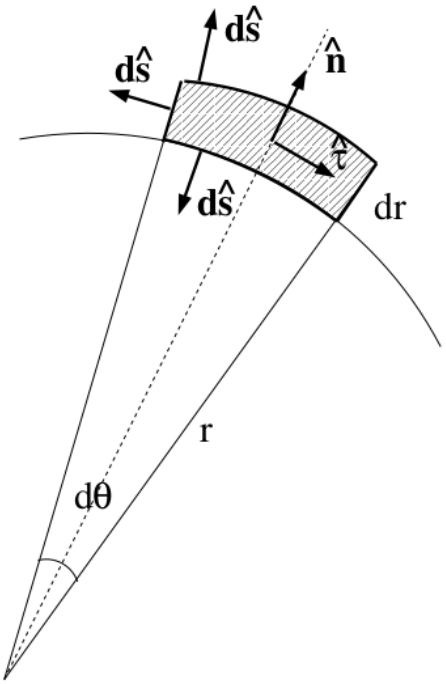

Figure D.2: Arc of a circle that locally approximates the interface. The colored region Ω is defined by the interval $[r, r + dr] \times [\theta, \theta + d\theta]$. At the boundary $\partial\Omega$, it is defined a vector field $d\hat{s}$ with a modulus of one and pointing outward from the colored region and orthogonal to the boundary. The flux of a vector field $\hat{f}$ through the boundary $\partial\Omega$ is given by the integral $\int_{\partial\Omega} \hat{f}\, d\hat{s}$.

Since the unit vectors $\hat{n}$ and $\hat{\tau}$ must be thought as centered at the point described by the coordinates (ξ, s), it follows that $(\hat{\tau} \cdot \nabla) = \partial_l$, where $l = rd\theta$ is the arc length along the interface.
The corresponding variation of the projection on the interface, ds, is given by

$$ds = Rd\theta,$$

which implies

$$dl = (R + \xi)d\theta = \left(1 + \frac{\xi}{R}\right) ds = (1 + \xi\kappa)ds,$$

where $\kappa = \frac{1}{R}$ is the curvature. Therefore,

$$(\hat{\tau} \cdot \nabla) = \partial_l = \frac{1}{1 + \xi\kappa}\partial_s,$$

and not simply ∂_s.
The Laplacian operator is defined as

$$\Delta = \nabla \cdot \nabla = \nabla \cdot [\hat{n}(\hat{n} \cdot \nabla) + \hat{\tau}(\hat{\tau} \cdot \nabla)] = \nabla \cdot (\hat{n}\partial_\xi + \hat{\tau}\partial_l)\,.$$

Now, using the chain rule, we have

$$\nabla \cdot (\hat{n}\partial_\xi) = (\nabla \cdot \hat{n})\partial_\xi + (\hat{n} \cdot \nabla)\partial_\xi,$$

and similarly for the tangential component $\hat{\tau}$. Thus, we need to calculate the divergence of $\hat{n}$ and $\hat{\tau}$. To do this, we can use the *divergence theorem*.
We consider the flux of the vector field $\hat{n}$ through the boundary $\partial\Omega$ of the colored region Ω in Figure D.2:

$$\int_{\partial\Omega} \hat{n}\, d\hat{s} = -r d\theta + (r + dr)d\theta = dr\, d\theta.$$

Using the divergence theorem, this can also be expressed as

$$\int_{\partial\Omega} \hat{n}\, d\hat{s} = \int_\Omega (\nabla \cdot \hat{n})\, dx\, dy \simeq (\nabla \cdot \hat{n}) dA,$$

where we approximate $(\nabla \cdot \hat{n})$ to be uniform within the small colored region Ω of area $dA = r\, dr\, d\theta$.
Therefore, we have

$$(\nabla \cdot \hat{n}) = \frac{1}{r} = \frac{1}{R + \xi} = \frac{\kappa}{1 + \kappa\xi}.$$

Similarly, for the vector field $\hat{\tau}$,

$$\int_{\partial\Omega} \hat{\tau} \cdot d\hat{s} = dr - dr = 0,$$

and using the divergence theorem again,

$$\int_{\partial\Omega} \hat{\tau} \cdot d\hat{s} = \int_\Omega (\nabla \cdot \hat{\tau})\, dx\, dy \simeq (\nabla \cdot \hat{\tau})\, dA.$$

This implies that $(\nabla \cdot \hat{\tau}) = 0$.
Using these results in the expression for the Laplacian:

$$\Delta = (\nabla \cdot \hat{n})\partial_\xi + (\hat{n} \cdot \nabla)\partial_\xi + (\nabla \cdot \hat{\tau})\partial_l + (\hat{\tau} \cdot \nabla)\partial_l,$$

we get

$$\Delta = \frac{1}{r}\partial_\xi + \partial_{\xi\xi} + \partial_{ll} \simeq \frac{\kappa}{\kappa\xi + 1}\partial_\xi + \partial_{\xi\xi} + \frac{1}{1 + \xi\kappa}\partial_s\left(\frac{1}{1 + \xi\kappa}\partial_s\right).$$

Appendix E

The Fredholm alternative

In this appendix, we present a proof of the theorem known as the "Fredholm Alternative." This theorem allows us to establish relationships between the parameters appearing in a differential equation without solving it.
The Fredholm Alternative theorem states that, for a linear inhomogeneous differential equation of the form

$$\hat{L}u(x) = f(x)$$

where $\hat{L}$ is a self-adjoint operator, meaning that

$$\langle \hat{L}u, v\rangle = \langle u, \hat{L}v\rangle$$

with the scalar product defined as

$$\langle u, v\rangle \equiv \int_{\Omega} u(x)v(x)\,dx$$

then, for any solution $v(x)$ of the corresponding homogeneous equation

$$\hat{L}v(x) = 0$$

it follows that

$$\langle f, v\rangle = 0$$

This result holds because

$$\langle f, v\rangle = \langle \hat{L}u, v\rangle = \langle u, \hat{L}v\rangle = \langle u, 0\rangle = 0$$

This is the conventional statement of the theorem. However, we use it in a context where the operator $\hat{L}$ may not be self-adjoint. Specifically, in Eq. 2.3.10, we have:

$$\hat{L} = \left(\partial_{\xi\xi} + C - 3m_0^2\right)$$

While the term $+C - 3m_0^2$ is clearly self-adjoint, we need to examine the derivative term more closely.
In general,

$$\langle \partial_{xx} u, v \rangle = \langle u, \partial_{xx} v \rangle + [\partial_x uv - u\partial_x v]_{\partial\Omega}$$

where Ω is the domain of integration in the definition of the scalar product. From this relationship, Eq. 2.3.10 follows:

$$\langle f, v \rangle = [\partial_x uv - u\partial_x v]_{\partial\Omega}$$

Appendix F

Extended Proof of Eq. 4.3.13

In the text we derived Eq. 4.3.13

$$(V_1 + K_1)\partial_\xi m_0 T = 0 \quad \forall \xi \tag{F.0.1}$$

from Eq. 4.3.12

$$\mathbf{0} = m_0 \int_{\tau_{-1}}^{\tau_{-1}+T} D_0(t_{-1})dt_{-1} \int_{\tau_{-1}}^{t_{-1}} D_0(t'_{-1})dt'_{-1} + \tag{F.0.2}$$

$$-2m_0^2 \int_{\tau_{-1}}^{\tau_{-1}+T} dt_{-1} \int_{\tau_{-1}}^{t_{-1}} D_0(t'_{-1})dt'_{-1} + (V_1 + K_1)\partial_\xi m_0 T$$

noticing that the three terms in the sum have different dependencies on ξ and the equation holds for all ξ, so each of the coefficients multiplying m_0, m_0^2, and $\partial_\xi m_0$ must individually equal zero.
In this appendix, we prove a necessary condition for the following assertion: there exists a value for $\tau_{-1} \in [0, T]$ such that both

$$I_A \equiv \int_{\tau_{-1}}^{\tau_{-1}+T} D_0(t_{-1})dt_{-1} \int_{\tau_{-1}}^{t_{-1}} D_0(t'_{-1})dt'_{-1} = 0$$

$$I_B \equiv \int_{\tau_{-1}}^{\tau_{-1}+T} dt_{-1} \int_{\tau_{-1}}^{t_{-1}} D_0(t'_{-1})dt'_{-1} = 0$$

For simplicity of notation, in the following calculations, we will use $D_0(t_{-1}) \equiv D(t)$ and $\tau_{-1} \equiv \tau$. To prove that $I_A = 0$, let's define the function

$$F(t) \equiv \int_\tau^t D(t')\,dt' \implies \frac{dF}{dt} = D(t).$$

With this definition, we can rewrite I_A as follows:

$$I_A = \int_\tau^{\tau+T} D(t)F(t)\,dt = \int_\tau^{\tau+T} \frac{dF}{dt}F(t)\,dt.$$

This can be further simplified by recognizing that the integral of a derivative times the function can be written as:

$$I_A = \frac{1}{2}\int_\tau^{\tau+T} \frac{dF^2}{dt}\,dt = \frac{1}{2}\left[F^2(\tau+T) - F^2(\tau)\right].$$

Since the average value of $D(t)$ over one period is zero, it follows that $F(\tau+T) = F(\tau) = 0$. Therefore $I_A = 0$
To prove that $I_A = 0$, it was not necessary to choose a specific value of τ, unlike in the case of I_B. We can express I_B as

$$I_B = \int_{\tau}^{\tau+T} F(t)\, dt.$$

By integrating by parts, where we write $F(t) = F(t) \cdot 1$ (and differentiate $F(t)$ while integrating the constant), we get:

$$I_B = [(\tau+T)F(\tau+T) - \tau F(\tau)] - \int_{\tau}^{\tau+T} D(t)t\, dt.$$

Given that $F(\tau+T) = F(\tau) = 0$, we simplify this to:

$$I_B = -\int_{\tau}^{\tau+T} D(t)t\, dt. \tag{F.0.3}$$

Now we write I_B as

$$I_B = \int_0^{\tau} \frac{dI_B}{dt} dt + I_B(0)$$

First we derive I_B respect to τ

$$\frac{dI_B}{d\tau} = -\frac{d}{d\tau}\int_{\tau}^{t^*} D(t)tdt - \int_{t^*}^{\tau+T} D(t)tdt \quad \forall t^*$$

$$\frac{dI_B}{d\tau} = \tau D(\tau) - (\tau+T)D(\tau+T)$$

And using $D_0(\tau) = D(\tau)$, it follows

$$\frac{dI_B}{d\tau} = -TD_0(\tau)$$

Now we re-integrate in $d\tau$

$$I_B(\tau) = I_B(0) - \int_0^{\tau} TD_0(t)dt$$

and recalling the definition of $I_B(\tau)$ (Eq. F.0.3) for $\tau = 0$

$$I_B(0) = -\int_0^{\tau} D(t)tdt$$

So

$$I_B(\tau) = -\int_0^{T} D(t)tdt - T\int_0^{\tau} D(t)dt$$

Our goal is to prove that it exists a value of τ such that $I_B(\tau) = 0$. This is equivalent to state that

$$\int_0^{T} D(t)tdt = -T\int_0^{\tau} D(t)dt \tag{F.0.4}$$

We define the function

$$f(t) \equiv \int_0^t D(t')dt'$$

So, integrating by parts the left hand side of Eq. F.0.4

$$\int_0^T D(t)tdt = T\int_0^T D(t')dt' - \int_0^T dt' \int_0^{t'} D_0(t'')dt'' = -\int_0^T f(t')dt'$$

where we used that $\int_0^T D(t)dt = 0$. Using this result in Eq. F.0.4

$$-\int_0^T f(t')dt' = -Tf(\tau)$$

At this point, we can state that there exists a value of $\tau \in [0, T]$ such that the above equation holds, due to the *Mean Value Theorem*. In fact the expression $\frac{1}{T}\int_0^T f(t')\,dt'$ represents the mean value of $f(t)$ over the interval $[0, T]$, and since $f(t)$ is continuous within this interval, the theorem guarantees the existence of a value $\tau \in [0, T]$ such that $f(\tau)$ is equal to the mean value.

Appendix G

Characteristic lengths ℓ and ℓ_{DW}

In the text, two characteristic lengths of the system, ℓ and ℓ_{DW}, were defined in Eqs. 3.1.2 and 2.3.15. In this appendix, we will first recall their definitions. Following that, we will prove that in a 2D system, during the asymptotic dynamics, it is possible to express one as a function of the other. As we will show, this relationship allows us to verify the coarsening law $\ell_{DW} \sim t^{\frac{1}{2}}$, which is expected during asymptotic dynamics, by checking whether $\ell \sim t^{\frac{1}{4}}$.
The first characteristic length, ℓ, describes the typical scale of the features of the system. It is defined as:

$$\ell \equiv \frac{2\pi}{\sqrt{\langle q^2 \rangle}}$$

where

$$\langle q^2 \rangle \equiv \frac{\int q^2 |M(\mathbf{q})|^2 d\mathbf{q}}{D \int |M(\mathbf{q})|^2 d\mathbf{q}}$$

Here, D is the dimension of the system and $M(\mathbf{q})$ is the amplitude of the Fourier component of the order parameter $m(\mathbf{x})$ associated to the wavelength $\lambda_{\mathbf{q}} = \frac{2\pi}{\sqrt{q^2}}$. As a feature appearing in the state $m(\mathbf{x})$, of order $\lambda_{\mathbf{q}}$, is described by the amplitude of the corresponding Fourier component $M(\mathbf{q})$, ℓ can be interpreted as the typical scale of the features within the system.
The second characteristic length, ℓ_{DW}, describes the typical size of the domains within the system. It is defined for a 2D system as:

$$\ell_{DW}^{(2D)} \equiv \frac{L^2}{\int |\nabla m(\mathbf{x})|^2 \, dx \, dy} \int \left(\partial_\xi m_0(\xi)\right)^2 d\xi$$

where

$$m_0(\xi) = \sqrt{C} \tanh\left(\xi \sqrt{\frac{C}{2}}\right)$$

is the stable stationary state of the 1D TDGL) equation. Here, L is the size of the system, and L^2 represents the total area of the system. When $D = 1$, the characteristic length is defined as:

$$\ell_{DW}^{(1D)} \equiv \frac{L}{\int |\partial_x m(x)|^2 \, dx} \int \left(\partial_x m_0(x)\right)^2 dx \tag{G.0.1}$$

In this case, if the parameter C is constant, the shape of each kink resembles the profile given by Eq. G.0.1. As a consequence, the ratio between the two integrals in the expression for $\ell_{DW}^{(1D)}$ is an estimate of $\frac{1}{N}$, where N is the number of kinks. It follows the interpretation of ℓ_{DW} as the average size of the domains, also if $D = 2$.

Relation between ℓ and ℓ_{DW} in a 2D system

Let's consider the definition of ℓ:

$$\left(\frac{2\pi}{\ell}\right)^2 \equiv \langle q^2 \rangle$$

Using the *Parseval's theorem* and the identities:

$$\mathcal{F}[|\nabla m|^2] = q^2 |M(\mathbf{q})|^2 \quad \text{and} \quad \mathcal{F}[m^2] = |M(\mathbf{q})|^2$$

it follows that:

$$\langle q^2 \rangle \equiv \frac{\int q^2 |M(\mathbf{q})|^2 d\mathbf{q}}{D \int |M(\mathbf{q})|^2 d\mathbf{q}} = \frac{1}{D} \frac{\int |\nabla m|^2 \, dx \, dy}{\int m^2(\mathbf{x}) \, dx \, dy}$$

Now, we observe that $|\nabla m|^2$ is significantly non-zero only near the interfaces between neighboring domains and is almost zero inside the domains. We also notice that, asymptotically, the curvature of any interface becomes small, so along a direction perpendicular to the interface, the profile of the order parameter $m(\mathbf{x})$ resembles the 1D stationary solution given by Eq. G.0.1. Therefore, we can approximate:

$$\int |\nabla m|^2 \, dx \, dy \simeq \mathcal{L} \int_{-\infty}^{+\infty} \left(\partial_\xi m_0(\xi)\right)^2 \, d\xi \equiv \mathcal{L} I_1$$

where $\mathcal{L}$ is the total length of the interfaces, while $I_1 = \int_{-\infty}^{+\infty} \left(\partial_\xi m_0(\xi)\right)^2 \, d\xi$ is a measure of the thickness of the interface.
A similar reasoning can be applied to calculate the other integral, $\int m^2(\mathbf{x}) \, dx \, dy$. Specifically, the function $C - m^2$ is also peaked at the interfaces and nearly zero inside the domains.
Thus, asymptotically:

$$\int m^2 \, dx \, dy = \int \left(C - (C - m^2)\right) \, dx \, dy = CL^2 - \int (C - m^2) \, dx \, dy$$

$$\int (C - m^2) \, dx \, dy \mathcal{L} \int_{-\infty}^{+\infty} \left(C - m_0(\xi)^2\right) d\xi \equiv \mathcal{L} I_2$$

Using these results, asymptotically we obtain:

$$\langle q^2 \rangle = \frac{1}{D} \frac{\mathcal{L} I_1}{CL^2 - \mathcal{L} I_2}$$

Dividing the numerator and denominator by $\mathcal{L}$, and remembering that $\ell_{DW} = \frac{L^2}{\mathcal{L}}$ in a 2D system, we find an equation that connects ℓ and ℓ_{DW} in the asymptotic regime:

$$(2\pi)^2 \ell^{-2} \equiv \langle q^2 \rangle = \frac{1}{D} \frac{I_1}{C\ell_{DW} - I_2}$$

(G.0.2)

$$I_1 \equiv \int_{-\infty}^{+\infty} \left(\partial_\xi m_0(\xi)\right)^2 d\xi, \quad I_2 \equiv \int_{-\infty}^{+\infty} \left(C - m_0(\xi)^2\right) d\xi$$

and

$$m_0(\xi) = \sqrt{C} \tanh\left(\xi \sqrt{\frac{C}{2}}\right)$$

This equation provides the relationship between the two characteristic lengths ℓ and ℓ_{DW} during the asymptotic dynamics in a 2D system. However, it is possible to make a further approximation that is valid asymptotically. At long times, the system undergoes coarsening dynamics, where the typical size of the domains grows as a power law of time, $\ell_{DW} \sim t^{\frac{1}{2}}$. As a result, eventually, $C\ell_{DW}$ becomes much larger than I_2, allowing us to simplify the previous equation:

$$(2\pi)^2 \ell^{-2} \simeq \frac{I_1 \ell_{DW}^{-1}}{DC} \tag{G.0.3}$$

where $D = 2$ in a 2D system. This asymptotic relation has been verified in a simulation (Figure G.1).
This result can be useful, as it allows the verification of the coarsening law $\ell_{DW} \sim t^{\frac{1}{2}}$ by checking that $\ell \sim t^{\frac{1}{4}}$.
Since we have the analytical expression for $m0(\xi)$, it is indeed possible to calculate the integrals I_1 and I_2 explicitly.

Calculating I_1 and I_2

To calculate I_1, we notice that

$$I_1 = \int_{-\infty}^{+\infty} (\partial_x m_0)^2 dx = \int_{-\infty}^{+\infty} (\partial_x m_0)(\partial_x m_0) dx = \int_{-\infty}^{+\infty} (\partial_x m_0) \frac{dm_0}{dx} dx$$

Simplifying the differentials, it follows that we can write I_1 as

$$I_1 = \int_{-\sqrt{C}}^{+\sqrt{C}} (\partial_x m_0) dm_0$$

where the extremes of integration changed, as now we're integrating in dm_0 and $m_0(\pm\infty) = \pm\sqrt{C}$. So now we need to express $(\partial_x m_0)$ as a function of m_0 to calculate the integral.

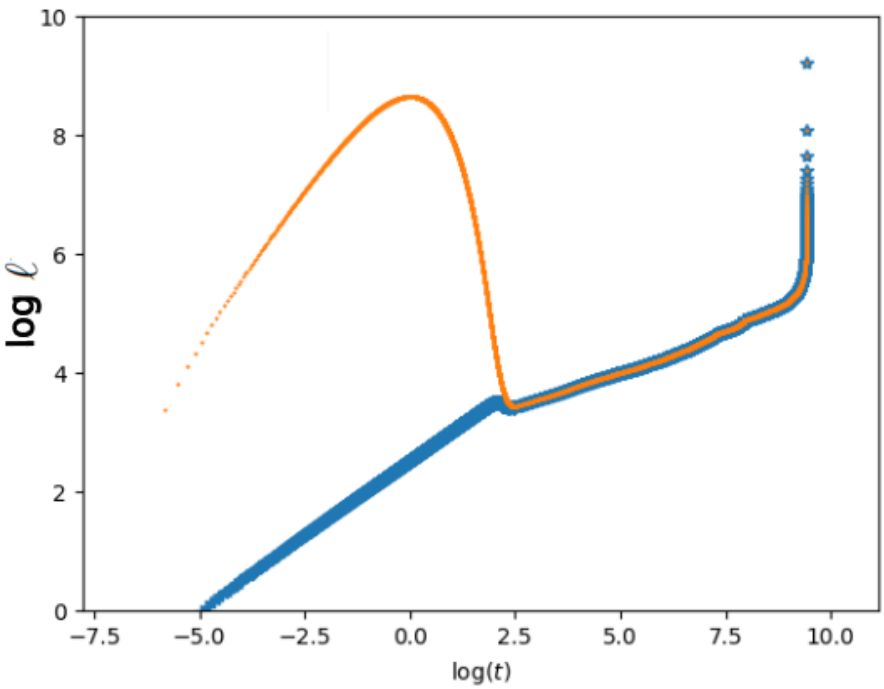

Figure G.1: In a 2D TDGL equation simulation starting from random initial conditions ($m(t = 0)$ is a small random perturbation around zero), both characteristic lengths $\ell(t)$ and $\ell_{DW}(t)$ were measured over time. The plot shows $\ell(t)$ from the simulation in **blue**, and $\ell(t)$ calculated using the measured values of $\ell_{DW}(t)$ within the asymptotic formula (Eq. G.0.3) in **orange**. The parameter C was kept constant at 1.

We recall that $m_0(x)$ is a stationary state of the 1D TDGL equation, so it's a solution of

$$\partial_{xx} m_0 + C m_0 - m_0^3 = 0$$

In Sec. 2 we saw that the stationary states correspond to the trajectories $m(x)$ of a particle moving in a potential

$$V(m) = -\frac{1}{4}m^4 + \frac{C}{2}m^2$$

In particular, the only stable state $m_0(x)$ is the available trajectory with higher energy $E = V(\pm\sqrt{C})$. Writing the energy as the sum of kinetic and potential energy

$$E = V(\pm\sqrt{C}) = \frac{1}{2}(\partial_x m_0(x))^2 + V(m_0(x))$$

so it follows that we can write the derivative of $m_0(x)$ as

$$(\partial_x m_0) = \sqrt{2}[V(\pm\sqrt{C}) - V(m_0)]^{\frac{1}{2}}$$

We can calculate explicitly the right member of the equation, as

$$V(\pm\sqrt{C}) - V(m_0) = \frac{1}{4}C^2 + \frac{1}{4}m_0^4 - \frac{1}{2}C m_0^2 = \frac{1}{4}(C - m_0^2)^2$$

Finally we can put this result inside the expression for I_1

$$I_1 = \frac{\sqrt{2}}{2}\int_{-\sqrt{C}}^{+\sqrt{C}} [C - m_0^2] dm_0 = \frac{2}{3}\sqrt{2}C^{\frac{3}{2}} \tag{G.0.4}$$

Calculating I_2 is easier, as

$$I_2 \equiv \int_{-\infty}^{+\infty} (C - m_0(x)^2) dx$$

and we notice that

$$\partial_x m_0 = \frac{1}{\sqrt{2}}(C - m_0^2)$$

It follows that

$$I_2 = \sqrt{2}\int_{-\infty}^{+\infty} (\partial_x m_0(x)) dx = \sqrt{2}[m_0(\infty) - m_0(-\infty)] = 2\sqrt{2}C^{\frac{1}{2}} \tag{G.0.5}$$

Appendix H

Latest numerical results

In this section, we present the available results from our simulations investigating the dynamics under a slowly varying temperature $T(t)$ that occasionally exceeds the critical temperature T_C. This case was not addressed analytically, as in our analysis of the limit where the oscillations of $T(t)$ are slow relative to the intrinsic timescale of the system, we assumed $T(t) < T_C \quad \forall t$. We're still investigating this limit at a simulation level and no theoretical explanation of the observed phenomena is currently available.
So far, we have studied the effect of this type of $T(t)$ modulation on a one-dimensional system with an isolated pair of neighboring kinks and on a two-dimensional system with an isolated circular domain.

1D system: two neighbouring kinks

We prepared the initial state with a kink and an anti-kink separated by a distance d_0. As we're using periodic boundary conditions, to avoid interactions between each kink and the periodic image of the other, we ensured that $d_0 \ll L$, where L is the length of the simulation box.
Next, we varied $C(t)$ so that it oscillates periodically around an average value $\bar{C} > 0$, with occasional intervals where $C(t) < 0$. The period T of the oscillations was chosen to be much larger than the system's intrinsic timescale, $\tau_{\text{linear}} \sim \frac{1}{\bar{C}}$.
Throughout the simulation, we tracked the distance between the kinks, $d(t)$, as a function of time. To calculate this distance, we identified the kink positions x_1 and x_2 as the points where the magnetization $m(x)$ changes concavity, corresponding to the zeros of $\partial_{xx} m(x)$. To estimate x_1 and x_2, we computed the second derivative of $m(x)$ using the Fourier transform properties:

$$\partial_{xx} m(x) = \mathcal{F}^{-1}[-q^2 \mathcal{F}[m(x)]],$$

We then identified the zeros of $\partial_{xx} m(x)$ by scanning the array containing the values of the second derivative and locating the points x_1 and x_2 where the sign changes.
In Figure H.1, we show how the distance between the kinks, $d(t)$, is affected by $C(t)$'s oscillations, for different values of its amplitude. Where the amplitude controls how much time the system spends with $C(t) < 0$. The simulations reveal that increasing the amplitude of the oscillation accelerates the annihilation of the kinks, reducing

the time it takes for them to merge. This suggests that the typically slow mechanism by which one kink approaches the other can be accelerated.
Notably, during the periods when $C(t) < 0$, the distance between the kinks decreases, but the domains gradually vanish (the height of the kinks gradually approaches zero). However, once $C(t) > 0$ again, the domains emerge again, while maintaining the newly reduced distance between the kinks.
One can find additional simulations, with animations that show explicitly the evolution of the state $m(x)$ here: `https://github.com/suanno/stage2/blob/main/notes/1D%20accelerate%20kinks/on_dist_oscillations.md`

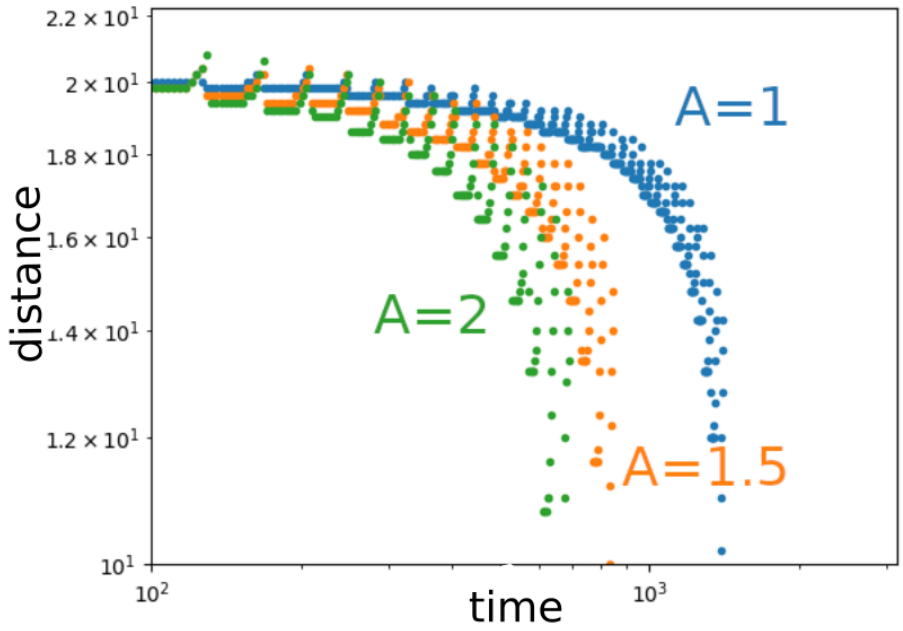

Figure H.1: We performed simulations of the one-dimensional time-dependent Ginzburg-Landau (TDGL) equation preparing the initial state as $m(x) = \tanh\left((x-x_1)\sqrt{\frac{1}{2}}\right) + \tanh\left((x-x_2)\sqrt{\frac{1}{2}}\right) - 1$, where the positions of the kinks x_1 and x_2 are initially separated by $x_2 - x_1 = d_0 = 20$ while the length of the simulation box is $L = 128$ and $dx = 0.1, dt = 0.1$. The parameter $C(t)$ varies over time according to the equation $C(t) = \bar{C} + A\sin(2\pi t/T)$, where $\bar{C} = 0.5$, $T = 40$, and A takes values of 1, 1.5, and 2 for the different curves. The plot illustrates the measured distance between the kinks, $d(t)$, as a function of time on a log-log scale.

2D system: isolated circular domain

We initialized the system with an isolated circular domain of initial radius R_0. At the start of the simulation ($t = 0$), the system was set in the state

$$m(r) = -\tanh\left((r - R_0)\sqrt{\frac{1}{2}}\right),$$

where r is the radial coordinate.

We varied $C(t)$ to oscillate periodically around an average value $\bar{C} > 0$, with occasional intervals where $C(t) < 0$. The period T of the oscillations was chosen to be much larger than the system's intrinsic timescale, $\tau_{\text{linear}} \sim \frac{1}{\bar{C}}$.
Throughout a simulation, we tracked the radius of the circular domain, $R(t)$, over time. To measure $R(t)$, we used the following expression:

$$R^2(t) = \frac{\int r^2 |\nabla m|^2 \, dx \, dy}{\int |\nabla m|^2 \, dx \, dy} \tag{H.0.1}$$

which represents the average of the radial coordinate squared, r^2, weighted by the squared modulus of the gradient of the state $m(x, y)$. This formula is based on the expectation that the value $m(x, y)$ changes significantly in space only near the interface, where $r \simeq R$.
In Figure H.2 (left), we observe that $R^2(t)$ decays linearly, as it happens in the case when C is constant. However, deviations from this linear decay occur with the same period of $C(t)$, and the slope of the linear decay differs from what would be expected for a constant C (red dashed line).
These deviations from the linear decay are found in the intervals when $C(t)$ returns to positive values after reaching its minimum value $C_{\text{min}} = -0.5$. Within these intervals, as shown in Figure H.2 (right), the estimate of $R(t)$ obtained using Eq. H.0.1 differs from the estimate obtained by measuring the actual positions of the peaks of $|\nabla m|^2$. If the interface position is defined as the location of these peaks, then Eq. H.0.1 tends to overestimate the radius of the domain. And this overestimation is consistent with the direction of the deviation from linear decay seen in Figure H.2 (left). Thus, probably these deviations from linear decay are not an inherent feature of the dynamics but rather just a result of the method used to estimate the domain radius.
Regarding the slope of the linear decay, Figure H.2 (left) shows that the decay is faster than the one expected for the case where C is constant. In Figure H.3, simulations with different values of the discrete time step dt are compared, and it can be seen that as dt decreases, the slope of the decay approaches the one expected if C were constant. However, this is not enough to conclude that the faster decay is purely a numerical phenomenon. We can only state that the effect is magnified by using a larger time step dt, but further investigation is required to fully understand its origin.

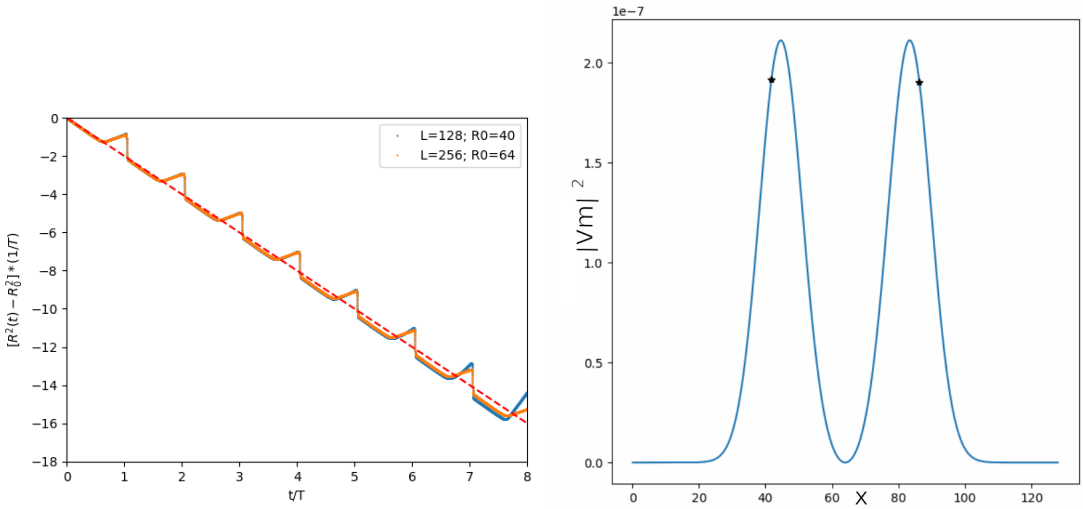

Figure H.2: We conducted simulations of the 2D time-dependent Ginzburg-Landau (TDGL) equation, where the initial state is prepared as $m(r) = -\tanh\left((r - R_0)\sqrt{\frac{1}{2}}\right)$, with initial radii $R_0 = 40$ and $R_0 = 64$. The size of the simulation box is either $L = 128$ or $L = 256$, with spatial and temporal discretization $dx = 0.1$ and $dt = 0.1$, respectively. During the simulations, the parameter $C(t)$ oscillates as $C(t) = \bar{C} + A\sin(2\pi t/T)$, with $\bar{C} = 1$, $A = 1.5$, and $T = 100$. On the **left**, the plot shows the deviation from the initial radius $(R^2(t) - R_0^2)$ as a function of time t, where $R(t)$ is the radius of the circular domain at time t, and $R_0 \equiv R(0)$. The axes have been rescaled with respect to the period T. For constant C, we expect a linear decay given by $R^2(t) - R_0^2 = -2t$, represented by the red dashed line. On the **right**, the plot shows $|\nabla m(x, y)|^2$ evaluated along the line $y = L/2$, making it a function ony of the variable x, at time $t = 600$. This corresponds to the simulation on the left with $L = 128$ and $R_0 = 40$. The black stars indicate the points $x = L/2 \pm R(t)$, where $R(t)$ is estimated using Eq. H.0.1.

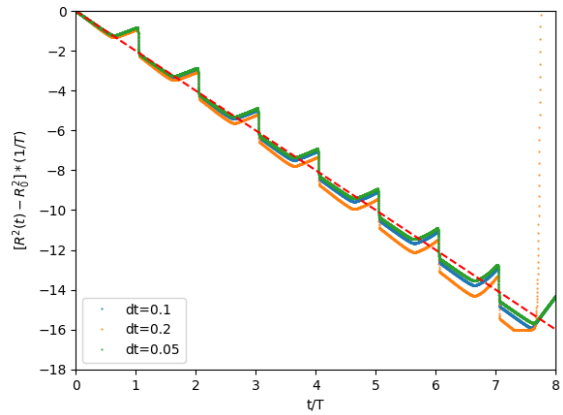

Figure H.3: The simulations of the 2D time-dependent Ginzburg-Landau (TDGL) equation, reported in Figure H.2 (left), were repeated for different values of the time step dt. In these simulations, the parameters are set as $R_0 = 40$, $L = 128$, and $dx = 0.1$, with $C(t) = 1 + 1.5\sin(2\pi t/T)$ and $T = 100$. The red dashed line represents the expected decay if C were constant.

Appendix I

Computational toolbox

This appendix is dedicated to explicitly describing the technique used to **simulate** the studied dynamics. Whenever we refer to simulations, we mean the numerical integration of the time-dependent Ginzburg-Landau (TDGL) equation with *periodic boundary conditions*. The method we employed for this purpose is the **Crank-Nicholson method in Fourier space**. In the following paragraphs, we will thoroughly explain this method, following a brief introduction to basic numerical methods. The concept has been implemented in a C code, available at `https://github.com/suanno/stage2/tree/main/codes_tdgl`.

I.1 Introduction to numerical methods for differential equations

Many differential equations, like the time-dependent Ginzburg-Landau (TDGL) equation, lack known analytical solutions. Numerical methods are crucial for *approximating* these solutions. This introduction highlights the two most popular methods: Euler's implicit and explicit methods, and the more sophisticated Crank-Nicholson method. Although Euler's methods are popular for their low execution time, they are not suitable for solving the TDGL equation. Instead, the Crank-Nicholson method is preferred, providing the best balance between accuracy and execution time.

I.1.1 Implicit and explicit Euler schemes

In this paragraph, we will present the two simplest methods for solving an *ordinary differential equation* (ODE), where derivatives are taken with respect to a single independent variable (e.g., time):

$$\partial_t u = f(u,t) \qquad \text{where: } u = u(t)$$

In contrast, p*artial differential equations* (PDEs) involve derivatives with respect to multiple variables (e.g., time and position), as seen in the time-dependent Ginzburg-Landau (TDGL) equation:

$$\partial_t u = \partial_{xx} u + Cu - u^3 \qquad \text{where: } u = u(x,t)$$

However, we'll later show that it is possible to recover an ODE from certain classes of PDEs, by applying a Fourier transform only in space. This means we can utilize the methods for solving some PDEs, such as the TDGL equation.

Explicit Euler method

The idea behind of this method is that it's possible to approximate the value of $u(t)$ at a future time $t_0 + dt$ knowing its value at time t_0 as

$$u(t_0 + dt) \simeq u(t_0) + \partial_t u(t_0) dt = u(t_0) + f(u(t_0), t_0) dt \tag{I.1.1}$$

This approximation is good when the time step dt is small. In particular we can find the order of magnitude of the error of this approximations, by taylor expanding $u(t)$ around $t = t_0$

$$u(t + dt) = u(t_0) + \partial_t u(t_0) dt + O(dt^2)$$

So we find the error of this approximations is proportional to dt^2. If we consider a larger simulation, over a time $\Delta t = N dt$ with $N >> 1$, we can estimate the order of the *global* the approximated solution

$$NO(dt^2) = NO((\frac{T}{N})^2) = TO(\frac{T}{N}) = O(dt)$$

So the global error scales faster, as $\sim dt$.

Implicit Euler method

The implicit Euler method is based on an alternative approach:

$$u(t_0) \simeq u(t_0 - dt) + \partial_t u(t_0) dt = u(t_0 - dt) + f(u(t_0), t_0) dt \tag{I.1.2}$$

This method is termed *implicit* because it does not provide an explicit formula for calculating $u(t_0 + dt)$; the function f on the right-hand side depends on the unknown future value $u(t_0 + dt)$. While $u(t_0 + dt)$ can be estimated using iterative methods, we will discuss an alternative approach suitable for a specific class of differential equations, including the TDGL equation.
Consider a partial differential equation (PDE) where derivatives with respect to space x and time appear together, focusing on the class of PDEs given by:

$$\partial_t u = \hat{L}[\partial_x, t] u; \quad u = u(x,t)$$

Here, $\hat{L}[\partial_x, t]$ is a linear operator containing space derivatives. The linearized TDGL equation (Eq. 2.1.1) belongs to this class, and it is possible to reduce the PDE to an ODE by applying a Fourier transform with respect to the spatial coordinate.
Defining the Fourier transform with respect to x as:

$$U(q,t) = \frac{1}{\sqrt{2\pi}} \int u(x,t) e^{iqx} dx$$

it follows from the Fourier transform's derivative property that:

$$\partial_t U = \hat{L}[iq]U$$

In this case, within the operator $\hat{L}$, each derivative ∂_x is replaced by iq, converting $\hat{L}$ into **a multiplicative term** with no space derivatives. Applying Eq. I.1.2 gives:

$$\begin{aligned} U(t_0) &\simeq U(t_0 - dt) + \hat{L}[iq]U(t_0)dt \\ U(t_0) &\simeq \frac{U(t_0 - dt)}{1 - \hat{L}[iq]dt} \end{aligned} \tag{I.1.3}$$

This method is particularly interesting because it is *numerically stable*, a property that cannot be generally claimed for the explicit Euler method. To define what is a numerically stable method, we need to notice that the trajectories $u(x,t)$ of a real system, which are the solutions of its correspondent differential equation, are always bounded: they never diverge as $t \to \infty$. However, the approximated solution found with a numerical method can present such kind of divergence, enhancing a non-physical behaviour. A method is called numerically stable if, *independently* on the equation to solve and on the choice of dt, the *numerical* solution is *bounded*.
To prove that the implicit Euler is a numerically stable method, is sufficient to notice that the formula for the approximated solution, corresponds to the equation describing the evolution of a discrete-time linear system

$$u_{n+1} = \hat{M}u_n \quad \text{where: } \hat{M} = (1 - \hat{L}dt)^{-1}$$

From the theory of discrete-time linear systems, the solution $\{u_n\}_n$ of this discrete-time system is bounded, if all the eigenvalues of $\hat{M}$ satisfy $|\lambda| \leq 1$. Going back to the original continuos-time equation

$$\partial_t u = \hat{L}u$$

from the theory of continuos-time linear systems, the solution $u(t)$ is bounded if all the real eigenvalues of $\hat{L}$ satisfy $\lambda \leq 0$.
As the two linear operator are related by

$$\hat{M} = \frac{1}{1 - \hat{L}dt)}$$

and the eigenvectors of a linear operator $\hat{A}$ are the same one of the inverse $\hat{A}^{-1}$

$$\hat{A}^{-1}\hat{A}u = \hat{A}^{-1}\alpha u \implies \alpha^{-1}u = \hat{A}^{-1}u$$

Then also the eigenvalues of $\hat{M}$ and $\hat{L}$ are related in the same fashion

$$\lambda^{(M)} = \frac{1}{1 - \lambda^{(L)}dt}$$

So the fact that $|\lambda^{(L)}| \leq 0$, implies that the denominator is > 1 for any value of dt. As a consequence, the eigenvalues of $\hat{M}$ all satisfy $\lambda^{(M)} \leq 1$, so the approximated solution is always bounded.

This method is referred to as an *implicit method* because in the equation

$$u(t_0) = u(t_0 + dt) + f(u(t_0)),$$

the term $u(t_0)$ appears on both sides, meaning the value of $u(t_0)$ is not given explicitly. A general property of implicit methods is their stability, a characteristic that cannot be proven for the explicit Euler method.

Formulas for the TDGL equation

Even though the TDGL equation contains a nonlinear term, we can *naively* adapt the implicit Euler formula to handle this case. The TDGL equation is given by

$$\partial_t u = \Delta u + C(t)u - u^3.$$

Taking the Fourier transform of both sides, we obtain

$$\partial_t U = \hat{L}U - \mathcal{F}[u^3]; \quad \hat{L} = -q^2 + C(t).$$

We can incorporate the term $\mathcal{F}[u^3]$ (the Fourier transform of the function u^3) into the implicit Euler formula as

$$U(t_0) \simeq U(t_0 - dt) + \{\hat{L}[iq]U(t_0) - \mathcal{F}[u^3](t_0)\}\, dt,$$

leading to the equation

$$U^{\mathbf{implicit}}(t_0) = \frac{U(t_0 - dt) - \mathcal{F}[u^3](t_0 - dt)\, dt}{1 + \hat{L}(t_0)\, dt}, \tag{I.1.4}$$

where the term $\mathcal{F}[u^3]$ is evaluated at time $t_0 - dt$ instead of t_0 to produce an explicit formula for $U(t_0)$.
In contrast, the explicit Euler method yields the simpler formula:

$$U^{\mathbf{explicit}}(t_0 + dt) = U(t_0) + \{\hat{L}(t_0)U(t_0) - \mathcal{F}[u^3](t_0)\}\, dt. \tag{I.1.5}$$

I.1.2 The Cranck-Nicholson method

A less commonly known method is the Crank-Nicholson method. This method is constructed by averaging the implicit and explicit Euler formulas. Specifically, for

$$\partial_t U = \hat{L}[iq, t]U; \quad U = U(q, t),$$

an approximation for the increment $dU = U(t_0 + dt) - U(t_0)$ is given by

$$U(t_0 + dt) - U(t_0) \simeq \frac{1}{2}\left(\hat{L}(t_0 + dt)U(t_0 + dt)\Delta t + \hat{L}(t_0)U(t_0)dt\right).$$

This expression is precisely the average of the implicit and explicit Euler formulas. As a result, the formula to calculate $U(t_0 + dt)$ is

$$U(t_0+dt) = U(t_0)\frac{\left(1+\frac{dt}{2}\hat{L}(t_0)\right)}{\left(1-\frac{dt}{2}\hat{L}(t_0+dt)\right)}.$$

And naively adapting this formula to the TDGL equation

$$U(t_0+dt)-U(t_0) \simeq \frac{1}{2}\left(\hat{L}(t_0+dt)U(t_0+dt) - \mathcal{F}[u^3](\mathbf{t_0}) + \hat{L}(t_0)U(t_0) - \mathcal{F}[u^3](t_0)\right)dt$$

$$U^{\textbf{Cranck-Nicholson}}(t_0+dt) = U(t_0)\frac{(1+\frac{dt}{2}\hat{L}(t_0))}{(1-\frac{dt}{2}\hat{L}(t_0+dt))} - \frac{\mathcal{F}[u^3]dt}{(1-\frac{dt}{2}\hat{L}(t_0+dt))} \quad \text{(I.1.6)}$$

Since this method is derived by averaging the implicit and explicit Euler methods, it is considered a *semi-implicit* algorithm and it is typically numerically stable.
The reason why we present this method, is that we discovered that the implicit and explicit Euler algorithm are not suitable for long simulations. Instead, the Cranck-Nicolson algorithm manages to integrate correctly the dynamics for longer times and this is enhanced in the following example.

Example: 0D TDGL Equation

Here, we compare the numerical solutions obtained using three different algorithms (Eqs. I.1.5, I.1.4, and I.1.6) for the time-dependent Ginzburg-Landau (TDGL) equation, starting from an initial *homogeneous* state:

$$u(x, t=0) = u_0 \quad \forall\, x.$$

This scenario corresponds to the *zero-dimensional case* discussed in Section 4, where the analytical solution is known (Eq. 4.1.2). In the following simulations, we consider $C(t)$ to be periodic and oscillating around $\bar{C} = 0$, so the expected behavior is, up to oscillations of the same period of $C(t)$

$$u(t) \sim t^{-\frac{1}{2}}$$

As shown in Figure I.1, Euler's methods are not suitable for long simulations. The explicit Euler algorithm exhibits a decay that is much faster than the expected power-law decay, resembling an exponential decay. The implicit Euler algorithm, on the other hand, causes $u(t)$ to converge to a nonzero value. In contrast, the Crank-Nicholson method accurately reflects the expected decay of $\sim t^{-\frac{1}{2}}$.

I.2 Fourier transform

In the previous paragraphs, we demonstrated the usefulness of the Fourier transform in developing methods to approximate solutions to the TDGL equation. In this section, we will define the Fourier transform and discuss the properties relevant to our work. The primary goal is to show how this tool, originally defined for continuous-time functions, can be adapted for discrete-time functions, which are the type of data that a computer can process. To achieve this, we will introduce the

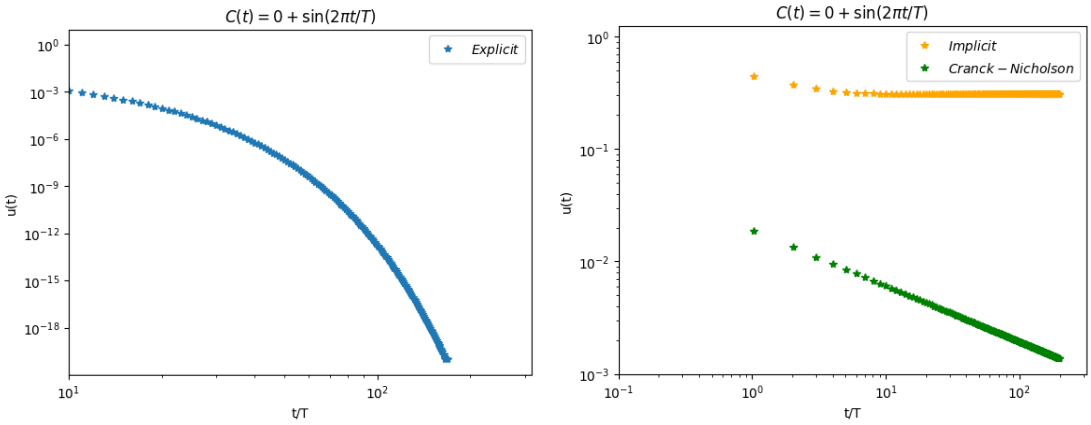

Figure I.1: Simulations of the 1D TDGL equation with a homogeneous initial state $u(x, t = 0) = u_0$ for all x. $C(t) = 0 + \sin(2\pi t/T)$ with $T = 10$. Three algorithms were compared: explicit Euler (**left**), implicit Euler, and Crank-Nicholson (**right**). The state remains homogeneous $u(x, t) = u(t)$ as time progresses. Measurements are taken at times that are multiples of the period ($t = nT; n \in \mathbb{N}$) to eliminate oscillations in $u(t)$ and verify the expected asymptotic decay $\sim t^{-\frac{1}{2}}$. Data points are shown on a log-log scale, where a power-law decay appears as a straight line with a negative slope.

discrete Fourier transform (DFT), the algorithm used by computers to approximate the Fourier transform of a continuos-time function.
The Fourier transform of a function $f(t)$ of a real variable $t \in \mathbb{R}$ is defined as:

$$\mathcal{F}[f(t)] = \hat{f}(q) \equiv \frac{1}{\sqrt{2\pi}} \int_{-\infty}^{\infty} f(t) e^{-iqt}\, dt.$$

The inverse Fourier transform is defined as:

$$f(t) = \mathcal{F}^{-1}[\hat{f}(q)] \equiv \frac{1}{\sqrt{2\pi}} \int_{-\infty}^{\infty} \hat{f}(q) e^{iqt}\, dq.$$

This formula provides an intuitive explanation of the Fourier transform: it expresses $f(t)$ as a sum of waves with different frequencies, where $\hat{f}(q)$ represents the amplitude of the wave with momentum q.
The Fourier transform satisfies several properties, but the ones most relevant to us are:

- Linearity:
$$\mathcal{F}[f(t) + g(t)] = \mathcal{F}[f(t)] + \mathcal{F}[g(t)];$$
- Derivative:
$$\mathcal{F}\left[\frac{d^n f(t)}{dt^n}\right] = (iq)^n \mathcal{F}[f(t)].$$
- Parceval's theorem:
$$\int_{-\infty}^{\infty} f(t) dt = \int_{-\infty}^{\infty} \hat{f}(q) dq$$

We used the derivative property to eliminate the space derivative in the TDGL equation, reducing it to an equation with only a time derivative.
However, computers cannot handle continuous-time functions $f(t)$. Instead, a function on a computer is represented by a discrete set of values $\{f_n\}$, corresponding to the continuous function $f(t)$ evaluated at discrete times $t_n = n\,dt$. For these discrete-time functions, the equivalent of the Fourier transform is known as the discrete Fourier transform (DFT), which still satisfies the linearity and derivative properties.
The easiest way for introducing the DFT is as the natural way of extending the Fourier serie definition to a discrete-time function.

Fourier serie

Given a continuous-time function $f(t)$ that is periodic with period T and differentiable, it can be expressed as its Fourier serie:

$$f(t) = \sum_{k=-\infty}^{\infty} \hat{f}_k e^{i\frac{2\pi}{T}kt}.$$

The sum extends from $-\infty$ to $+\infty$ because it includes all frequencies $\omega_k = \frac{2\pi}{T}k$ that are *compatible* with the period T, meaning the corresponding periods are divisors of T. To construct a function with period T, only these compatible frequencies are needed, though there are still *infinitely* many of them.
The exponentials in the sum form an orthonormal basis for functions with period T (with respect to the inner product $\langle f, g\rangle = \int_0^T f^*(t)g(t)\,dt$):

$$\hat{f}_k = \langle e^{i\frac{2\pi}{T}kt} \mid f(t)\rangle = \frac{1}{T}\int_0^T f(t)e^{-i\frac{2\pi}{T}kt}\,dt,$$

where the factor $\frac{1}{T}$ is included to ensure consistency between the Fourier series and the formula for the coefficients $\hat{f}_k$.

Discrete Fourier transform (DFT)

Let's now consider a finite sequence $\{f_n\}_{n=1,2,\ldots,N}$. We can view this as a periodic function $f(t)$ defined only at discrete time points $t \in \mathbb{Z}$, with a period $T \in \mathbb{Z}$.
Since

$$e^{i\frac{2\pi}{T}(k+T)} = e^{i\frac{2\pi}{T}k},$$

and T is an integer, the frequencies ω_k and ω_{k+mT} are equivalent $\forall m, k \in \mathcal{Z}$.
Therefore, to construct a discrete-time function, only the frequencies $\omega_k = \frac{2\pi}{T}k$ with $k \in \{0, \ldots, T-1\}$ are necessary. Alternatively, if you wish to maintain symmetry in the range of k, you can use $k \in \{-T/2, \ldots, T/2-1\}$. The function can be expressed as its Fourier series, incorporating each distinct frequency only once:

$$f(n) = \sum_{k=-N/2}^{N/2} \hat{f}_k e^{i\frac{2\pi}{N}kn}; \quad n = 0, 1, \ldots, (T-1)$$

where we have labeled $N = T$ and $n = t$ to emphasize that $t, T \in \mathbb{Z}$. The **finite** sequence $\{\hat{f}_k\}$ with $k = -N/2, \ldots, 0, \ldots, N/2 - 1$ is known as the discrete Fourier transform (**DFT**) of the sequence $\{f(n)\}_{n=1,2,\ldots,N}$ and can be calculated using the formula:

$$\hat{f}_k = \frac{1}{N} \sum_{n=0}^{N-1} f(n) e^{-i\frac{2\pi}{N}kn}, \quad k = -N/2, \ldots, 0, \ldots, N/2 - 1$$

This expression, when substituted back into the original series, exactly reconstructs $f(n)$.
The DFT retains the two key properties of the Fourier transform: linearity and the derivative property. To state the derivative property explicitly for the DFT, consider the sequence:

$$\{q_k\}; \quad q_k = \frac{2\pi}{T}k, \quad k = -N/2, \ldots, N/2 - 1$$

Given a continuous-time function $g(t)$, its Fourier transform $\mathcal{F}[g(t)]$ can be approximated by the DFT of the sequence $\{g_n\}_{n=1,2,\ldots,N}$ obtained by sampling $g(t)$ at discrete times $t = n \in \mathbb{Z}$. If we denote by $\{g'_n\}$ the sequence obtained by evaluating the derivative $\frac{d}{dt}g(t)$ at these discrete times, the derivative property for the DFT is expressed as:

$$g'_k = -iq_k g_k; \quad k = -N/2, \ldots, 0, \ldots, N/2 - 1$$

This relationship allows us to recover the sequence $\{g'_n\}_{n=1,2,\ldots,N}$ through the Fourier series.

Remark for C implementation

In C, the recommended library for implementing the DFT is the **FFTW** library. In this library, the coefficients $\{\hat{f}_k\}$ of the DFT are stored as elements of an array $\hat{\mathbf{f}}$. However, associating each element of the array with its corresponding frequency ω_k is not straightforward.
To assist users with this association, we can define an array $\mathbf{k}$ containing the values $k = -\frac{N}{2} + 1, \ldots, 0, \ldots, \frac{N}{2}$ as follows:

```
for (i = 1; i < (N/2); i++) {
    k[i] = i;
    k[N - i] = -i;
}
k[0] = 0;
k[N/2] = N/2;
```

Bibliography

[1] O. Zingera, G. Zhaob, Z. Schwartzb J. Simpsone, M. Wielande, D. Landolta, Barbara Boyanb, Differential regulation of osteoblasts by substrate microstructural features, Biomaterials **26** (2005) 1837–1847.

[2] Barada K. Nayak, Mool C. Gupta, Self-organized micro/nano structures in metal surfaces by ultrafast laser irradiation, Optics and Lasers in Engineering **48** (2010) 940–949.

[3] S. Curiotto, P. Müller, A. El-Barraj, Olivier Pierre-Louis, et al. 2D nanostructure motion on anisotropic surfaces controlled by electromigration, Applied Surface Science, 2019, **469** (1), 463-470.

[4] R. Livi, P. Politi, Nonequilibrium statistical physics, a modern perspective (Chapter 6)

[5] P.L. Krapivsky, S. Redner, E. Ben-Naim, A Kinetic View of Statistical Physics. Cambridge University Press; 2010.

[6] M. Allen, John W. Cahn, A microscopic theory for antiphase boundary motion and its application to antiphase domain coarsening, Acta Metallurgica **27** (1979)

[7] P. C. Hohenberg, B. I. Halperin, Theory of dynamic critical phenomena (Model A), Rev. Mod. Phys. **49** (1977), 435

[8] T. Gibaud, P. Schurtenberger 2009 J.Phys. Condensed Matter **21**

[9] R. Kurita, Control of pattern formation during phase separation initiated by a propagated trigger, Scientific Reports, 7: 6912.

[10] C. N. Yang and T. D. Lee, Statistical Theory of Equations of State and Phase Transitions. I. Theory of Condensation, Phys. Rev. **87**, 404

[11] E. A. G. Jamie, R. P. A. Dullens, D. G. A. L. Aarts, Spinodal decomposition of a confined colloid-polymer system, THE JOURNAL OF CHEMICAL PHYSICS **137**, 204902 (2012)

[12] H. Wang, X. Zhao, J. Wang, Enhanced dropwise condensation on heterogeneously hybrid patterned surfaces, Case Studies in Thermal Engineering, **27** (2021).

[13] J.-N. Aqua, I. Berbezier, L. Favre, T. Frisch, A. Ronda, Growth and self-organization of SiGe nanostructures J.-N., Physics report **522** (59-189).

[14] Q. Wang, Y.F. Chen, S.B. Long, Fabrication and characterization of single electron transistor on SOI, Microelectronic Engineering **84** (2007) 1647–1651.